SCUOLA DI DOTTORATO
UNIVERSITÀ DEGLI STUDI DI MILANO-BICOCCA

Department of Earth and Environmental Sciences (DISAT)

PhD program in Chemical, Geological and Environmental Sciences (SCGA)
Cycle XXXVIII
Curriculum in Environmental Sciences

The use of advanced geomorphological mapping techniques for innovative research in the science of marine geohazard and environmental changes in coastal environments

Varzi Andrea Giulia

Registration number 793000

Tutor: Prof. Claudia Pasquero

Supervisor: Prof. Alessandra Savini

Co-supervisor: Prof. Aaron Micallef

Coordinator: Prof. Marco Giovanni Malusà

ACADEMIC YEAR 2024/2025

Table of Contents

Abstract

Coastal environments represent transitional systems where terrestrial and marine processes interact dynamically, shaping highly diverse and fragile landscapes that are increasingly threatened by natural and anthropogenic pressures. Understanding the morphology and evolution of these areas requires integrated approaches capable of bridging the methodological gap between terrestrial and marine domains. This thesis addresses this challenge by developing and applying advanced geomorphological mapping techniques and multi-sensor data integration strategies to investigate coastal and marine geohazards and environmental changes across different spatial and temporal scales. The research follows a multi-layered methodological framework that combines conceptual, technical, and quantitative integration of data and approaches. Through this framework, the study seeks to demonstrate that seamless geomorphological analysis can provide a comprehensive understanding of the coastal zone as a single, continuous system, and that such understanding is essential for geohazard assessment, environmental monitoring, and sustainable management.

The CresciBluReef project provides a conceptual case study focused on the integration of geomorphological and biological evidence to reconstruct the environmental evolution in the area off Marzamemi, southeastern Sicily. High-resolution bathymetry and Remotely Operated Vehicle (ROV) imagery reveal submerged terraces and coralligenous buildups shaped by the interplay of Holocene sea-level oscillations, crustal uplift, and biogenic accretion. These findings refine local uplift rates, define morphological indicators of tectonic stability, and offer new insights into the resilience of bioconstructions under changing environmental conditions.

The BridgET project embodies technical integration by developing workflows for producing seamless, high-accuracy Digital Elevation Models (DEMs) that connect land and sea. By combining Uncrewed Aerial Systems (UAS) photogrammetry, terrestrial LiDAR, and Multibeam Echosounder (MBES) data, this project demonstrates how seamless models improve hazard modelling and morphological analysis. Furthermore, BridgET highlights the potential of immersive Virtual Reality (VR) environments to visualize geological data and foster participatory learning in hazard awareness and coastal planning. These applications represent a step toward digital transformation in marine sciences, where spatial data become interactive tools for research, education, and decision-making.

The Methane Seep Hunting project is focused on quantitative analyses by combining bathymetric, seismic, chemical, and biological data to characterize methane seeps and pockmark fields in the Colombian Caribbean. The identification of active fluid escape features and the analysis

of their spatial relationships with structural and sedimentary controls reveal their geohazard potential. Collectively, the results demonstrate that integrating terrestrial and marine datasets enhances the accuracy, interoperability, and interpretive power of geomorphological analyses.

The thesis highlights the relevance of these methods for identifying and managing geohazards such as coastal erosion, slope instability, and fluid-driven seafloor deformation, as well as for understanding processes related to sea-level change and climate impacts. The research also emphasizes the role of advanced visualization technologies and digital infrastructures in promoting open, reproducible, and participatory coastal science. By bridging traditional disciplinary boundaries, this work contributes to the development of a unified geomorphological framework for coastal and marine environments. It provides methodological foundations for future applications in Digital Twin technologies, immersive geospatial education, and integrated environmental management, supporting the transition toward a systemic understanding of the coastal zone as an interconnected, evolving landscape.

Introduction

Significance of Integrating Terrestrial and Marine Datasets

Coastal zones represent the environments where terrestrial and marine processes converge, extending from the high-water mark to the continental shelf. They are inherently transitional environments, where processes such as sediment transport, erosion, tectonic uplift/subsidence, and sea-level fluctuations, operate simultaneously across both the terrestrial and marine realms. From a geomorphological perspective, however, the spatial and temporal boundaries of coastal systems are far from straightforward, as they exhibit pronounced variability across both space and time (Masselink et al., 2011; Armynot du Châtelet et al., 2016; Prampolini et al., 2020). Inman and Brush (1973) define these spatial boundaries as the elevational range affected by coastal processes throughout the Quaternary period, a time marked by sea-level fluctuations of up to approximately 140 m. Within this framework, the coastal system encompasses the coastal plain, the shoreface, and the continental shelf (Figure 1).

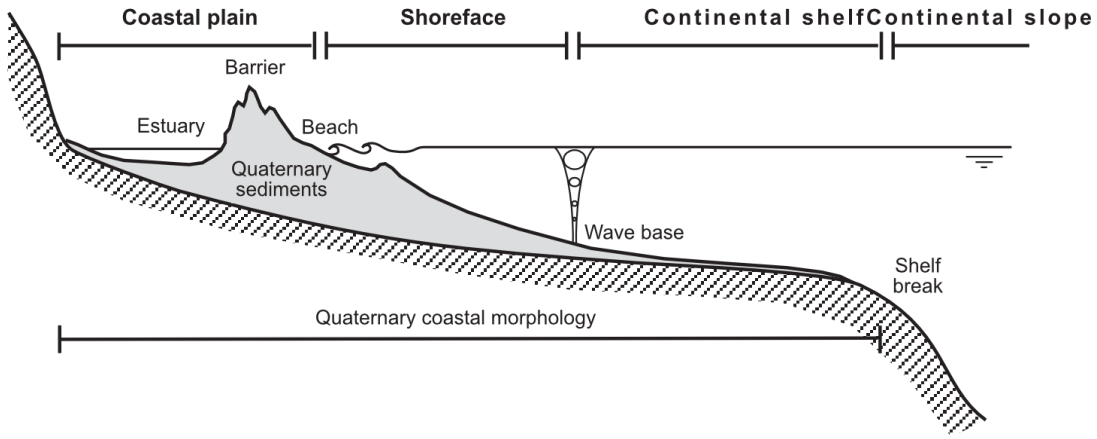

Figure 1. Spatial boundaries of the coastal zone. Extracted from Masselink et al. (2011).

The terrestrial limit corresponds to the coastal and marine erosional landforms generated during high sea-level stands, typically associated with interglacial, warmer periods, whereas the marine limit is represented by surfaces formed during glacial lowstands, when sea levels

reached their minimum and the shoreline approached the shelf break, generally located at water depths (wd) of 100–200 m. Consequently, Quaternary climate oscillations induced significant shifts in the position and extent of the coastal zone. In terms of temporal dynamics, Cowell and Thom (1994) identified four overlapping time scales over which coastal processes are in action. At the shortest, instantaneous scales, morphological changes occur within a single hydrodynamic cycle, such as the formation and destruction of wave ripples or the onshore migration of intertidal bars within a tidal cycle. Over slightly longer event scales, processes span from individual wave or tidal events to seasonal variations, encompassing phenomena such as barrier erosion during major storms or the seasonal closure of estuaries by sand bars. On engineering time scales, ranging from years to centuries, coastal evolution includes the migration of tidal inlets, the progradation of beaches, and the accumulation of sediments in foredunes, processes of particular concern to coastal engineers and managers. Finally, at geological time scales, extending from decades to millennia, long-term directional trends in sea level, climate, and tectonics dominate, driving large-scale changes such as tidal basin infilling, onshore barrier migration, and delta-lobe switching.

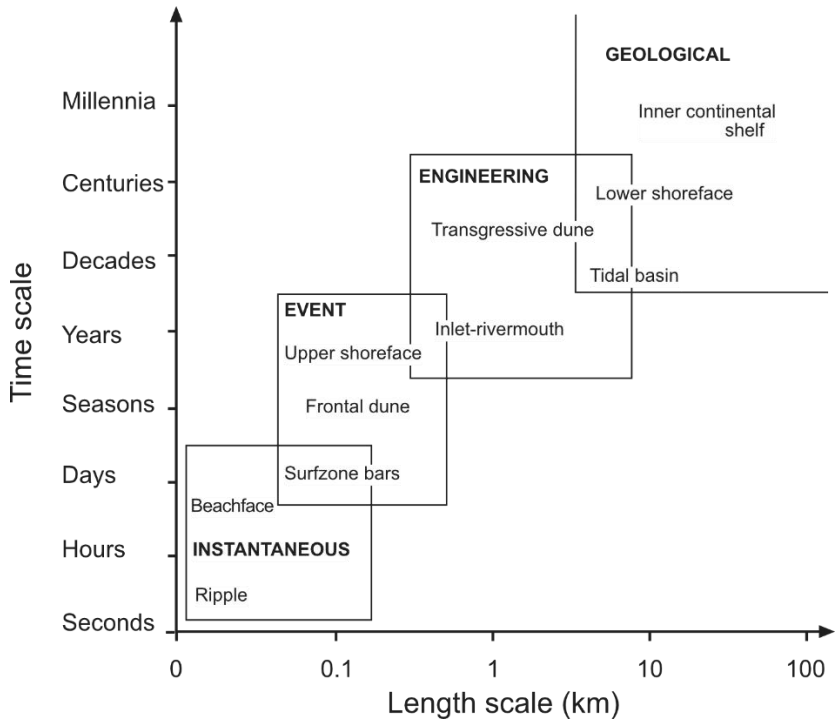

Figure 2. Definition of spatial and temporal scales involved in coastal evolution. Extracted from Masselink et al. (2011).

Beyond their geomorphic complexity, coastal areas have immense ecological and socio-economic importance, hosting more than 40% of the global population (Muñoz Sevilla et al., 2019; Kieu & Law, 2021), providing food and livelihoods for millions (FAO, 2020b), and serving as centres for recreation and tourism (Mishra & Gould, 2016). They also deliver critical ecosystem services, including shoreline protection, nutrient cycling, and carbon sequestration (Selig et al., 2019; Cooley et al., 2022). As the world is facing increasing economic, social, and environmental challenges, there is the urge of measures to improve the capacity of adapting to the impacts of climate change and geohazards. This is particularly true for these regions, where economic activity and environmental issues are more climate-sensitive. For decades, geomorphologists have tended to treat terrestrial and marine domains separately, employing different methodologies, sensors, and analytical frameworks. This disciplinary division has often resulted in fragmented datasets and a limited ability to reconstruct the coastal system as a continuum. Indeed, this area is now notably known as the *white ribbon* area, which term was first coined by the British Geological Survey referring to the nearshore and intertidal zone where both terrestrial and marine survey techniques face severe limitations. As such, this zone represents a persistent data gap all around the world, both spatially and methodologically challenging to map (Mason et al., 2006; Leon et al., 2013). Nevertheless, despite the common knowledge of their ecological, economic, and social importance, coastal zones continue to deteriorate due to both natural and anthropic pressures (Cooley et al., 2022). To fully understand these dynamics, the integration of datasets across the land-sea boundary is not only desirable but necessary, and this is the reason such a topic is becoming increasingly significant in coastal and marine sciences.

One of the main scientific benefits of this integration is the ability to reconstruct cross-shore profiles and to study morpho-stratigraphic features such as submerged paleoshorelines, coastal terraces, reef systems, and other geomorphic markers of environmental changes and crustal vertical movements. By combining high-resolution terrestrial topography, often acquired through Light Detection And Ranging (LiDAR),

Uncrewed Aerial Systems (UAS)-based photogrammetry, with marine bathymetry obtained through the use of Multibeam Echosounders (MBESs) and subseafloor information by seismic profiling, researchers can better quantify crustal vertical movements (Varzi et al., 2024), identify long-term rates of tectonic deformation, and provide robust constraints on past sea-level fluctuations (Rovere et al., 2019). This comprehensive approach improves the resolution of paleoenvironmental reconstructions and supports interpretations of both natural and anthropogenic drivers of coastal evolution (Prampolini et al., 2021).

Integrated datasets are equally crucial for geohazard assessment and risk management. Many natural geohazards, such as cliff collapses, submarine landslides, tsunami generation, or extreme storm events, are not confined to either land or sea but develop across their boundary. Seamless Digital Elevation Models (DEMs) that merge topography and bathymetry provide the essential input for numerical modelling of flooding scenarios, wave run-up, and storm surge propagation. Without accurate representation of the nearshore and intertidal zone, model predictions can be significantly biased, resulting in under- or overestimation of hazard exposure (Barnard et al., 2019). The improvement of hazard modelling through integrated datasets has been highlighted by recent applications in coastal flood assessments, where updated topo-bathymetry has been shown to drastically increase predictive reliability.

Ecological and habitat studies also benefit from such integration. Many benthic ecosystems, such as seagrass meadows, coral reefs, and coralligenous habitats, are tightly coupled with terrestrial processes that regulate sediment supply, nutrient fluxes, and freshwater input (e.g. Bialik et al., 2022; Varzi et al., 2023; Bracchi et al., 2025). The ability to integrate land-derived data on catchment characteristics with marine mapping of seabed morphology and substrate composition supports more accurate habitat models and biodiversity assessments (Casella et al., 2016). For instance, studies combining airborne LiDAR, UAS-derived DEMs, and shallow-water MBES bathymetry have demonstrated the potential of integrated products to guide marine conservation planning and to quantify

anthropogenic pressures such as dredging, trawling, or coastal development (Specht, 2023, 2025).

Apart from research, the societal significance of integrated datasets lies in their application to coastal planning and environmental management. Integrated Coastal Zone Management (ICZM) and Marine Spatial Planning (MSP) rely on comprehensive spatial information that crosses jurisdictional and disciplinary boundaries. Seamless DEMs and combined terrestrial-marine geodatabases are strategic assets for sustainable decision-making in the face of accelerating climate change, sea-level rise, and urban expansion along coasts (Barnard and Hoover, 2010). In this sense, the integration of terrestrial and marine datasets represents not only a scientific advancement but also a critical step towards sustainable governance of coastal and marine environments.

Methodological Challenges and Technological Advancement

Mapping the seafloor at a global scale is fundamental for understanding ocean processes, supporting marine spatial planning, and enabling sustainable management of marine resources. In recent years, several international and regional mapping initiatives have been launched to accelerate the systematic acquisition and dissemination of bathymetric data. At the global scale, the GEBCO project and the Nippon Foundation-GEBCO Seabed 2030 initiative coordinate efforts to compile and share bathymetric data from hydrographic offices, research institutions, industry, and crowdsourced contributions. These are supported by complementary programs such as the IHO Data Centre for Digital Bathymetry (DCDB) and the Crowdsourced Bathymetry Initiative, as well as by satellite-derived gravity models that provide baseline coverage in unmapped regions. At the regional level, initiatives like EMODnet Bathymetry in Europe, NOAA's National Bathymetric Source (NBS) in the United States, and national or thematic programs, such as AusSeabed and Arctic mapping collaborations, contribute high-resolution data within their respective domains. Together, these coordinated efforts have significantly expanded the mapped portion of the global seafloor. According to the latest GEBCO and Seabed 2030 data release, 27.3% of the world's ocean floor has now been mapped to modern standards (Seabed 2030, 2025), reflecting the growing contribution of governmental, commercial, and research hydrographic surveys (Figure 3)

In this context, the so-called *white ribbon* problem still persists, as the integration of terrestrial and marine datasets remains methodologically complex and technologically demanding. Land-based methods such as UAS photogrammetry or terrestrial LiDAR often cannot capture data below the waterline, while marine methods such as MBES cannot operate effectively in shallow or turbulent waters. As a result, the transition zone between topographic and bathymetric datasets is frequently left unresolved, creating discontinuities in DEMs and undermining their reliability for research and applied purposes (Leon et al.,

2014; Carvalho et al., 2017). This persistent lack of detailed coverage hampers the capacity to build seamless DEMs and to provide accurate inputs for coastal hazard assessments and ecological modelling. Bridging these knowledge gaps requires not only technological advances but also methodological frameworks for systematic mapping and integration of heterogeneous datasets.

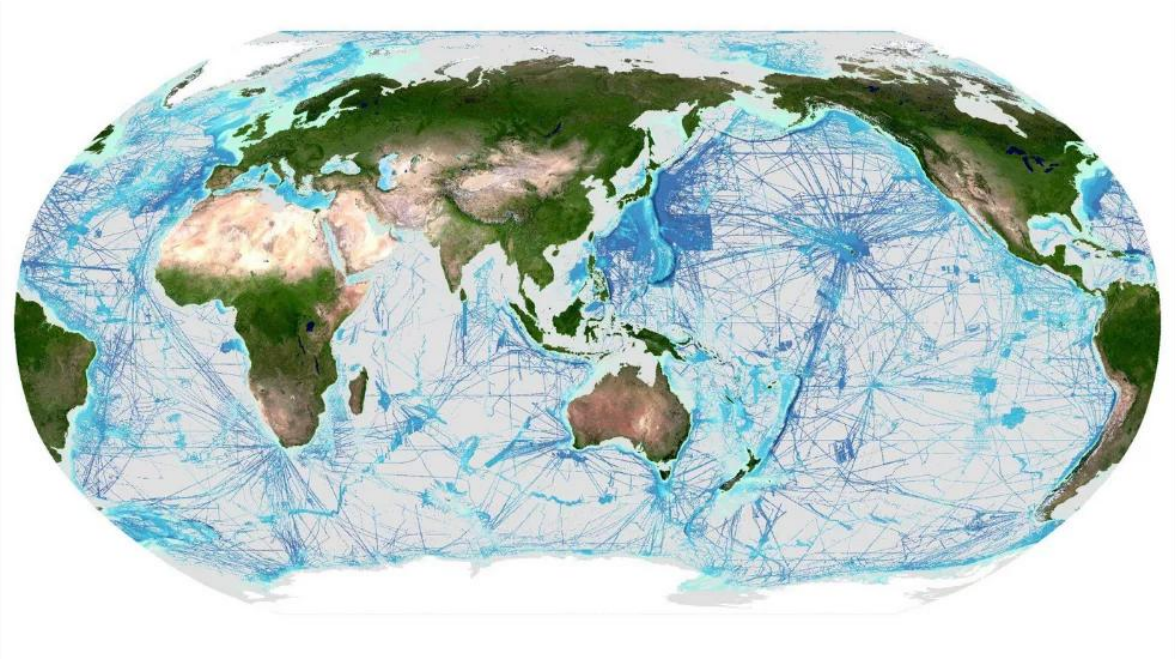

Figure 3. Areas in shaded blue represent parts of the seafloor considered mapped in the GEBCO 2025 Grid. © Seabed 2030

In addition to the spatial gap, there are substantial differences in the nature of terrestrial and marine datasets. They often differ in resolution, positional accuracy, coordinate reference systems, and acquisition time frames. For example, terrestrial surveys may provide centimetric resolution through UAS-based photogrammetry, while marine bathymetric surveys cover larger extents at coarser resolutions, often collected at different times and under variable tidal or sea-state conditions. Reconciling these differences requires meticulous georeferencing, the application of tidal and vertical datum corrections, and the development of robust error propagation frameworks (Westoby et al., 2012; Barnard and Hoover, 2010). Temporal mismatch poses an additional challenge, as dynamic coastal processes such as storms, sediment transport, or human interventions can alter the

morphology between successive surveys, complicating the interpretation of integrated datasets.

To fully understand the environmental changes affecting coastal regions, both natural and human-induced, it is of primary importance to integrate terrestrial and submerged datasets (Prampolini et al., 2021). New strategies have been lately suggested worldwide, carefully considering biotic, abiotic, and anthropogenic components (see Tribbia & Moser, 2008), in order to evaluate system susceptibility. This includes advanced mapping techniques and the creation of Spatial Data Infrastructures (SDIs), which are dedicated configurations of data infrastructures to manage and deliver geospatial data that not only includes hardware, networking, and software required to physically manage the data, but also the appropriate policies, standards, and personnel to operate the infrastructure (Simmons, 2018). This is particularly necessary for the management of coastal environments under an ecosystem-based approach. Spatial data management tools and Coastal SDI (CSDI) are key instruments (Kelly & Tuxen, 2003; Rodríguez et al., 2009; Oliveira et al., 2014), simplifying data organization and sharing among experts and stakeholders (Conti et al., 2018). Data collection in coastal areas, however, remains complex and expensive, especially due to water depth constraints, with zones often too shallow for traditional bathymetric surveys but too deep for optical land-based methods (Prampolini et al., 2021). Additionally, coastal environments lack well-defined limits (Najdawi & Ghatasha, 2012; Conti et al., 2018), which leads to the use of spatial datasets from multiple sources with differing resolutions and standards, thereby complicating georeferencing and integration (Leon et al., 2013; Prampolini et al., 2021).

Technological advancements over the past decade, however, are progressively addressing these challenges. Structure-from-Motion (SfM) algorithms, in particular, have revolutionized the acquisition of terrestrial and shallow-water topography. SfM reconstructs three-dimensional surfaces from overlapping images by identifying and matching features across photographs, producing dense PCs and high-resolution DEMs with relatively low-cost equipment (James & Robson, 2012; Westoby et al., 2012; Fonstad

et al., 2013; Clapuyt et al., 2016; Smith et al., 2016). When combined with Ground Control Points (GCPs) and integrated with MBES bathymetry, SfM allows the generation of seamless DEMs that extend continuously from subaerial to subaqueous environments (Casella et al., 2016; Pulido Mantas et al., 2023). SfM is particularly valuable for capturing fine-scale geomorphic features, intertidal zones, and shallow coastal areas where traditional survey methods are limited. In parallel, Object-Based Image Analysis (OBIA) has emerged as a powerful technique for extracting meaningful information from these high-resolution datasets. OBIA segments images or PCs into discrete objects based on spectral, spatial, and textural characteristics, rather than individual pixels, enabling more accurate classification of benthic habitats, geomorphic units, and land cover (Baatz, 2000; Blaschke, 2010; Phinn et al., 2012; Ma et al., 2017; Ierodiaconou et al., 2018; Hossain & Chen, 2019). Applied to SfM-derived orthophotos and PCs, OBIA allows the creation of semantically rich layers suitable for ecological mapping and geomorphometric analyses. By combining SfM and OBIA, researchers can generate both detailed topography and interpretable representations of the coastal landscape, which are essential for quantitative analyses and predictive modelling. Another critical advancement lies in multi-sensor data fusion, where heterogeneous datasets, from Satellite-Derived Bathymetry (SDB) to UAS topography and shipborne sonar, are combined using statistical interpolation, machine learning algorithms, and reliability ranking methods. These workflows allow researchers to weight datasets according to their accuracy, correct systematic errors such as refraction in optical bathymetry, and produce seamless DEMs with quantified uncertainties (Leon et al., 2014; Carvalho et al., 2017). The increasing computational capacity available for handling dense PCs and large-scale MBES surveys also supports these more complex integration workflows.

Beyond data acquisition and processing, visualization technologies such as Virtual Reality (VR) and immersive three-dimensional environments are beginning to play a transformative role in both research and teaching. They allow scientists to interact with integrated terrain and seabed models at multiple scales, enhancing interpretation and

communication of complex geospatial phenomena. While such immersive technologies are still emerging in applied geoscience, they hold promise for supporting inclusive education, public engagement, and stakeholder participation in coastal planning (Barnard et al., 2019).

What remains essential is the establishment of standardized workflows and best practices that ensure data comparability and reproducibility across different coastal contexts. Only through such methodological consolidation can integrated datasets fulfil their potential in advancing our understanding and sustainable management of dynamic coastal and marine environments.

Application for Coastal and Marine Geospatial Modelling

The increasing availability of integrated seamless datasets has opened new frontiers in marine and coastal geospatial modelling. By extending the spatial, temporal, and thematic resolution of datasets across the land-sea interface, researchers can now address more complex questions, improve predictive accuracy, and better inform management decisions. The urgency of applying integrated datasets is further emphasized by the increasing pressures on coastal systems. Climate change is altering the diversity, abundance, and distribution of marine species, while weakening the ocean's capacity to provide essential ecosystem services such as food provision, carbon storage, and oxygen generation (Cooley et al., 2022). At the same time, human activities such as fishing, coastal development, shoreline hardening, and habitat destruction significantly reshape the land-sea interface, modifying hydrodynamics and even driving local subsidence (Steneck and Pauly, 2019; Suchley and Alvarez-Filip, 2018; Newton et al., 2020). In this context, systematic morphological mapping, coupled with geomorphological interpretation and subsurface geophysical data, is indispensable to assess both anthropogenic impacts and geohazards. Recent studies illustrate how such integration has moved from aspiration to operational use, revealing multiple domains of application where this approach is particularly relevant.

A first and significant application is found in habitat mapping and ecological modelling. Maruca et al. (2025) developed a semiautomated GIS-based workflow to map coralligenous bioconstructions off Calabria, Italy, combining high-resolution MBES bathymetry, backscatter, and geomorphometric indices to identify and classify seabed morphologies. Their procedure not only delineated the extent of habitat types but also quantified their 2D and 3D attributes, supporting geomorphological interpretation and providing a basis for monitoring and conservation of benthic biogenic structures. Similarly, Sullivan et al. (2025) combined UAS imagery with Sentinel-2 satellite data to classify

benthic cover in the NEOM region, Saudi Arabia, successfully mapping coastal habitat types, such as algae, corals, and seagrasses and, over 225 km^2 of the seafloor. These approaches demonstrate how integrated datasets can provide ecological baselines and guide management strategies for biodiversity conservation. Nevertheless, biological and ecological studies still tend to focus either on the terrestrial domain or in the marine one, leaving the transition zone less investigated.

Integrated data also play a central role in coastal hazard assessment and morphological monitoring. Specht (2023) produced high-resolution coastal DEMs for the Polish shoreline by integrating UAS-based topography with Single-Beam Echosounder (SBES) bathymetric data collected via an Uncrewed Surface Vehicle (USV). The study tested multiple terrain-modelling methods, demonstrating such models are suitable for shoreline change detection and coastal flood modelling. Spadaro et al. (2025) present a multi-sensor workflow integrating UAV-based SfM photogrammetry, USV-borne SBES bathymetry, and GNSS/total-station topography to produce seamless coastal DEMs. By applying refraction correction and testing various interpolation techniques, they extended effective depth measurements to 4-5 meters, exceeding typical optical limits and demonstrated the potential of integrated DEMs for hydraulic, geomorphological, and environmental studies.

Another important field of application is Marine Spatial Planning (MSP) and decision support. In this regard, the "Statewide Marine Habitat Map 2023" in Victoria, Australia, combined ground-truth records with 28 environmental predictor layers, including bathymetry, terrain metrics, and other parameters, to train a Random Forest model that predicted 24 marine and coastal habitat-complex classes at about 10 m resolution, covering 83 % of the area via modelling. The resulting product serves as a broad-scale dataset for MSP, habitat condition assessment, cumulative-impact, and risk tools, and as a baseline for monitoring and management of Victoria's state waters (Mazor et al., 2023). More broadly, reviews of geospatial technologies for MSP (Schwartz-Belkin and Portman, 2023) stress that integrating topography, bathymetry, and habitat datasets is critical for

evidence-based planning, though many initiatives still suffer from data gaps or mismatched scales.

Applications also extend to ecosystem functioning and environmental monitoring. Piazzolla et al. (2025) combined USV bathymetry, ROV surveys, and multimetric ecological indices to assess benthic habitat quality in three coastal sites in the northeastern Tyrrhenian Sea. By integrating spatial data, such as substrate type, vegetation height, and percent cover, with taxonomic and functional metrics, they generated composite habitat quality indices. This integrated approach provides a rapid, scalable method for evaluating coastal benthic habitats, supporting monitoring, management, and decision-making under frameworks such as the Marine Strategy Framework Directive (MSFD) and MSP, while highlighting differences in habitat status across sites of varying protection levels.

Finally, integrated terrestrial and marine datasets are fundamental for predictive modelling under climate change and anthropogenic pressure scenarios. Seamless DEMs and substrate or habitat layers serve as essential inputs to spatially explicit models of sea-level rise impacts, storm surge flooding, and species distribution. For example, habitat mapping of the Croatian Adriatic Sea combined EMODnet bathymetry, substrate, and geology data to inform conservation planning and provide baseline layers for ecosystem services and spatial modelling (EMODnet, 2024).

In this evolving geospatial landscape, the concept of a Digital Twin (DT) represents a major advancement in how physical systems are monitored, simulated, and understood. A DT can be broadly defined as a dynamic, data-driven virtual representation of a real-world system that is continuously updated through the integration of observations, models, and sensor data (Yao et al., 2023). This approach is characterised by the real-virtual mapping of objects or processes, real-time synchronization, and feedback loops that enable continuous calibration and prediction. Originally developed in industrial and engineering contexts, digital twins are increasingly applied in Earth and environmental sciences, where they provide an integrative framework for combining heterogeneous datasets, assimilating real-time observations, and conducting scenario-based simulations (Yao et al., 2023).

Within the marine and coastal domain, this paradigm has evolved into the concepts of the Digital Twin of the Ocean (DTO) and Coastal Digital Twins (CDTs). These are virtual systems that integrate high-resolution bathymetric, topographic, hydrodynamic, biogeochemical, and ecological information to reproduce, analyse, and forecast the behaviour of coastal and marine environments (Jiang et al., 2021; Chen et al., 2023). By merging observations, models, and Artificial Intelligence (AI), such frameworks enable near-real-time monitoring, predictive simulations, and scenario testing under changing climatic and anthropogenic conditions. In this sense, digital twins represent a natural extension of seamless land-sea integration, offering a platform where terrestrial and marine datasets can interact dynamically to support early warning systems, ecosystem management, and sustainable coastal planning.

Rationale

Coastal systems are intrinsically cross-boundary: geomorphic, ecological, and anthropogenic processes operate continuously from the terrestrial shore to the offshore seabed. These environments are among the most dynamic and fragile on Earth, shaped by the interplay of climatic, tectonic, and oceanographic processes. They host dense human populations, critical infrastructures, and ecologically valuable habitats, yet they are increasingly exposed to the combined effects of sea-level rise, coastal erosion, and anthropogenic pressures. Despite their complexity and importance, coastal zones have long been studied through a disciplinary divide: terrestrial and marine domains have traditionally been analysed using different platforms and conceptual frameworks. This separation has produced fragmented datasets and hindered our ability to understand the coastal system as a single, continuous environment.

The persistent absence of detailed information in the nearshore, the *white ribbon gap* (Mason et al., 2006; Leon et al., 2013), exemplifies this fragmentation, where both terrestrial and marine methods struggle to capture accurate data in shallow waters. Consequently, many fundamental questions about coastal evolution, habitat distribution, and geohazard dynamics remain unresolved. Integrating terrestrial and marine datasets therefore represents not merely a technical challenge but a conceptual and methodological frontier: it allows us to move from a dualistic to a holistic understanding of coastal systems, bridging the subaerial and subaqueous domains. Within this context, my research seeks to develop and test approaches that enable such integration, both in theory and in practice, by combining geomorphological reasoning with technological innovation.

In this PhD thesis, I adopt a structured framework that distinguishes between *Conceptual Integration*, *Technical Integration*, and *Quantitative analysis*, which together define the methodological and analytical core of the thesis. *Conceptual integration* refers to the use of terrestrial observations and datasets as interpretative frameworks for marine geomorphology, for example, applying onshore stratigraphy, landforms, and geomorphic

indicators to interpret submerged features, constrain sediment sources, and reconstruct paleo-shorelines or crustal movements. *Technical integration*, on the other hand, refers to the geospatial fusion of heterogeneous datasets, such as LiDAR-derived topography, UAS-based photogrammetry, and MBES bathymetry, into seamless DEMs and unified PCs that represent the land-sea continuum with quantified uncertainties. The third, cross-cutting pillar of this research is the *Quantitative analysis* aimed at assessing anthropogenic impacts and geohazards. Once datasets are integrated, they enable systematic morphological mapping, geomorphometric extraction, and spatial modelling that quantify the magnitude and direction of change across coastal environments. Such analyses are fundamental for distinguishing natural variability from human-induced transformations, evaluating the stability of coastal slopes and seabed features, and assessing the health and resilience of benthic habitats.

Within this framework, each of these concepts is associated with a reference project: CRESCIBLUREEF illustrates the conceptual integration of terrestrial and marine perspectives for interpreting biogenic and geomorphic structures; BridgET focuses on the technical integration of geospatial datasets and the development of seamless DEMs across the land-sea interface; and Methane Seep Hunting (MSH) demonstrates the application of quantitative analyses. Comprehensive details for each project are reported in the Methodology section, which has been organised according to the three main concepts investigated here. The Results section follows the same structure, presenting published or under-review papers developed within each framework. Together, these projects define a coherent approach through which this research advances both the scientific understanding and the practical management of dynamic coastal and marine systems.

Aims and Research Questions

This PhD thesis aims to overcome the long-standing separation between terrestrial and marine approaches to coastal research by developing and testing methods that allow the coastal zone to be treated as a continuous, interacting system. The overarching objective is to advance both the conceptual understanding and the technical capability required to integrate land and sea datasets, and to apply such integration to the quantitative analysis of environmental change and geohazard processes. In particular, the research is structured around the following specific aims:

1. To demonstrate how land-derived data can improve the interpretation of submarine features and palaeoenvironmental reconstructions.

2. To develop and validate a transferable, reproducible workflow for producing high-resolution, seamless land-sea DEMs that integrate multi-sensor terrestrial and marine datasets, with explicit treatment of positional, temporal and measurement uncertainty.

3. To apply quantitative analyses that identify and measure anthropogenic impacts and geohazard signatures, producing actionable information for management and hazard mitigation.

Together, these aims define a coherent and complementary framework through which the thesis advances the integration of terrestrial and marine perspectives, conceptually, technically, and analytically, towards a unified understanding of coastal systems and their evolution.

Building upon these aims, the research is guided by a series of questions that address the conceptual, technical, and analytical dimensions of land-sea integration. These questions are designed to test how terrestrial and marine datasets can be effectively combined, how such integration can enhance the interpretation of coastal and submarine

processes, and how the resulting information can be applied to quantify environmental change and assess geohazard potential. The main research questions are therefore as follows:

1. To what extent does incorporating terrestrial geomorphological and stratigraphic information improve the interpretation of submarine features and the reconstruction of past sea-level or vertical movement rates?

2. How can multi-sensor terrestrial and marine datasets be combined into a seamless, reproducible DEM of the land-sea continuum while preserving and propagating measurement uncertainties?

3. Which geomorphometric or statistical indicators derived from integrated datasets best discriminate between natural variability and anthropogenic impacts in vulnerable coastal habitats?

4. Can the workflow and indicators developed in the case studies be generalised into best-practice guidelines for CSDIs and applied in management or decision-support contexts?

Together, these questions guide the thesis from methodological development to applied interpretation.

Methodology

Conceptual Integration

I. CresciBluReef project

CresciBluReef – "Cresciuto nel blu: nuove tecnologie per la conoscenza e la conservazione dei reef del Mediterraneo" is a national research initiative funded under the FISR 2019 (Fondo Integrativo Speciale per la Ricerca). The project brings together a multidisciplinary consortium of Italian universities and research groups, combining expertise in marine geology, geobiology, biogeochemistry, robotics, computer graphics, and virtual reality technologies. The University of Milano-Bicocca leads the national coordination, including the Marine Geology and Geobiology group and GeoVires Laboratory from the Department of Earth and Environmental Sciences (DISAT), alongside with expertise in AI, from the Department of Informatics, and marine zoology, thanks to the involvement of the University of Genova. Two additional research units complement the consortium: the University of Calabria, with competences in mechanical engineering, marine robotics, geomicrobiology, and biogeochemistry; and the University of Catania, with expertise in marine geobiology and (paleo)ecology. Together, these teams are advancing a new frontier in the study and preservation of Mediterranean reefs, integrating technological development, geoscientific research, and digital innovation toward a deeper understanding and sustainable management of these fragile underwater landscapes.

The project was indeed conceived in response to a significant knowledge gap concerning Mediterranean bioconstructions, which, despite their ecological and geological relevance, remain far less studied than their tropical counterparts. Along the Mediterranean continental shelf, various types of reef-like bioconstructions have developed during the Holocene, acting as natural archives of past environmental changes. Among these, Coralligenous formations, complex structures primarily built by calcareous red algae, represent key ecosystems that record climatic and environmental fluctuations within their framework. CresciBluReef focuses on investigating the Coralligenous system off

Marzamemi, Southeastern Sicily, one of the most representative examples of these temperate reefs. The research aims to unravel the tempo and mode of Coralligenous inception and development, characterize the accretionary structures, and estimate their growth rates in relation to Holocene climate variability inferred from geobiological and geochemical proxies. This geological perspective complements ongoing biological studies that mainly address the biodiversity and ecological functioning of the living surface layer, thereby offering a more comprehensive understanding of these habitats.

In line with the European Blue Growth strategy, the project integrates technological innovation with fundamental research. A new ROV is being developed and tested to enable minimally invasive sampling and high-resolution seabed observation. This ROV incorporates original mechanical and robotic solutions with potential applications beyond the project's scope. The planned activities also include geo-paleontological and biogeochemical analyses, environmental monitoring, seafloor mapping, and sub-bottom profiling, alongside 3D photogrammetric reconstructions of the investigated bioconstructions.

The resulting multi-scale datasets will be digitally archived and made accessible through immersive virtual reality environments, enabling remote exploration and analysis of these deep and complex reef systems. This digital dimension not only enhances the scientific value of the collected data but also promotes educational and outreach activities, fostering greater public awareness and appreciation of Mediterranean marine ecosystems.

Technical Integration

II. BridgET project

The BridgET project, "Bridging the gap between the land and the sea in a virtual environment for innovative teaching and community involvement in the science of climate change-induced marine and coastal geohazard" is a transnational Erasmus+ KA220-HED Cooperation Partnership in Higher Education, running from February 2022 to February 2025. Coordinated by the University of Milano-Bicocca, Italy, BridgET involves a strong consortium of European universities and research institutions, including partners from Germany, Malta, Greece, Norway, Belgium, and Italy, bringing together expertise in marine geosciences, geohazard assessment, digital mapping, and immersive learning technologies. The project was conceived in response to a growing need for highly skilled professionals in coastal and marine geosciences, capable of innovating in the visualization, analysis, and interpretation of complex geological and environmental datasets. The recent advances in digital mapping have dramatically improved the ability to generate high-resolution 3D terrain models. These advances make it possible to integrate terrestrial and submarine datasets seamlessly, enabling a more integrated approach for understanding coastal systems and their evolution in the context of climate change, sea-level rise, tectonic processes, and marine geohazards.

BridgET's primary aim is to transform the way marine and coastal geosciences are taught and learned, through the development of standardized workflows and innovative teaching methodologies that leverage VR. By bringing detailed, reality-based 3D models of complex and often inaccessible environments into immersive virtual spaces, the project facilitates new forms of interactive, inclusive, and experiential learning. This is especially significant in marine geosciences, where traditional fieldwork is often logistically challenging and costly, and where certain groups of students, such as those with physical disabilities, have historically faced barriers to participation. To achieve these aims, BridgET

implemented a series of interconnected activities. Central to the project are the three international summer schools held in Santorini, Greece, Mount Etna, Italy, and the Maldives, locations selected for their geological diversity and exposure to different types of climate- and tectonics-driven geohazards. During these schools, MSc students have the possibility to gain hands-on experience in terrestrial, aerial, and underwater data acquisition, data processing, and 3D model construction. These multiscale and multisource datasets can then be used to build immersive VR environments, allowing students to analyse geological processes and human-environment interactions in real time. This not only strengthens technical skills but also encourages students to propose management and mitigation strategies for coastal geohazard scenarios.

Quantitative Analysis to Assess Anthropogenic Impacts and Geohazard

III. Methane Seep Hunting Project

The project "Methane seep hunting: A multi-scale and multi-method approach" (Project Code 80733) is a 24-month research initiative funded under Colombia's national program for science, technology, and innovation in geosciences, within the call 877-2020 for hydrocarbon sector research. Led by the Universidad Pontificia Bolivariana (UPB) in Medellín, in collaboration with the Universidad Nacional de Colombia (UNAL), GMAS SAS, Geomares S.A.S., the Asociación Colombiana de Geólogos y Geofísicos del Petróleo (ACGGP), the University of Milano-Bicocca, the University of Malta, and the Kiel University, the project addresses critical knowledge gaps in the understanding of methane seep dynamics in the Colombian Caribbean, particularly in the Sinú offshore basin. Its central aim is to develop and implement a standardized, cost-effective, and technologically advanced methodology to identify hydrocarbon seep fields, as a means of improving exploration strategies and basin analysis.

The project area is located offshore the Gulf of Morrosquillo, within the Sinú basin, an underexplored region with high geological complexity due to the interaction of the Caribbean and South American plates. This margin exhibits widespread fluid flow features such as mud diapirs, mud volcanoes, pockmarks, and methane seeps, yet seep fields have never been systematically studied despite their significance as indicators of active petroleum systems. Traditional exploration methods like seismic reflection and drilling are costly and time-intensive; by contrast, methane seep detection offers an innovative, lower-cost exploration pathway. The project seeks to answer key scientific and industrial questions: i) what is the origin and nature (microbial vs. thermogenic) of seeped hydrocarbons? ii) what morphological and ecological signatures accompany seeps? iii) how are seep distributions

controlled by geological structures such as diapirs? iv) how can seeps be detected rapidly and reliably across large areas?

To address these questions, the project adopts a multi-scale, multi-method workflow combining remote sensing, geophysics, geochemistry, and biological analyses. At the large scale, Synthetic Aperture Radar (SAR) imagery were analyzed to detect oil slicks and potential seep zones on the sea surface. At the meso-scale, marine geophysical surveys employed MBES and high-resolution SBP to map seafloor morphology, subsurface structures, and active gas plumes. At the fine scale, targeted sampling campaigns collected water column profiles, piston cores, and biological samples at selected seep sites. These samples the underwent geochemical and isotopic analyses (e.g., GC-MS, $\delta^{13}C$ measurements) to determine the nature and origin of seep fluids, sedimentation rates, and the depth of the sulphate-methane transition zone. Biological analyses focused on foraminifera assemblages and chemosymbiotic communities, both of which provide valuable indicators of seep activity, flux intensity, and environmental change.

An innovative aspect of this project is its integration of geological, geochemical, and biological proxies to reconstruct both current and past seep activity, thereby improving the understanding of seep dynamics in space and time. Ultimately, it aims at generating a workflow specific to Colombian waters, applicable to other basins, and designed to be cost-efficient, replicable, and scalable. Scientifically, the project builds upon decades of prior work on methane seepage, pockmarks, mud volcanism, and cold seep ecosystems worldwide, adapting these approaches to the Colombian Caribbean margin, a region with distinctive geological features and tectonic history. Through this integrative framework, the Methane Seep Hunting project positions Colombia at the forefront of methane seep research in Latin America, contributing to both fundamental science and applied exploration strategies, while fostering sustainable and informed use of offshore resources.

Results

CresciBluReef Project

a) Geomorphology of coralligenous reefs offshore southeastern Sicily (Ionian Sea)

This work is published as:

Varzi, A. G., Fallati, L., Savini, A., Bracchi, V. A., Bazzicalupo, P., Rosso, A., Sanfilippo, R., Bertolino, M., Muzzupappa, M., & Basso, D. (2023). Geomorphology of coralligenous reefs offshore southeastern Sicily (Ionian Sea). *Journal of Maps*. https://doi.org/10.1080/17445647.2022.2161963

Abstract

Coralligenous (C) include calcareous build-ups of biogenic origin, formed since the Holocene transgression. Peculiar columnar-shaped C outcrops were documented offshore Marzamemi village (SE Sicily, Ionian Sea), although the actual extension and distribution were not assessed. Project 'CRESCIBLUREEF' produced a new, 17 km^2 high-resolution bathymetric map, leading to good knowledge about their extent in this area. C bioconstructions are largely distributed along two depth ranges 36–42 m and 86–102 m water depth. By coupling the documented uplift rate in this region and the Holocene sea-level curve, we were able to interpret the distribution of C outcrops over terraces. However, additional investigation is required to understand: (1) the role of the inherited continental shelf landscape, in creating a favourable substrate for the settlement and growth of C habitats during the Holocene, and (2) the extent to which C bioconstructions can impact the evolution of present-day continental shelf landforms and landscapes.

Introduction

Coralligenous (C) habitats consist of calcareous formations of biogenic origin and are a characteristic of subtidal systems located within the Mediterranean Sea (Peres, 1982; Ballesteros, 2006). Calcareous structures are largely composed of encrusting Rhodophyta belonging to the orders Corallinales and Hapalidiales (Ballesteros, 2006). C habitats generally develop on rocky coasts or sandy planes, whether or not stable conditions of temperature, salinity, and currents exist, and in areas where irradiance is reduced to 0.05–3% of surface irradiance (Garrabou & Ballesteros, 2000; Costanzo et al., 2021). The growth of C habitats largely depends on the delicate balance between bioconstruction and bioerosion processes (Sartoretto & Francour, 1997; Garrabou & Ballesteros, 2000; Costanzo et al., 2021), and can easily be altered by environmental changes and stressors such as increased sedimentation, biological invasion, and nutrient enrichment (Balata et al.,

2005, 2007; Piazzi et al., 2007, 2011; Costanzo et al., 2021). Since definitions and morphological classifications for C bioconstructions have always been difficult due to their variety and complexity (Riding, 2002), and since, at present, no unanimous consensus exists within the scientific community, here, when referring to C physical tridimensional structures, the terms reef, build-up, and bioconstructions are equally used as descriptions.

Documented C bioconstructions within the Mediterranean Sea show complex three dimensional structures (Bracchi et al., 2015; Marchese et al., 2020). Remarkable lateral growth is dominant (Bosence, 1985; Di Geronimo et al., 2002), although peculiar columnar-shaped structures have been observed that contain subhorizontal (Sartoretto, 1994; Di Geronimo et al., 2002) or vertical (Di Geronimo et al., 2001, 2002) growth. Within the Mediterranean Sea, the extent and biodiversity of C habitats and their role in the carbon cycle (Ballesteros, 2006; Boudouresque et al., 2015; Ingrosso et al., 2018; Costanzo et al., 2020) make them one of the most valuable and important marine habitats. Although these structurally complex bioconstructions provide heterogeneous habitats and suitable substrates for the settlement of a variety of organisms (Boudouresque et al., 2015; Costanzo et al., 2020; Bracchi et al., 2022), approximately 95% of C habitats have not been mapped (Martin et al. 2014; De Falco et al., 2022). Due to the fact that these habitats are protected by international conventions such as Habitat Directive 92/43/EEC, the SPA/BIO Protocol, the Barcelona Convention, the Bern Convention, and the European Union 1967/2006 Regulation (Costanzo et al., 2020), knowledge of C habitat distribution is fundamental for management and conservation (De Falco et al., 2022).

Offshore Marzamemi (SE Sicily) at the infra-circalittoral boundary, Di Geronimo et al. (2001, 2002) described intriguing columnar-shaped build-ups made by calcareous algae and subordinate invertebrates. In this area, columns rise from the seafloor and reach a height of approximately 1 m in water depths (w.d.) up to around 40 m, forming a sort of patch-reef subparallel to the coastline. Due to material collected by fishers and a map of the entire Gulf of Noto, produced using data acquired in 1981 (Violanti et al., 1990; Rosso & Sanfilippo, 2009), deeper C bioconstructions have been known for quite some time.

However, an accurate mapping of this marine habitat has, to date, not been done (Lo Iacono et al., 2018). The main goal of our study was to create a high-resolution, morpho-bathymetric map for the continental shelf offshore Marzamemi that contained a quantitative description for the distribution and extent of C reefs.

Study Area

The study area is located offshore Marzamemi village (Figure 1). The area is part of the Hyblean Plateau, the northernmost sector of the Pelagian block, and represents the emerging portion of the NE-SW-oriented bulge of the African foreland (Lentini et al., 1994; Distefano et al., 2021a). The plateau is bounded to the NW by a system of NE-SW trending, NW dipping normal faults, and is flanked by the Gela Basin towards the W (Lentini & Carbone, 2014). Towards the E, the plateau is bordered by the Ragusa-Malta Escarpment, a dominant feature of the Central Mediterranean, which represents a regional system of NW-SE/NNW-SSE oriented extensional faults (Grasso & Lentini, 1982; Grasso & Pedley, 1990; Distefano et al., 2021a) that controls the tectonic evolution of the eastern Sicilian offshore region (Grasso et al., 1992; Distefano et al., 2021a). Eastern Sicily, along with the Calabrian Arc region, is one of the most tectonically active regions of Southern Italy. A regional tectonic uplift began around 0.6 Ma (Westaway, 1993; Tortorici et al., 1995; Catalano et al., 2008) and has been continuous over the entire Holocene, leading to the occurrence of an uplifted paleo-shoreline (Firth et al., 1996; Stewart et al., 1997; De Guidi et al., 2003; Antonioli et al., 2004; Ferranti et al., 2007; Catalano et al., 2008). The area we investigated is characterised by a regional uplift of approximately 0.2 mm/yr since the Late Pleistocene (see Bianca et al., 1999; Catalano et al., 2008; Lambeck et al., 2011; Pavano et al., 2019; Distefano et al., 2021a). Coupled with eustatic sea level changes, uplift produced the deep entrenchment of rivers on land and marine terracing along the margin. Stratigraphic succession of the Hyblean Plateau consists of carbonate sediments of Triassic to Quaternary age. Carbonate facies reflect distribution of the following paleogeographic

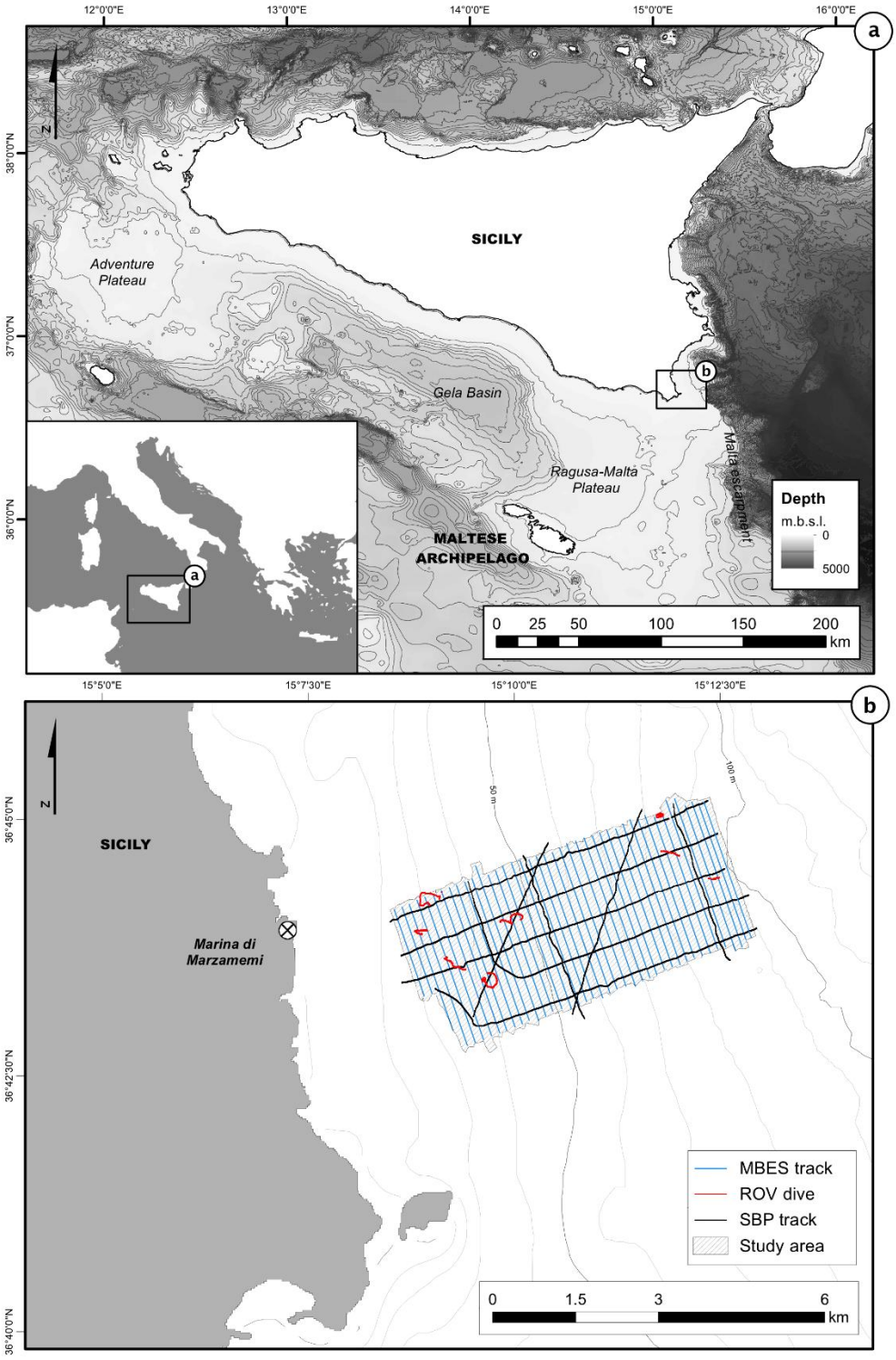

Figure 1. (a) Bathymetric map of the central Mediterranean Sea showing Sicily and the main geomorphological features characterising the area (isobath at 100 m interval). Background bathymetry from EMODnet (https://www.emodnet-bathymetry.eu/). (b) Bathymetric map of the central Mediterranean Sea showing Sicily and the main geomorphological features characterising the area (isobath at 100 m interval). Background bathymetry from EMODnet

domains: a basin known as the 'Siracusa Sector' towards the E and the carbonate shelf of the 'Ragusa Sector' towards the W (Distefano et al., 2021a). The study area is included within the Siracusa domain. Using stratigraphic logs of Quaternary deposits located close to the Marzamemi village, Distefano et al. (2021a) produced a detailed geological sketch-map of the area. Succession in the area begins with limestones of the Priolo Formation (Upper Cretaceous) associated with the products of subaerial events. An overlying sedimentary succession of Paleocene-Eocene age then occurs, followed by marls of the Tellaro Formation (Middle to Late Miocene). Pliocene units are represented by Trubi Formation (Early Pliocene) and Late Pliocene marls. The final layer, consisting of Quaternary deposits, is represented by calcarenites of the Marzamemi Formation (Late Pleistocene), Holocene alluvial and lagoon sediments, and present-day beach deposits.

Both subaerial and submerged geomorphological features have revealed evidence for erosional forms cut into carbonate units. The submerged morphologies of sublittoral and inner shelf zones, indeed, resemble characteristics typical of karst depressions (Distefano et al., 2021a, 2021b). Subaerial erosional surfaces over the area mark the height reached by relative sea level during the Late Quaternary coupled with regional uplift. Late Pleistocene marine terraces were approximately 15 m above sea level (Gracia & Gutiérrez, 2002; Distefano et al., 2021a). The following evolution produced sedimentary deposition and transformation of river valleys into progressively infilling (estuary Distefano et al., 2021a, 2021b).

Methods

Our study is based on three data sets acquired during June 2021 for the first marine expedition of project 'CRESCIBLUREEF – Grown in the blue: new technologies for knowledge and conservation of Mediterranean reefs' (Figure 1(b)). Data acquisition was performed onboard the minor vessel Valerio. Positional data were provided by a Trimble RTK GNSS receiver that was connected, in real-time, to a NTRIP network (Leica SmartNet ItalPoS).

The first data set was collected during a Multibeam Echosounder (MBES) survey using a pole-mounted, R2-Sonic 2022 system combined with an Integrated Inertial Navigation System (I2NS), which provided accurate and robust georeferencing and motion compensation, and the Sound Velocity Sensor – Valeport miniSVS. Data was collected in 45 tracks (Figure 1 (b)) performed at an average speed of 5 knots during three days of field work. The lateral range was kept between 70 and 100 m, with a swath overlap of 10–50%. Approximately 17 km^2 of seafloor was investigated, with depth ranging from approximately 20 to over 100 m w.d.. A couple of sound velocity profiles were collected each working day, before starting the acquisition in the morning and in the afternoon, using a Sound Velocity Profiler – Valeport miniSVP. The multibeam survey provided both bathymetry and backscatter (BS) data (see Main Map in the original submission).

The second data set consists of underwater video surveys obtained by using a SEAMOR Steelhead inspection-class Remotely Operated Vehicle (ROV). We identified possible interesting spots on the basis of the MBES data and we planned eight transects (Figure 1(b)) along which visual investigations were performed. Each dive had a duration of about one hour, including the drop-off and drop-on of the ROV. Positional information, with respect to ship position, was obtained with an Ultra-Short Baseline Applied Acoustic Micor Beacon 1200A. Low-definition (LD) videos were acquired using the incorporated camera of the ROV. To obtain high-definition (HD) imagery, we equipped the ROV with a GoPro HERO5. LD and HD videos were used to ground-truth MBES data. The video analysis allowed us to confirm the presence/absence of C and its morphotypes, other than the type of substrate.

The third data set consists of seismic lines, acquired using an Innomar SES-2000 smart, and the SESWIN data acquisition software. Data was collected along 11 tracks (Figure 1(b)). In particular, five were performed following the depth gradient throughout the whole study area, and they were spaced about 600 m to each other to laterally investigate the whole area of interest. Three were conducted perpendicular to those mentioned above, at about 44, 50, and 93 m w.d.. Finally, three were executed following a diagonal

course, two with a SW-NE orientation, and one with a NW-SE orientation.

The post-processing of MBES data was performed using QPS Qimera; and included a correction for heading, heave, pitch, and roll. Sound velocity correction process was fulfilled using the sound velocity profiles obtained with the Valeport miniSVP. Corrections for tide were applied considering measurements registered by the Catania station of the Rete Mareografica Nazionale RMN (Istituto Superiore per la Protezione e la Ricerca Ambientale – ISPRA). Finally, soundings were cleaned to remove spikes. The bathymetric dataset was exported as a 32-bit raster file with a cell size of 3 m. Backscatter data processing was performed using QPS Fledermaus FMGT. Output was exported as an 8-bit raster file with a cell size of 0.3 m.

Mapping operations were conducted using ESRI ArcGIS. Whenever possible, we implemented a semi-automatic approach in order to detect positive morphologies from bathymetric data (Gafeira et al., 2018). The computation of basic land surface parameters, such as the slope gradient and profile curvature, supported the manual mapping of other significant submarine landforms on bathymetry and backscatter data. The processing and interpretation of seismic profiles were performed using the Kingdom Software 2020. RAW data were converted to SEG-Y files using SES Convert software. Seismic data were used to perform seismostratigraphic correlations with published results obtained from seismic reflection surveys conducted offshore Marzamemi (i.e. Distefano et al., 2021a, 2021b).

Results

MBES data

MBES data processing resulted in a Digital Terrain Model (DTM) with a resolution of 3 m (Figure 2). The bathymetric dataset reveals a marked topographic complexity within the shallower region of the study area resulting from positive landforms, which form distinct banks arranged in a rough pattern between 10 and 40 m w.d.. Moving offshore, seafloor complexity drastically decreases, with the exception of deeper areas where the

presence of positive morphologies and elongated narrow ridges are evident between 75 and 100 m w.d.. The analysis of DTM-derived local morphometric variables (i.e. slope and curvature) further led to the clear identification of marked breaks in slope (see Main Map in the original submission), mainly oriented along two perpendicular axes:

- NW-SE, arranged from the shore to the offshore at: (i) 44–48 m, (ii) 62–70 m, (iii) 80–86 m, and (iv) 98–102 m below sea level. The couples of numbers refer to the upper and lower rims of each escarpment, defining the terrace height-drop at the outer rim. The surveyed area results thus to be shaped by four terraces. Additional smaller escarpments clearly denote the presence of two narrow ridges over the third and fourth terraces.
- SW-NE, marking distinct incisions on the seabed in the form of discrete channel-like morphologies. The first one has a mean section of 95 m, and its path yielded two main changes in direction, running a total length of roughly 3 km over the first terrace; the mean vertical relief is of about 2 m. The second one has a larger mean section of approximately 145 m, it also crosses the second terrace over a distance of 3 km but follows a more linear path; the mean vertical relief is, again, of about 2 m despite. Both morphologies are characterised by the presence of sub-circular small depressions (between 30 and 60 m in diameter) along the track, with a vertical relief between 0.2 and 0.5 m (Figure 2).

BS data

We determined a dependable match between backscatter and topographic complexity. A rough appearance in bathymetric data is, indeed, normally associated with a complex backscattering fabric, while flat areas are defined by a more regular and homogeneous pattern. Since the first terrace is the most complex region, maximum variability in BS is seen throughout this area. The shallower portion is characterised by an intermittent speckled fabric of moderate BS (Table 1(a)). Articulate positive features dominating the area are characterised by a complex fabric of moderate to low BS (Table

1(c)). The transition between these two patterns is gradual and delimited by a complex fabric of moderate backscatter (Tab1e 1(b)). Besides sub-circular depressions that have an exceptionally low backscatter, flat areas display a more homogeneous pattern of moderate to high intensity (Table 1 d). A pattern of moderate to high BS typifies the flat seafloor of the second and third terraces. Patches with a dotted pattern of slightly lower signal intensity (Table 1(e)) are locally found over this region. Channels are marked by a more homogeneous BS, although inner sub-circular concavities show much lower intensities. Within the deeper fourth terrace, a high BS intensity (Table 1(g)) typifies the featured mound-like morphologies. The surrounding seafloor displays a homogeneous pattern of low BS (Table 1(f)).

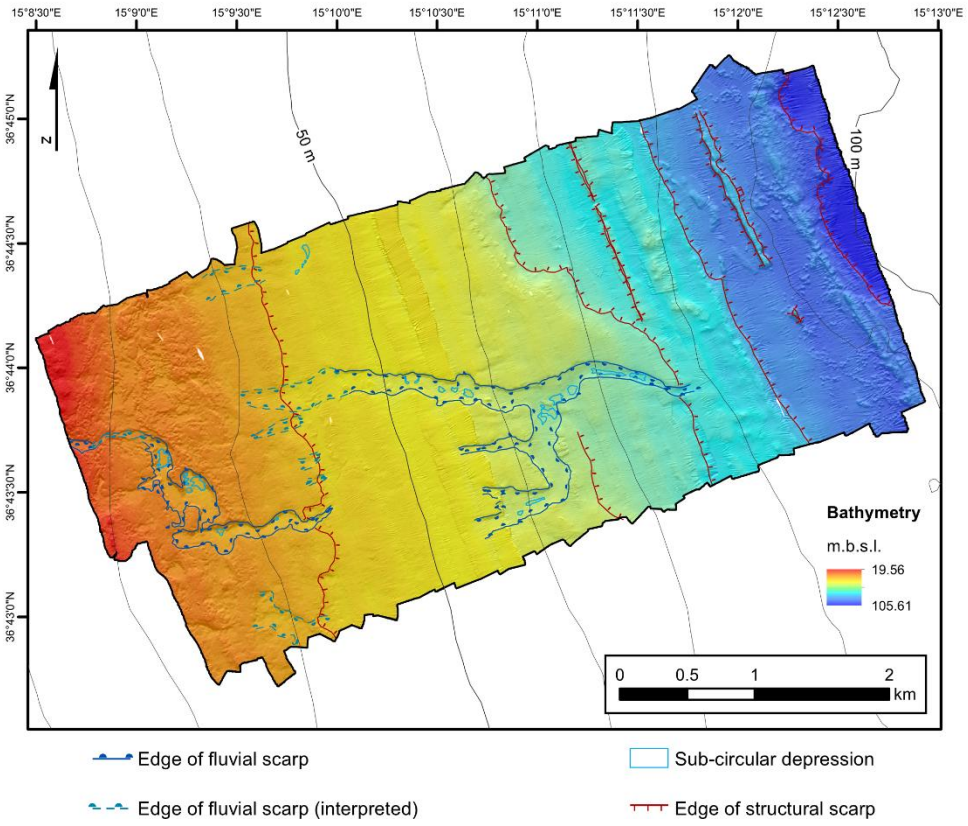

Figure 2. Processed bathymetric data draped on shaded relief map, with a focus on the main geomorphological characteristics that typify the area (isobath at 10 m interval). High-resolution data collected by the MBES survey (R2-Sonic 2022 system) as part of the CRESCIBLUREEF project.

Table 1. Morpho-acoustic facies identified by combining bathymetric and backscatter data with ROV videos interpretation.

Bathymetry 19.56 105.61 m.b.s.l.	**Backscatter** Low High	**Texture description**	**Seabed image**	**Seabed description**
		Intermittent speckled fabric of moderate backscatter	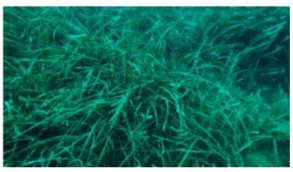	Bedrock covered by dense *Posidonia oceanica* meadows
	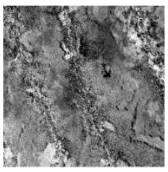	Complex fabric of moderate backscatter		Mobile sediment with blocks of C and patches of seagrass
	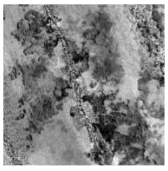	Complex fabric of moderate to low backscatter		Banks of C of columnar aspect
	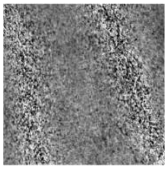	Homogeneous pattern of moderate backscatter		Medium to coarse sediment with rhodoliths
	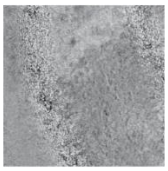	Dotted pattern of moderate backscatter		Small discrete C build-ups surrounded by medium to coarse sediment with rhodoliths
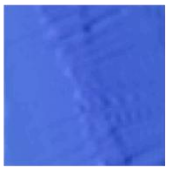	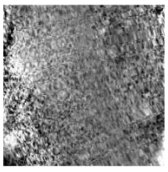	Homogeneous pattern of low backscatter		Bioturbated fine sediment
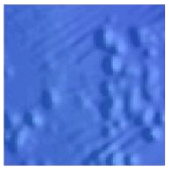	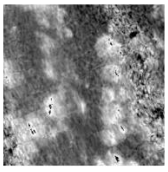	Complex fabric of high backscatter		Blocks of C populated by CWC surrounded by fine sediment

Notes: First and second columns show the bathymetry and backscatter imagery (area of 100 × 100 m). High backscatter is represented by light colours while low backscatter by dark colours. Third column reports backscatter textures description. Representative photographs of the seabed composition and its interpretation are reported as well in the fourth and fifth columns, respectively.

Visual inspections

ROV videos were crucial for recognising the widespread distribution of C habitats throughout the area, as well as the general layout of various habitats. *Posidonia oceanica* (L.) (Delile, 1813) is abundant up to a depth of about 30 m. Discrete, small build-ups (between 20 and 40 cm in diameter) are scattered over the seafloor among Posidonia meadows and are sometimes associated with sparse rhodoliths. Moving offshore, seagrasses become sparser, leaving spaces for positive irregular reefs (e.g. banks) that form shallow outcrops of approximately 1 m in height. Within the central portion of the surveyed area, C bioconstructions are more sparsely distributed and are not organised in banks. Across the deepest area, C build-ups are visibly larger in both size and height as compared to the shallower counterparts. An in-depth analysis of ROV videos also allowed the identification of several macro-organisms associated with C build-ups (Table 2).

Detected habitats

The combination of video and bathymetric data, and the associated backscattering pattern led to the identification of seven distinctive morpho-acoustic facies (Table 1). We were able to map five main habitats that characterise the surveyed area, and two categories corresponding to mobile substrate, which are 'Fine sediment' and 'Medium to coarse sediment' (Figure 3). C habitats and morphotypes were categorised by referring to Bracchi et al. (2017). More information about their identification are reported here below:

- *Posidonia oceanica* meadows: typical P. oceanica BS signal was recognised in the shallower region of our study area, up to 30 m w.d.. Here, P. oceanica meadows dominate and span 0.27 km^2 of the seafloor.

- Mosaic of C and Posidonia meadows: in the area from 30 to 36 m w.d., typical P. oceanica BS signal gradually attenuates. Indeed, ROV videos show that C outcrops begin to be gradually discernible, and P. oceanica starts to be less compact. Indeed,

Table 2. List of the species we were able to identify thanks to ROV video surveys.

	IUCN Category		International Legal Instrument	European Legal Instrument	Regional Legal Instrument		
	MED (a)	GLO (b)	CITES (c)	EU Habitats Directive (d)	Protocol SPA/BD (e)	Bern Convention (f)	GFCM Reccomendations (g)
Chlorophyta							
Caulerpa cylindracea	NE	NE					
Codium bursa	NE	NE					
Flabellia petiolata	NE	NE					
Halimeda tuna	NE	NE					
Rhodophyta							
Osmundaria volubilis	NE	NE					
Tracheophyta							
Posidonia oceanica	LC	LC			II	I	
Porifera							
Chondrilla nucula	NE	NE					
Phorbas fictitius	NE	NE					
Cnidaria							
Antipathella sp.	NT	NE	II		II		GFCM/43/2019/6 on a establishment of a set of measures to protect vulnerable marine ecosystems formed by cnidarian (coral) communities in the Mediterranean Sea
Dendrophyllia ramea	VU	NE	II		II		
Eunicella cavolini	NT	NE					
Paramuricea macrospina	DD	DD					
Anellida							
Bonellia viridis	NE	NE					
Hermodice carunculata	NE	NE					
Bryozoa							
Margaretta cereoides	NE	NE					
Myriapora truncata	NE	NE					
Reteporella sp.	NE	NE					
Arthropoda							
Calappa granulata	NE	NE					
Echinodermata							
Achantaster sp.	NE	NE					
Astrospartus mediterraneus	NE	NE					
Centrostephanus longispinus	NE	NE		IV	II	II	
Peltaster placenta	NE	NE					
Stylocidaris affinis	NE	NE					
Chordata							
Halocynthia papillosa	NE	NE					
Muraena helena	LC	LC					

Notes: We verified whether such species would have been assessed for the IUCN Red List of Threatened Species both at the Mediterranean (a) and Global (b) level (Vulnerable, VU; Near Threatened, NT; Least Concern, LC; Data Deficient, DD; Not Evaluated, NE) or under other Legal Instruments: (c) CITES, Convention on International Trade in Endangered Species of wild fauna and flora, ratified by all Mediterranean States; Appendix II-Species (see http://www.cites.org for full definitions) list of taxa not necessarily threatened now with extinction, but that may become so unless trade is closely controlled. (d) EU Habitats Directive, Council Directive 92/43/EEC on the Conservation of natural habitats and of wild fauna and flora, it must be implemented in all European States of the Mediterranean; Annex IV, species of interest to Europe which need strict protection. (e) Protocol SPA/BD, concerning Specially Protected Area and Biological Diversity in the Mediterranean, ratified by all Mediterranean States (except Greece, Israel, Bosnia, and Libya); Annex II, species that are endangered or threatened. (f) Bern Convention on the Conservation of European Wildlife and Natural Habitats, ratified by all Mediterranean States of the study, except Algeria, Egypt, Israel, Lebanon; Appendix I, strictly protected flora species; Appendix II, strictly protected fauna species. (g) GFCM Recommendations, adopted by the General Fisheries Commission for the Mediterranean, must be implemented in all Contracting Parties of the GFCM in the Mediterranean.

we classified a transitional belt that occupies 0.81 km^2 of the seafloor, to be a mosaic of C habitats and P. oceanica meadows.

- C sensu stricto: deeper than 36 m w.d., upon close ROV inspection, P. oceanica is not present anymore. Discrete C build-ups are well imaged by ROV. We easily noticed lateral continuity due to the coalescence of C build-ups, especially within the NW region between 36 and 42 m w.d.. In this area, C habitats form hybrid banks with metrical topographic relief, displaying typical cavernous aspects. Intra-areas sensu Bracchi et al. (2017) are characterised by medium to coarse sediment. This morphotype represents the transition between isolated build-ups and tabular banks. We classified these areas, which extend over 0.91 km^2 of the seafloor from approximately 36 to 42 m w.d., as C sensu stricto.

- Mosaic of C and detritic bottom: towards the outer rim of the first terrace and along the entire rim of second and third terraces, large C banks are no longer visible. Nevertheless, ROV dives reveal the presence of discrete, small build-ups often associated with coarse sediments and sparse rhodoliths. Since backscatter signal is similar throughout the whole central part of the investigated area, we, therefore, mapped this area as a mosaic of C habitats and detritic bottom that extends from 42 up to 80 m w.d.. Anyways, small, isolated patches of slightly lower backscatter were recognised throughout this area; ROV videos confirmed in such areas C build-ups are more relevant in respect to the surroundings. Whenever possible, these patches were outlined using another symbology; they span a total area of 0.77 km^2.

- Mosaic of C and muddy bottom: ROV surveys over deeper regions revealed that topographic complexity, once again, corresponds to the presence of C habitats. Since the mobile substrate surrounding C outcrops is finer in respect to that found in shallower areas, we mapped this habitat, spanning 1.38 km^2 and extending up to

100 m w.d., as a mosaic of C habitats and muddy bottom. Although these habitats tend to be clustered together, it is often possible to easily discern single build-ups. For this reason, we no longer refer to these C outcrops as banks, but as single discrete build-ups (Bracchi et al., 2017). The sub-circular build-ups in this area have a mean diameter of approximately 20 m and reach heights of approximately 2 m. A total of 295 entities, with a mean area of approximately 365 m^2, were mapped with a different symbology within this habitat.

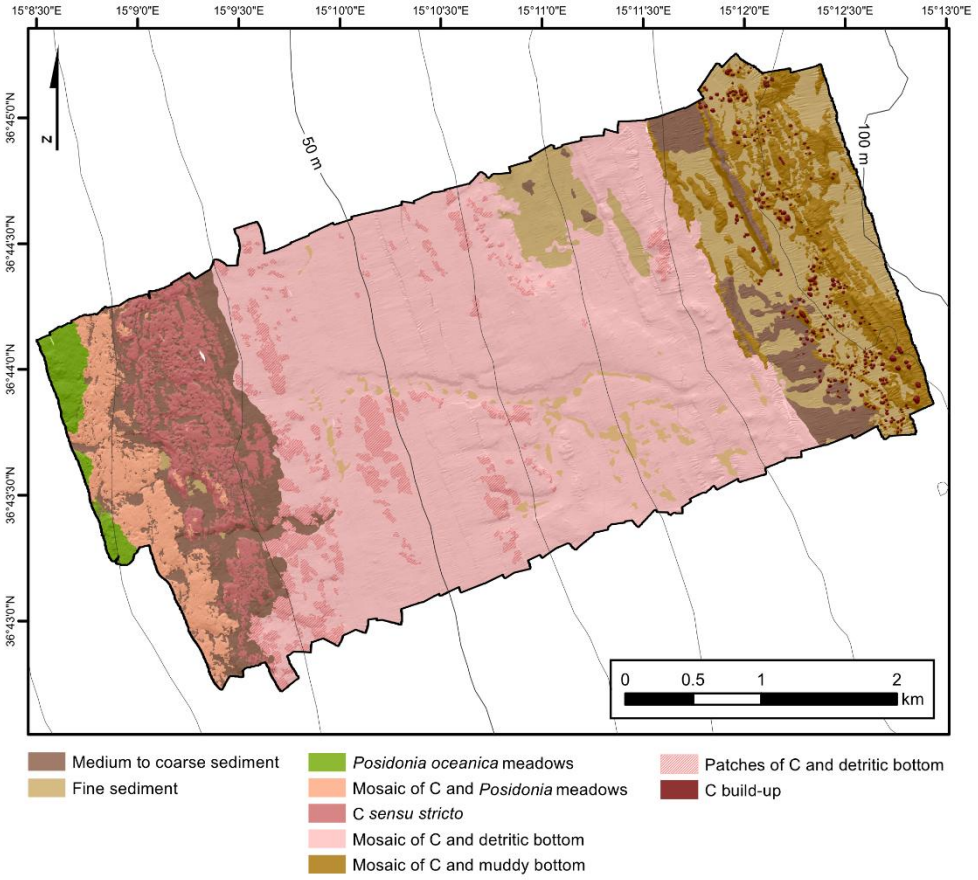

Figure 4. Habitat map of the study area. We identify five major habitats: Posidonia oceanica meadows, Mosaic of C and Posidonia meadows, C sensu stricto, Mosaic of C and detritic bottom, Mosaic of C, and muddy bottom. Whether possible, noticeable areas of C and detritic bottom have been delimited as Patches of C and detritic bottom. Likewise, we mapped recognisable isolated C build-ups in the deep region of the area as C build-up.

Discussion

Climate change and tectonic uplift are the dominant forcing mechanisms responsible for the formation of long and narrow terraced landforms in a variety of geomorphic settings. Marine terraces are largely used for reconstructing Quaternary glacial and interglacial climatic phases (Pirazzoli, 1993). With the exception of a few recent studies on the significance of submarine depositional terraces (see Chiocci & Orlando, 1996; Chiocci et al., 2004; De Pippo & Pennetta, 2004; Fraccascia et al., 2013; Pepe et al., 2014; Quartau et al., 2014; Casalbore et al., 2010, 2020), submerged terraced landforms have been poorly investigated (Prampolini et al., 2020), especially with regard to their possible erosive nature as wave-cut or abrasion platforms over outcropping bedrock on the shelf (Bilbao-Lasa et al., 2020; Savini et al., 2020). Throughout the Calabrian Arc region, marine terraces actually represent typical landforms well mapped on-land (Bianca et al., 1999; Catalano & De Guidi, 2003; Tortorici et al., 2003; Catalano et al., 2003, 2008) and associated with main interglacial marine isotope stages (MIS) for the Quaternary period. Based on the distribution for our bathymetric values, submerged terraces were determined to range from: (i) 35–44 m, (ii) 48–62 m, (iii) 70–80 m, and (iv) 86–98 m w.d.. Scarps distinctively mark their outer rims.

By correlating the depth range for such escarpments with the eustatic sea-level curve, some hypotheses can be formulated regarding driving processes and the time of formation. However, due to documented regional uplift (0.2 mm/yr – Distefano et al., 2021a), directly correlating a specific depth value with respect to lowstand periods or transgressive/regressive events is difficult. The scarp delimiting the deepest terrace (98–102 m) offshore actually demands an association with paleo-cliffs likely formed during lowstand periods (MIS 6?). A reasonable hypothesis is that shallower terraces likely formed between MIS 5 and MIS 2 as wave-cut shore platforms and were likely generated during lowstand periods or transgressive events that promoted erosion. However, further investigations are needed to exactly date their origin. C reefs within the surveyed area are associated with

different morphotypes (Bracchi et al., 2017), and their arrangement seems to be correlated with zonation imposed by mapped submerged marine terraces (Figure 4). These exposed, flat bedrock surfaces became available for C settlement and growth at the beginning of the most recent transgressive event (Flandrian) and were favoured by low sedimentation rates.

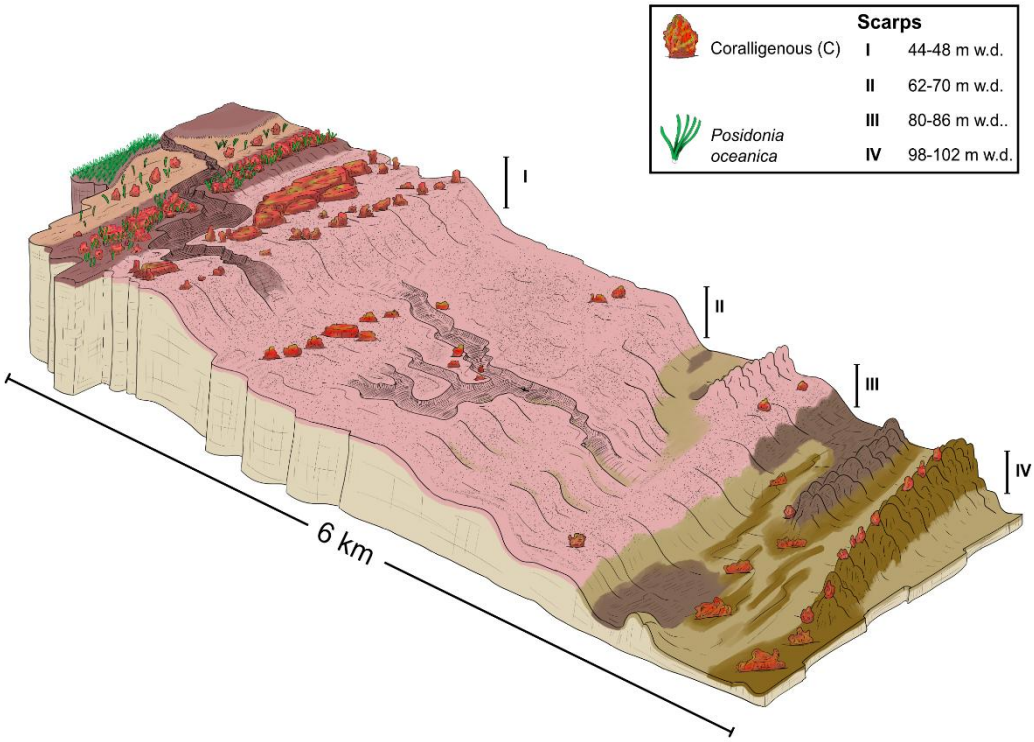

Figure 5. 3D schematic representation of the study area. The four main scarps have been indicated, with a reference to their height. C outcrops are spread all over the area, although as different morphotypes. C reefs result to be more abundant over the shallowest and deepest terraces

In agreement with Distefano et al. (2021a), Late Holocene and transgressive sedimentation seem to be concentrated over our two mid-terraces, where considerable C outcrops are not present. In contrast, our analysis indicates that the first and last terraces were likely the most suitable areas for reef development. ROV surveys revealed the presence of megaripples within the surrounding and intra-areas of shallow C bioconstructions, suggesting the presence of moderate currents and, thus, low sedimentation rates. The relationship between C outcrops and P. oceanica in defining the lower infralittoral limit within the area is of peculiar concern. In this sense, as the project progresses, further investigations are necessary and are currently being planned. Based on our analysis to date,

deep C build-ups appear to be quite different in their morphological expression, suggesting different environmental conditions during settling and growth.

The reefs we investigated, either shallow or deep, are hotspots of biodiversity. ROV videos revealed an abundance of life in association with C habitats, drawing attention to the need for protection and conservation actions. For example, deep C build-ups host anthozoa like *Dendrophyllia ramea* (Linneo, 1758) and Antipathella sp., which are both included in the IUCN Red List of Threatened Species at the Mediterranean level, as well as in other legal publications. Since we only performed a preliminary and qualitative analysis, the species recognised from ROV data only represent a snapshot of habitat richness. Given the level of detail in ROV data, we were not able to identify the genus or species of many organisms. Thus, some categories of species may be underestimated. For example, Porifera is known to be a major phyla associated with C habitats (Bertolino et al., 2013; Costa et al., 2019). However, given data quality, we were only able to identify two species.

A seismic-stratigraphic comparison of our data to data reported by Distefano et al. (2021a) suggests that channel-like landforms occupying the central portion of the surveyed area originated as a result of incisions in either Pleistocene or Pliocene carbonatic formations when the seafloor was under subaerial conditions. Due to configuration and, in particular, to small, infilled depressions along its track (relict pot-holes), we believe these formations correspond to a paleo rocky riverbed, which developed as a result of the bedrock karst condition. To better understand the geomorphological layout of the area and the correlation with C settling and distribution, further investigations are required.

Conclusions

Data collected within the CRESCIBLUREEF project allowed the realisation of a high-resolution, morpho-bathymetric map of the seafloor off Marzamemi. The Main Map (consultable in the original submission) was realized thanks to the interpretation of both bathymetry and backscatter data, together with ROV investigations, which led us to classify

the area into five habitats, as well as a geomorphological subdivision based on four distinct marine terraces. C habitats are recognisable throughout the entire surveyed area, and form more evident morphologies over the shallowest and deepest terraces. In particular, the shallow C habitat is in the form of banks, ranging from 30 to 42 m w.d.; deeper C is organised as single build-ups often clustered together, ranging from 86 to 92 m w.d.. Morphological complexity tends to decrease moving offshore. Morphology is highly related to the presence of C reefs, whose formation is likely correlated to late Quaternary lowstand periods or transgressive/regressive events coupled with the uplifting movements characteristic of this region.

The geomorphological map provides new information regarding extent and characteristics of a major Mediterranean habitat for which knowledge is limited.

Software

The processing of multibeam and backscatter data was done by using QPS Qimera and Fledermaus, respectively. Seismic data were visualised using Kingdom Software 2020. Final maps were produced by using ESRI ArcMap 10.8. Additional graphic operations were done using Affinity Designer. All software was licensed to the University of Milano-Bicocca.

Acknowledgment

This article is a contribution to the project 'CRESCIBLUREEF – Grown in the blue: new technologies for knowledge and conservation of Mediterranean reefs'. We would like to acknowledge the captain and crew of the survey vessel (M/B Valerio) of Arena Sub S.r.l..

Disclosure statement

No potential conflict of interest was reported by the author(s).

Funding

This work was funded by the Italian Ministry of Research and University – Fondo Integrativo Speciale per la Ricerca (FISR), project FISR2019_04543 CRESCIBLUREEF – Grown in the blue: new technologies for knowledge and conservation of Mediterranean reefs.

References

Antonioli, F., Dai Pra, G., Segre, A. G., & Sylos Labini, S. (2004). New data on Late Holocene uplift rates in the Messina Strait area, Italy. *Quaternaria Nova*, *8*, 45–67.

Balata, D., Piazzi, L., & Benedetti-Cecchi, L. (2007). Sediment disturbance and loss of beta diversity on subtidal rocky reefs. *Ecology*, *88*(10), 2455–2461. https://doi.org/10.1890/07-0053.1

Balata, D., Piazzi, L., Cecchi, E., & Cinelli, F. (2005). Variability of Mediterranean coralligenous assemblages subject to local variation in sediment deposition. *Marine Environmental Research*, *60*(4), 403–421. https://doi.org/10.1016/j.marenvres.2004.12.005

Ballesteros, E., Gibson, R. N., A Atkinson, R. J. A., Gordon, J. D. M., & Taylor, E. (2006). Mediterranean coralligenous assemblages: a synthesis of present knowledge. In *An Annual Review* (Vol. 44). Ballesteros, E. (2006). Mediterranean coralligenous assemblages: A synthesis of present knowledge. In *Oceanography and Marine Biology* (Vol. 44, pp. 123–195). https://doi.org/10.1201/9781420006391-7

Bertolino, M., Cerrano, C., Bavestrello, G., Carella, M., Pansini, M., & Calcinai, B. (2013). Diversity of Porifera in the Mediterranean coralligenous accretions, with description of a new species. *ZooKeys*, *336*, 1–37. https://doi.org/10.3897/zookeys.336.5139

Bianca, M., Monaco, C., Tortorici, L., & Cernobori, L. (1999). Quaternary normal faulting in southeastern Sicily (Italy): a seismic source for the 1693 large earthquake. In *Geophys. J. Int* (Vol. 139). https://academic.oup.com/gji/article/139/2/370/553202

Bilbao-Lasa, P., Jara-Muñoz, J., Pedoja, K., Álvarez, I., Aranburu, A., Iriarte, E., & Galparsoro, I. (2020). Submerged Marine Terraces Identification and an Approach for Numerical Modeling the Sequence Formation in the Bay of Biscay (Northeastern Iberian Peninsula). Frontiers in Earth Science, 8. https://doi.org/10.3389/feart.2020.00047

Bosence, D. W. J. (1985). The "Coralligène" of the Mediterranean — a Recent Analog for Tertiary Coralline Algal Limestones. In *Paleoalgology* (pp. 216–225). Springer Berlin Heidelberg. https://doi.org/10.1007/978-3-642-70355-3_16

Boudouresque, C. F., Blanfuné, A., Harmelin-Vivien, M., Personnic, S., Ruitton, S., Thibaut, T., & Verlaque, M. (2016). Where Seaweed Forests Meet Animal Forests: the Examples of Macroalgae in Coral Reefs and the Mediterranean Coralligenous Ecosystem. In *Marine Animal Forests* (pp. 1–28). Springer International Publishing. https://doi.org/10.1007/978-3-319-17001-5_48-1

Bracchi V., Savini A., Marchese F., Palamara S., Basso D., Corselli C., (2015). Coralligenous habitat in the Mediterranean Sea: a geomorphological description from remote data. Ital. J. Geosci. (Boll. Soc. Geol. It.). DOI: 10.3301/IJG.2014.16.

Bracchi, V. A., Basso, D., Marchese, F., Corselli, C., & Savini, A. (2017). Coralligenous morphotypes on subhorizontal substrate: A new categorization. *Continental Shelf Research*, *144*, 10–20. https://doi.org/10.1016/j.csr.2017.06.005

Bracchi, V. A., Bazzicalupo, P., Fallati, L., Varzi, A. G., Savini, A., Negri, M. pietro, Rosso, A., Sanfilippo, R., Guido, A., Bertolino, M., Costa, G., de Ponti, E., Leonardi, R., Muzzupappa, M., & Basso, D. (2022). The Main Builders of Mediterranean Coralligenous: 2D and 3D Quantitative Approaches for its Identification. *Frontiers in Earth Science*, *10*. https://doi.org/10.3389/feart.2022.910522

Casalbore, D., Falese, F., Martorelli, E., Romagnoli, C., & Chiocci, F. L. (2020). Submarine depositional terraces in the Tyrrhenian Sea as a proxy for paleo-sea level reconstruction: Problems and perspective. *Quaternary International*, *544*, 1–11. https://doi.org/10.1016/J.QUAINT.2016.07.051

Casalbore, D., Romagnoli, C., Chiocci, F., & Frezza, V. (2010). Morpho-sedimentary characteristics of the volcaniclastic apron around Stromboli volcano (Italy). *Marine Geology*, *269*(3–4), 132–148. https://doi.org/10.1016/j.margeo.2010.01.004

Catalano, S., De Guidi, G., Monaco, C., Tortorici, G., & Tortorici, L. (2008). Active faulting and seismicity along the Siculo-Calabrian Rift Zone (Southern Italy). *Tectonophysics*, *453*(1–4), 177–192. https://doi.org/10.1016/j.tecto.2007.05.008

Catalano, S., & De Guidi, G. (2003). Late Quaternary uplift of northeastern Sicily: relation with the active normal faulting deformation. *Journal of Geodynamics*, *36*(4), 445–467. https://doi.org/10.1016/S0264-3707(02)00035-2

Catalano, S., De Guidi, G., Monaco, C., Tortorici, G., & Tortorici, L. (2003). Long-term behaviour of the late Quaternary normal faults in the Straits of Messina area (Calabrian arc): structural and morphological constraints. *Quaternary International*, *101–102*(1), 81–91. https://doi.org/10.1016/S1040-6182(02)00091-5

Chiocci, F. L., D'Angelo, S., & Romagnoli, C. (2004). Atlas of submerged depositional terraces along the Italian coasts. *Memorie Descrittive Della Carta Geologica d'Italia*, *58*.

Chiocci, F. L., & Orlando, L. (1996). Lowstand terraces on Tyrrhenian Sea steep continental slopes. *Marine Geology*, *134*(1–2), 127–143. https://doi.org/10.1016/0025-3227(96)00023-0

Costa, G., Bavestrello, G., Micaroni, V., Pansini, M., Strano, F., & Bertolino, M. (2019). Sponge community variation along the Apulian coasts (Otranto Strait) over a pluri-decennial time span. Does water warming drive a sponge diversity increasing in the Mediterranean Sea? Journal of the Marine Biological Association of the United Kingdom, 99(7), 1519–1534. https://doi.org/10.1017/S0025315419000651

Costanzo, L. G., Marletta, G., & Alongi, G. (2021). Ecological status of coralligenous macroalgal assemblages in the marine protected area (Mpa) isole ciclopi (ionian sea). *Plants*, *10*(2), 1–15. https://doi.org/10.3390/plants10020329

De Falco, G., Conforti, A., Brambilla, W., Budillon, F., Ceccherelli, G., De Luca, M., Di Martino, G., Guala, I., Innangi, S., Pascucci, V., Piazzi, L., Pireddu, L., Santonastaso, A., Tonielli, R., & Simeone, S. (2022). Coralligenous banks along the western and northern continental shelf of Sardinia Island (Mediterranean Sea). *Journal of Maps*.
https://doi.org/10.1080/17445647.2021.2020179/SUPPL_FILE/TJOM_A_2020179_SM3526.PDF

De Guidi, G., Catalano, S., Monaco, C., & Tortorici, L. (2003). Morphological evidence of Holocene coseismic deformation in the Taormina region (NE Sicily). *Journal of Geodynamics*, *36*(1–2), 193–211. https://doi.org/10.1016/S0264-3707(03)00047-4

De Pippo, T., & Pennetta, M. (2004). Submerged depositional terraces in the Gulf of Policastro (Southern Tyrrhenian sea, Italy). *Memorie Descrittive Della Carta Geologica d'Italia*, *58*, 35–38.

Di Geronimo, I., Di Geronimo, R., Improta, S., Rosso, A., & Sanfilippo, R. (2001). Preliminary observations on a columnar coralline build-up from off SE Sicily. *Biologia Marina Mediterranea*, *8*(1), 229–237.

Di Geronimo, I., Di Geronimo, R., Rosso, A., & Sanfilippo, R. (2002). Structural and taphonomic analysis of a columnar coralline algal build-up from SE Sicily. *Geobios*, *35*(SUPPLEMENT), 86–95. https://doi.org/10.1016/S0016-6995(02)00050-5

Distefano, S., Gamberi, F., Baldassini, N., & Di Stefano, A. (2021a). Quaternary evolution of coastal plain in response to sea-level changes: Example from south-east sicily (southern italy). *Water*, *13*(11). https://doi.org/10.3390/w13111524

Distefano, S., Gamberi, F., Borzì, L., & Di Stefano, A. (2021b). Quaternary coastal landscape evolution and sea-level rise: An example from south-east sicily. *Geosciences (Switzerland)*, *11*(12). https://doi.org/10.3390/geosciences11120506

Ferranti, L., Monaco, C., Antonioli, F., Maschio, L., Kershaw, S., & Verrubbi, V. (2007). The contribution of regional uplift and coseismic slip to the vertical crustal motion in the Messina Straits, southern Italy: Evidence from raised Late Holocene shorelines. *Journal of Geophysical Research*, *112*(B6), B06401. https://doi.org/10.1029/2006JB004473

Firth, C., Stewart, I., McGuire, W. J., Kershaw, S., & Vita-Finzi, C. (1996). Coastal elevation changes in eastern Sicily: implications for volcano instability at Mount Etna. *Geological Society, London, Special Publications*, *110*(1), 153–167. https://doi.org/10.1144/GSL.SP.1996.110.01.12

Fraccascia, S., Chiocci, F. L., Scrocca, D., & Falese, F. (2013). Very high-resolution seismic stratigraphy of Pleistocene eustatic minima markers as a tool to reconstruct the tectonic evolution of the northern Latium shelf (Tyrrhenian Sea, Italy). *Geology*, *41*(3), 375–378. https://doi.org/10.1130/G33868.1

Gafeira, J., Dolan, M. F. J., & Monteys, X. (2018). Geomorphometric Characterization of Pockmarks by Using a GIS-Based Semi-Automated Toolbox. *Geosciences*, *8*(5), 154. https://doi.org/10.3390/geosciences8050154

Garrabou, J., & Ballesteros, E. (2000). Growth of mesophyllum alternans and lithophyllum frondosum (corallinales, rhodophyta) in the northwestern mediterranean. *European Journal of Phycology*, *35*(1). https://doi.org/10.1080/09670260010001735571

Gracia, F. J., & Gutiérrez, M. (2002). Origin and evolution of Gallocanta polje. *Zeistchrift Für Geomorphologie*, *46*, 245–262.

Grasso, M., & Lentini, F. (1982). Sedimentary and tectonic evolution of the eastern Hyblean Plateau (southeastern Sicily) during late Cretaceous to Quaternary time. *Palaeogeography, Palaeoclimatology, Palaeoecology*, *39*(3–4), 261–280. https://doi.org/10.1016/0031-0182(82)90025-6

Grasso, M., & Pedley, H. M. (1990). Neogene and Quaternary sedimentation patterns in the northwestern Hyblean Plateau (SE Sicily): the effects of a collisional process on a foreland margin. *Rivista Italiana Di Paleontologia e Stratigrafia*, *96*(2–3), 219–240.

Grasso, M., Reuther, C. D., & Tortorici, L. (1992). Neotectonic deformations in SE Sicily: The Ispica fault, evidence of late miocene-pleistocene decoupled wrenching within the central mediterranean stress regime. *Journal of Geodynamics*, *16*(1–2), 135–146. https://doi.org/10.1016/0264-3707(92)90023-L

Ingrosso, G., Abbiati, M., Badalamenti, F., Bavestrello, G., Belmonte, G., Cannas, R., Benedetti-Cecchi, L., Bertolino, M., Bevilacqua, S., Bianchi, C. N., Bo, M., Boscari, E., Cardone, F., Cattaneo-Vietti, R., Cau, A., Cerrano, C., Chemello, R., Chimienti, G., Congiu, L., … Boero, F. (2018). Mediterranean Bioconstructions Along the Italian Coast. In *Advances in Marine Biology* (Vol. 79, pp. 61–136). https://doi.org/10.1016/bs.amb.2018.05.001

Lambeck, K., Antonioli, F., Anzidei, M., Ferranti, L., Leoni, G., Scicchitano, G., & Silenzi, S. (2010). Sea level change along the Italian coast during the Holocene and projections for the future. *Quaternary International*, *232*(1–2), 250–257. https://doi.org/10.1016/j.quaint.2010.04.026

Lentini, F., & Carbone, S. (2014). Geologia della Sicilia-geology of Sicily. *Memorie Descr. Carta Geologica d'Italia*, *95*(7–414).

Lentini, F., Carbone, S., & Catalano, S. (1994). Main structural domains of the central Mediterranean region and their Neogene tectonic evolution. *Bollettino Di Geofisica Teorica Ed Applicata*, *36*(141–44), 103–125.

Lo Iacono C, Savini A, Basso D (2018). Cold-Water Carbonate Bioconstructions. In: Micallef A., Krastel S., Savini A, Submarine Geomorphology. p. 425-455, Springer, ISBN: 978-3-319-57851-4, doi: 10.1007/978-3-319-57852-1_22.

Marchese F., Bracchi V.A., Lisi G., Basso D., Corselli C. & Savini A. (2020). Assessing Fine-Scale Distribution and Volume of Mediterranean Algal Reefs through Terrain Analysis of Multibeam Bathymetric Data. A Case Study in the Southern Adriatic Continental Shelf. Water 12(1):157 DOI:10.3390/w12010157

Martin, C. S., Giannoulaki, M., De Leo, F., Scardi, M., Salomidi, M., Knittweis, L., Pace, M. L., Garofalo, G., Gristina, M., Ballesteros, E., Bavestrello, G., Belluscio, A., Cebrian, E., Gerakaris, V., Pergent, G., Pergent-Martini, C., Schembri, P. J., Terribile, K., Rizzo, L., … Fraschetti, S. (2014). Coralligenous and maërl habitats: predictive modelling to identify their spatial distributions across the Mediterranean Sea. *Scientific Reports*, *4*(1), 5073. https://doi.org/10.1038/srep05073

Pavano, F., Romagnoli, G., Tortorici, G., & Catalano, S. (2019). Morphometric evidences of recent tectonic deformation along the southeastern margin of the Hyblean Plateau (SE-Sicily, Italy). *Geomorphology*, *342*, 1–19. https://doi.org/10.1016/j.geomorph.2019.06.006

Pepe, F., Bertotti, G., Ferranti, L., Sacchi, M., Collura, A. M., Passaro, S., & Sulli, A. (2014). Pattern and rate of post-20 ka vertical tectonic motion around the Capo Vaticano Promontory (W Calabria, Italy) based on offshore geomorphological indicators. *Quaternary International*, *332*, 85–98. https://doi.org/10.1016/j.quaint.2013.11.012

Peres, J. M. (1982). Major benthic assemblages. *Mar. Ecol.*, *5*.

Piazzi, L., Balata, D., & Cinelli, F. (2007). Invasions of alien macroalgae in Mediterranean coralligenous assemblages. *Cryptogamie, Algologie*, *28*(3), 289–301.

Piazzi, L., Gennaro, P., & Balata, D. (2011). Effects of nutrient enrichment on macroalgal coralligenous assemblages. *Marine Pollution Bulletin*, *62*(8), 1830–1835. https://doi.org/10.1016/j.marpolbul.2011.05.004

Pirazzoli, P. A. (1993). Global sea-level changes and their measurement. Global and Planetary Change, 8(3), 135–148. https://doi.org/10.1016/0921-8181(93)90021-F

Prampolini M. Savini A., Foglini F., Soldati M. (2020) Seven Good Reasons for Integrating Terrestrial and Marine Spatial Datasets in Changing Environments. Water 2020, 12, 2221

Quartau, R., Hipólito, A., Romagnoli, C., Casalbore, D., Madeira, J., Tempera, F., Roque, C., & Chiocci, F. L. (2014). The morphology of insular shelves as a key for understanding the geological evolution of volcanic islands: Insights from Terceira Island (Azores). *Geochemistry, Geophysics, Geosystems*, *15*(5), 1801–1826. https://doi.org/10.1002/2014GC005248

Riding, R. (2002). Structure and composition of organic reefs and carbonate mud mounds: concepts and categories. *Earth-Science Reviews*, *58*(1–2), 163–231. https://doi.org/10.1016/S0012-8252(01)00089-7

Rosso, A., & Sanfilippo, R. (2009). The contribution of Bryozoans y and Serpuloideans p to coralligenous concretions from SE Sicily. *First Mediterranean Symposium on the Coralligenous and Other Calcareous Bioconcretions of the Mediterranean Sea*, 1–36. https://www.researchgate.net/publication/310258686

Sartoretto, S. (1994). Structure Et Dynamique D'Un Nouveau Type De Bioconstruction a Mesophyllum Lichenoides (Ellis) Lemoine (Corallinales, Rhodophyta). *Comptes Rendus de l'Academie Des Sciences - Serie III*, *317*(2), 156–160.

Sartoretto, S., & Francour, P. (1997). Quantification of bioerosion by sphaerechinus granularis on "coralligene" concretions of the western Mediterranean. *Journal of the Marine Biological Association of the United Kingdom*, *77*(2), 565–568. https://doi.org/10.1017/s0025315400071885

Savini, A., Bracchi, V. A., Cammarosano, A., Pennetta, M., & Russo, F. (2020). Terraced Landforms Onshore and Offshore the Cilento Promontory (South-Eastern Tyrrhenian Margin) and Their Significance as Quaternary Records of Sea Level Changes. *Water*, *13*. https://doi.org/10.3390/w

Shackleton, N. J. (1987). Oxygen isotopes, ice volume and sea level. In *Quaternary Science Reviews* (Vol. 6, Issues 3–4). https://doi.org/10.1016/0277-3791(87)90003-5

Stewart, I. S., Cundy, A., Kershaw, S., & Firth, C. (1997). Holocene coastal uplift in the Taormina area, northeastern sicily: Implications for the southern prolongation of the calabrian seismogenic belt. *Journal of Geodynamics*, *24*(1–4), 37–50. https://doi.org/10.1016/S0264-3707(97)00012-4

Tortorici, G., Bianca, M., De Guidi, G., Monaco, C., & Tortorici, L. (2003). Fault activity and marine terracing in the Capo Vaticano area (southern Calabria) during the Middle-Late Quaternary. *Quaternary International*, *101–102*(1), 269–278. https://doi.org/10.1016/S1040-6182(02)00107-6

Tortorici, L., Monaco, C., Tansi, C., & Cocina, O. (1995). Recent and active tectonics in the Calabrian arc (Southern Italy). *Tectonophysics*, *243*(1–2), 37–55. https://doi.org/10.1016/0040-1951(94)00190-K

Violanti V., Di Geronimo, I., & Saccà, R. (1990). Foraminiferal thanatocoenoses from the Gulf of Noto (Southeastern Sicily). Boll. Mus. Reg. Sci. Nat. Torino, Special Volume, 773–799.

Waelbroeck, C., Labeyrie, L., Michel, E., Duplessy, J. C., McManus, J. F., Lambeck, K., Balbon, E., & Labracherie, M. (2002). Sea-level and deep water temperature changes derived from benthic foraminifera isotopic records. *Quaternary Science Reviews*, *21*(1–3), 295–305. https://doi.org/10.1016/S0277-3791(01)00101-9

Westaway, R. (1993). Quaternary uplift of southern Italy. *Journal of Geophysical Research: Solid Earth*, *98*(B12), 21741–21772. https://doi.org/10.1029/93JB01566

b) New chronology for submerged relict paleoshorelines and associated rates of crustal vertical movements offshore the Marzamemi village, Sicily (Southern Italy)

This work is published as:

Varzi, A. G., Meschis, M., Fallati, L., Scicchitano, G., de Santis, V., Scardino, G., Basso, D., Bracchi, V. A., & Savini, A. (2024). New chronology for submerged relict paleoshorelines and associated rates of crustal vertical movements offshore the Marzamemi village, Sicily (Southern Italy). *Marine Geology*, *474*, 107326. https://doi.org/10.1016/J.MARGEO.2024.107326

Abstract

We investigated the Late Pleistocene-Holocene crustal vertical movements off the coast of Marzamemi village in SE Sicily, Italy. By using a Synchronous Correlation Approach (SCA), we analysed terraced landforms that characterize a submerged sector within one of Southern Italy's most seismically active regions. In this area, the emerging portion of the NE-SW oriented bulge of the African foreland structurally shapes the coastal and marine regions off Marzamemi village.

Based on a newly created 17 km^2 high-resolution bathymetric map generated from a Multibeam Echosounder (MBES) survey conducted in June 2021, we identified and examined four main paleo-shorelines identifying four submerged terraces. Terraced landforms play a crucial role in reconstructing Quaternary glacial and interglacial stages, offering insights into associated sea level fluctuations. Through the application of the SCA, our goal is to refine the chronology of these recently mapped and submerged marine terraces off the Marzamemi village, thereby contributing to the calculation of associated rates of crustal vertical movements. We demonstrate that these rates persist constantly throughout the Late Pleistocene-Holocene epoch, suggesting overall tectonic stability, with a slight and likely local fault-related subsidence. We explore a few chronology scenarios, raising questions about whether these submerged marine terraces are indeed recording the Late Pleistocene-Holocene limit or not. This research contributes to a better understanding of the geological dynamics in this region and sheds light on the potential factors influencing coastal landscape development over time.

Introduction

Terraced landforms are characterized by relatively flat surfaces bordered on both sides by steeper descending and ascending slopes (Anderson, 1999; Armijo et al., 1996; International Hydrographic Organization (IHO, 2008). Along coastal regions, these

features are used as crucial geomorphic indicators for reconstructing past sea level positions and estimating vertical deformation rates at both local and regional scales (e.g. Armijo, et al., 1996; Saillard et al., 2009; Jara-Muñoz and Melnick, 2015; Jara-Muñoz et al., 2017; Pedoja et al., 2018; Cerrone et al., 2021; De Santis et al., 2021, 2023; Robertson et al., 2023). Nevertheless, research on submerged terraces is less accessible than on land and has been inhibited primarily due to the (i) absence of high-resolution bathymetric data and (ii) challenges associated with direct measurements and sediment/rock sampling for absolute dating (Prampolini et al., 2020; Soldati et al., 2021). Terraced landforms currently situated beneath the sea surface may result from either depositional or erosional processes. Submarine Depositional Terraces (SDT) show a clinostratified internal structure with prograding growth towards the sea (Chiocci and Orlando, 1996). On the other hand, the erosive nature of submerged terraced landforms, likely formed on bedrock outcropping on the shelf, together with their correlation to former sea level positions and vertical movements, has received less attention (Bilbao-Lasa et al., 2020; Savini et al., 2013, 2021). To support our comprehension of the origin and geomorphological significance of submerged terraced landforms, we additionally correlate them with available regional information from onshore terraces in the absence of precise dating on key samples. This correlation is useful for interpreting their chronology.

Recent studies by Distefano et al. (2021a and b) and Varzi et al. (2023) have suggested the presence of potential marine terraces and paleoshorelines in the area offshore Marzamemi village, SE Sicily (Italy). This speculation is supported by the presence of coralligenous outcrops (Di Geronimo et al., 2002; Varzi et al., 2023), such as banks and discrete columns, which typically occur over flat surfaces controlled by suitable growth conditions (Ballesteros, 2006; Bracchi et al., 2015, 2017; Marchese et al., 2020), in addition to sediment starvation (Basso, 1998; Lo Iacono et al., 2018, Distefano et al., 2021a,b). Furthermore, constant uplift rates over the Late Quaternary have been estimated by investigating a sequence of raised marine terraces preserved onshore along the coastline from Augusta and Siracusa towns, a few tens kilometres north with respect to the

Marzamemi region (Bianca et al., 1999; Dutton et al., 2009; Meschis et al., 2020). Yet, the research and study for submerged sequences in the offshore of SE Sicily (Distefano et al., 2021b; Varzi et al., 2023) remains poorly constrained, leaving a gap of knowledge on the variety of processes that contribute to coastal landscape development driven by Late Pleistocene-Holocene sea level oscillations and the associated rates of crustal vertical movements. In this context, we propose to investigate the newly mapped offshore marine terraces by (i) correlating them with the preserved onshore sequence, considering the lack of datable sampling material, and (ii) refining their chronology to facilitate the calculation of associated rates of crustal vertical movements. This approach attempts to refine the geomorphological significance of submerged marine terraces, with the combination of terrestrial and marine geospatial dataset (Prampolini et al., 2020). Finally, our results are discussed within the regional tectonic context of the investigated area and the potential influence of the faulting activity by the active faults controlling the landscape.

Background

Geodynamic setting

The study area, situated offshore Marzamemi village in SE Sicily (Italy), is encompassed by the geodynamic province of the Hyblean Plateau (HP). This region is controlled by a quasi N-S oriented Neogene to Quaternary tectonic convergence between the African and Eurasian continental margins (e.g. Dewey et al., 1989; Faccenna et al., 2011). The Sicilian-Maghrebian chain has emerged as a consequence of the progressive and still ongoing tectonic collision, tectonically linked to the Apennines through the arc-shaped Calabrian-Peloritani forearc (Fig. 1a) (e.g. Malinverno and Ryan, 1986; Mattia et al, 2012; Palano et al., 2012; Meschis et al., 2020). The HP, forming part of the broad foreland domain of the Pelagian Block (e.g. Ben-Avraham and Grasso, 1991; Nicolich et al, 2000), boasts of a 25–30 km thick continental crust (e.g. Grasso and Lentini, 1982; Ben-Avraham and Grasso, 1991; Cultrera et al, 2015), and it is identified as a carbonate promontory of

the larger African paleomargin (Grasso and Lentini, 1982). Seismic investigations and geological assessments of the HP revealed a Meso-Cenozoic sedimentary carbonate succession, approximately 6 km thick, interwoven with volcanic layers and positioned atop the Paleozoic Basement. Additionally, Quaternary marine deposits, often associated with uplifted marine terraces, frequently overlay this carbonate succession (Lentini et al., 1987; Bianca et al., 1999; Meschis et al., 2020). Heading eastward, the transition from continental to oceanic crust is identified by the Malta Escarpment (Fig. 1), a Mesozoic passive margin potentially reactivated by oblique extension during the Quaternary (Bianca et al., 1999; Meschis et al., 2020).

Tectonic setting

Eastern Sicily, coupled with the Calabrian Arc region, stands as one of the Mediterranean's most dynamically active zones, marked by historical earthquakes surpassing magnitude 7 (Rovida et al., 2020). The region is influenced by multiple ongoing tectonic regimes, such as a (i) NNW-SSE oriented tectonic convergence with a geodetically measured rate of 10 mm/yr, accommodating around 50% of the total movement (Mattia et al., 2012; Palano et al., 2012), and a (ii) NW-SE oriented crustal extension at a rate of 2–3 mm/yr (Jacques et al., 2001; Serpelloni et al., 2005, 2010; Aloisi et al., 2013; Barreca et al., 2021; Meschis et al., 2022a, 2022b).

The offshore of Marzamemi area lies within the tectonically subsiding hanging wall of the "Avola Fault," associated with significant seismic activity, including the "Val di Noto" seismic sequence, one of the most the impactful reported in the Italian Earthquake Catalogue in 1693 (M 7.4) (Bianca et al., 1999; Monaco and Tortorici, 2000; Pavano et al., 2019; Rovida et al., 2020). This event is thought to have been triggered by an offshore N-S oriented normal fault (over 50 km long) (e.g. Azzaro and Barbano, 2000; Gambino et al., 2021; Scardino et al., 2022; Scicchitano et al., 2022), with an associated damaging tsunami (Piatanesi and Tinti, 1998; Scicchitano et al., 2022), highlighting the significance of active

fault systems in shaping seafloor geomorphic changes throughout the Quaternary (Bianca et al., 1999; Argnani and Bonazzi, 2005; Gross et al., 2016).

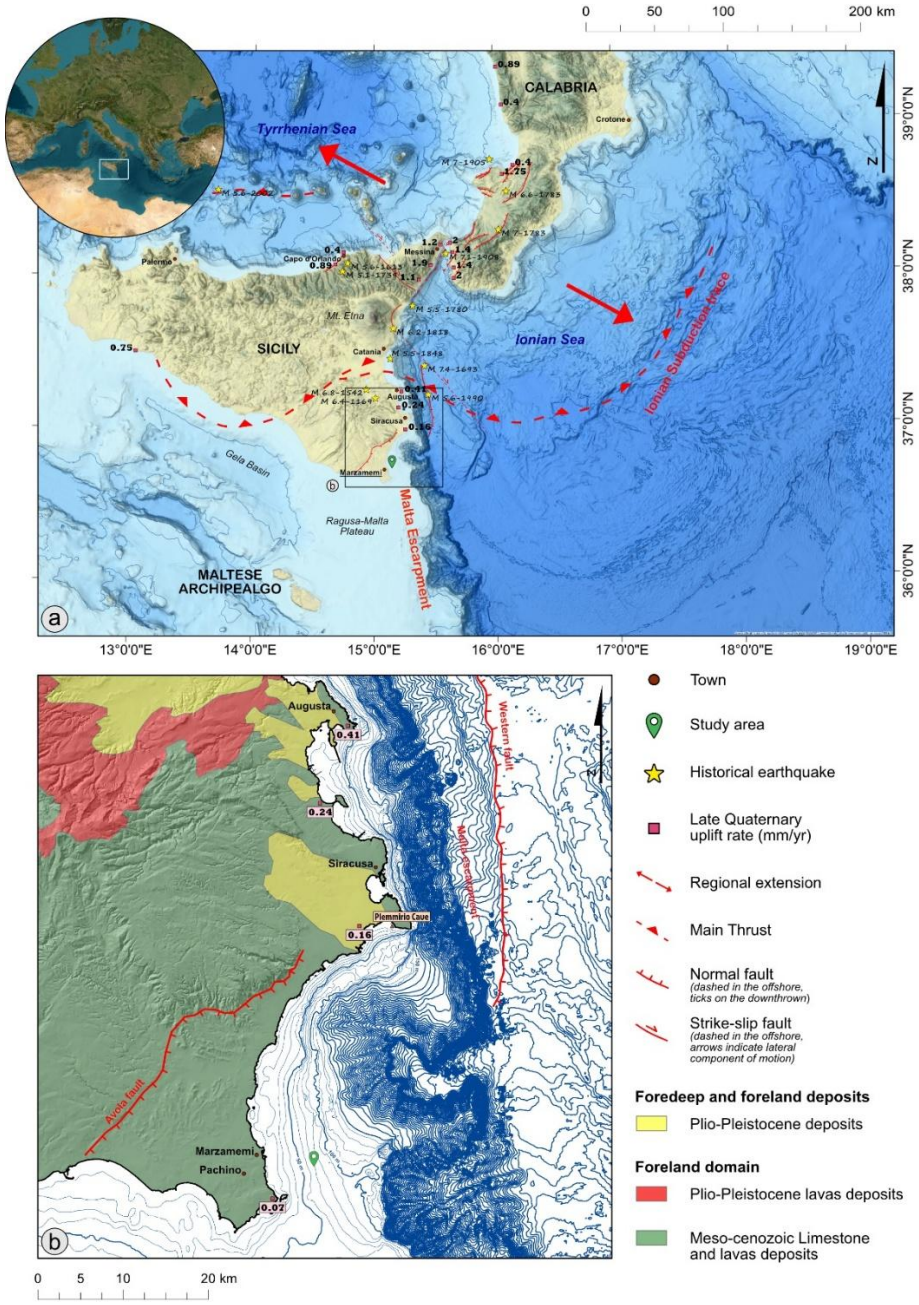

Figure 6. (a) Simplified tectonic map of Sicily and Southern Calabria. Red lines represent tectonic faults/lineaments from several previous investigations (e.g. Jacques et al., 2001; Gambino et al., 2021; Meschis et al., 2018, 2020; Roberts et al., 2013). Red arrows show the direction of regional extension derived by GPS investigations (Serpelloni et al., 2005). Yellow stars show historical seismic events (Rovida et al., 2020). Fuchsia squares indicate values of Late Quaternary uplift rates from several investigations (e.g. Ferranti et al., 2021; Meschis et al., 2018, 2020, 2022a, 2022b). Background basemap (GEBCO_2022) derived from the General Bathymetric Chart of the Oceans; isobath at 500 m interval. (b) Focus on SE Sicily showing the main geological deposits characterising the onshore (Lentini et al., 1995), and the location of the offshore study area. Red lines delineate the Avola normal fault (Pavano et al., 2019) and the Western fault (Gambino et al., 2021; Scicchitano et al., 2022).

Quaternary uplift processes

Worldwide, there is a widely acknowledged understanding that the interplay of crustal tectonic uplift and Quaternary sea level changes results in uplifted marine terraces carved in the coastal topography. This occurs when the rate of sea level rise during highstands (warm period) is outpaced by crustal uplift rates (Lajoie, 1986). In SE Sicily, this interaction has led to a significant series of preserved marine terraces, predominantly outcropping in the eastern part of the HP, associated with

Marine Isotope Stages (MIS) over the Middle-Late Pleistocene (around the last half a million years) (Bianca et al., 1999; Monaco et al., 2002; Meschis et al., 2020). Their studies have highlighted spatially varying uplift rates in the region, likely influenced by deep-seated subcrustal processes. Uplift rates gradually decrease from N (0.41 mm/yr near Augusta town) to S (0.16 mm/yr near Siracusa town) (Fig. 1b) (Meschis et al., 2020), showing almost tectonic stability.

Our study area is located a few tens of kilometres S of Siracusa, where a paleoshoreline was found within submerged caves at −20 m below the present sea level (Scicchitano and Monaco, 2006). Absolute dating methods, including 234U/230Th on calcite speleothems formed during lowstand periods and 14C dating of layers of calcitic serpulids encrusting the speleothems when caves were later flooded (Dutton et al., 2009), confirmed its belonging to MIS 5a (76.5 ka) (Table 1).

Table 1. Age constraint used for our synchronous correlation technique resulting from a submerged paleoshoreline available in literature

Reference	Dating Method	Dated sample description	Assigned Highstand (ka)	Paleoshoreline Elevations (m w.d.)
Dutton et al. 2009	U/Th	*"Three specimens of stalagmite."*	76.5 (MIS 5a)	-20

Methods

MBES data acquisition

Bathymetric data off the coast of Marzamemi were collected as part of the CRESCIBLUREEF project (FISR_04543) in June 2021, as detailed in Varzi et al. (2023). The data acquisition utilized a pole-mounted R2Sonic 2022 Multibeam Echosounder system (MBES) operating at 400 kHz. This advanced system transmitted a total of 1024 acoustic beams in a 150° fan configuration. The data acquisition was conducted using the QPS Qinsy software, maintaining an operational speed of 5 knots along closely spaced lines to ensure comprehensive coverage (at least 20% overlap). This methodology allowed for a complete mapping of approximately 17 km^2 of the continental shelf, spanning a water depth (w.d.) from approximately 15 to 100 m (Fig. 2b). To ensure data accuracy and quality, MBES data underwent thorough cleaning and filtering procedures using QPS Qimera software, culminating in the generation of a Digital Terrain Model (DTM) at a 3 m resolution. This bathymetric dataset provides a detailed and reliable representation of the underwater topography in the specified area, providing valuable insights for subsequent geomorphological analyses.

Mapping GIS-based submerged marine terraces

Geospatial data analyses were conducted using ESRI® ArcGIS software on the generated DTM (Fig. 2) to identify the presence of an offshore terraced sequence. The analysis primarily focused on detecting fault-like scarps (e.g.: edge of structural scarps in Varzi et al., 2023 – Fig. 3) used as reference points, to be used in conjunction with the slope gradient map. The bathymetric histogram, showing the distribution of depth values over distance, played a crucial role in pinpointing significant depths characterized by a higher abundance of pixels. This approach facilitated the identification of larger areas at the same depth, possibly indicative of terraced landforms. In this context, the depth at which this increase in pixel abundance occurred served as the reference for a paleoshoreline.

Additionally, ten bathymetric transects, oriented from SW to NE (Fig. 3), were extracted, each spanning approximately 6 km and spaced at intervals of about 250 m. This strategic arrangement allowed for a detailed examination of the lateral continuity of detected fault-like scarps and an assessment of the general bathymetric trend across the entire study area. The integration of these findings enabled us to (i) validate previously mapped escarpments outlined in Varzi et al. (2023) and (ii) make any necessary adjustments or dismissals based on the observed geospatial information.

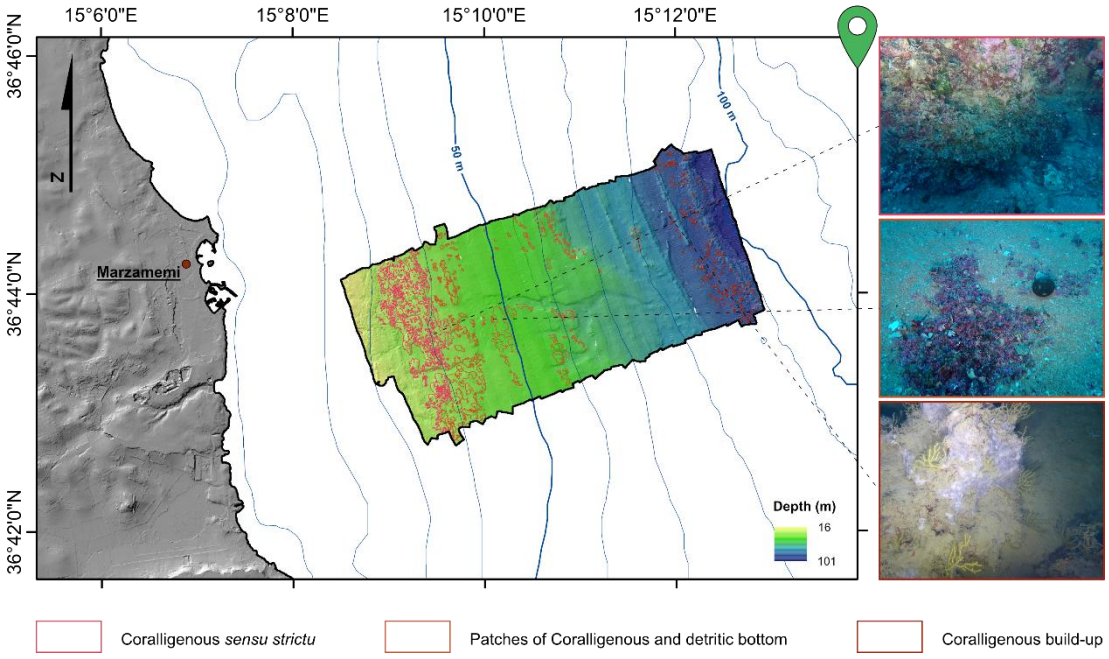

Figure 2. DTM of the study area offshore Marzamemi village (SE Sicily), resulted from the Multibeam Echosounder (MBES) survey performed during the first campaign of the CRESCIBLUREEF project in June 2021, together with the coralligenous habitat classified in Varzi et al. (2023) - ground-truth images of each one are visible on the right, extrapolated from the ROV surveys performed during the above mentioned campaign. Minor isobath at 10 m interval; major isobath at 50 m interval.

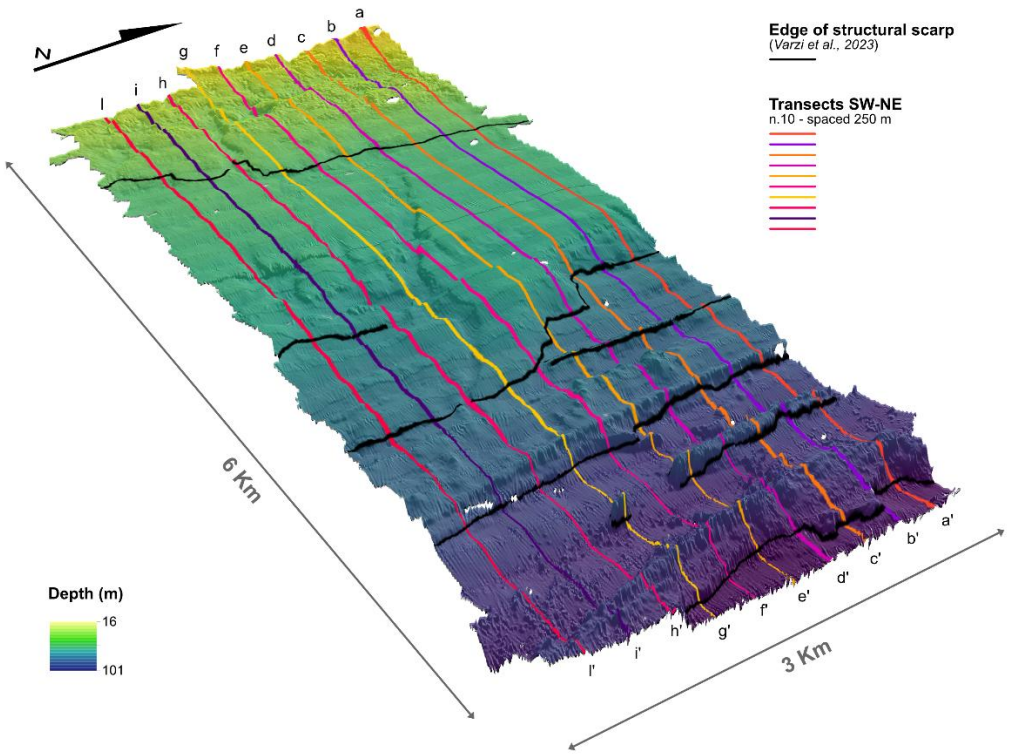

Figure 3. 3D visualisation DTM of the study area. Bathymetry ranges between 16 and 101 m of water depth (w.d.). Black lines delineate fault-like scarps mapped in Varzi et al. (2023). Colourful lines show the position of the n.10 SW-NE bathymetric transects.

Synchronous Correlation Approach (SCA)

The Synchronous Correlation Approach (SCA) is based on the idea that glacio-eustatic sea level highstands over the Quaternary are not evenly-spaced in time (Houghton et al., 2003; Roberts et al., 2009, 2013; Pedoja et al., 2018; Meschis et al., 2018, 2020, 2022a,b; Robertson et al., 2019, 2023; De Santis et al., 2021, 2023). This implies that the resulting raised paleoshorelines will not exhibit uniform elevations, given a constant through time uplift rate scenario (e.g. Roberts et al., 2013; Roberts et al., 2009; Robertson et al., 2023; Robertson et al., 2019; Westaway, 1993). The versatility of this method becomes evident as it is applicable to scenarios with either constant or varying uplift rates, as demonstrated by prior studies (e.g. Roberts et al., 2009, 2013; Meschis et al., 2022a,b). This approach proves valuable in overcoming the "re-occupation" problem, preventing the assignment of inaccurate ages to undated marine terraces (e.g., Meschis, et al., 2018; De Santis et al., 2023). Furthermore, SCA can be effectively employed when at least one

absolutely dated paleoshoreline is available, allowing for an initial examination of the simplest scenario of a constant uplift rate over time. This iterative process allows us to calculate sea level highstand elevations systematically, guided by age controls derived from established literature or newly obtained absolute dating. This approach enables us to identify the optimal correlation between the mapped paleoshorelines and iteratively-calculated sea level highstand elevations. If the initial test with the simplest scenario of having a constant uplift rate is not satisfied, we then proceed to test a fluctuating uplift rate scenario, driven by age controls (Meschis et al., 2018; Robertson et al., 2019; De Santis et al., 2021). Considering we are testing if this sequence of submarine terraces is recording the transition period between the Late Pleistocene and Holocene, we opted for a more detailed and recent sea level curve with higher resolution proposed by Gowan et al. (2021), describing the "MIS 5 - MIS 1 period (80 ka to present)" (Table 2). Table 1 shows reliable age controls used in this study, driving iterations of uplift/subsidence. Moreover, linear regression analysis was performed to quantify the relationship between measured and predicted paleoshoreline elevations, with the aim of maximizing the coefficient of determination (R2). It is essential to note that the margin of error associated with paleoshoreline elevations mapped on the DTM is roughly 3 m. The sea level curve employed in our analysis incorporates 2σ error bars for both sea level and the ages of sea level highstands. These error bars represent a confidence interval indicating a 95% probability that the true value falls within the range defined by the error bars. To pinpoint the optimal match and determine the most accurate values for uplift/subsidence rates, we conducted Root-Mean-Square (RMS) deviation calculations, following an established approach outlined in previous studies (Robertson et al., 2019; Meschis et al., 2018, 2020). From the transects depicted in Fig. 3, precise rates were derived by (i) iterating uplift/subsidence rates within the range of −0.3 to 0.2 mm/yr at intervals of 0.05 mm/yr (Fig. 4), and (ii) plotting the RMS deviation values obtained from comparing the values of mapped versus predicted marine terrace bathymetric depths.

Table 3. Values of sea level derived from Gowan et al. (2021) used for our synchronous correlation modelling to calculate predicted paleoshoreline elevations/depths iterating values of uplift/subsidence rates.

Age (ka)	Elevation of paleo-sea level (mm)
0	0
2.5	0
5.0	-4600
7.5	-8400
10	-28200
12.5	-54200
15	-80400
17.5	-107300
20	-116400
22.5	-111600
25	-97600
30	-61300
35	-43600
40	-38500
42.5	-36500
45	-46600
50	-39400
55	-57300
60	-78900
65	-50700
70	-26700
72.5	-19200

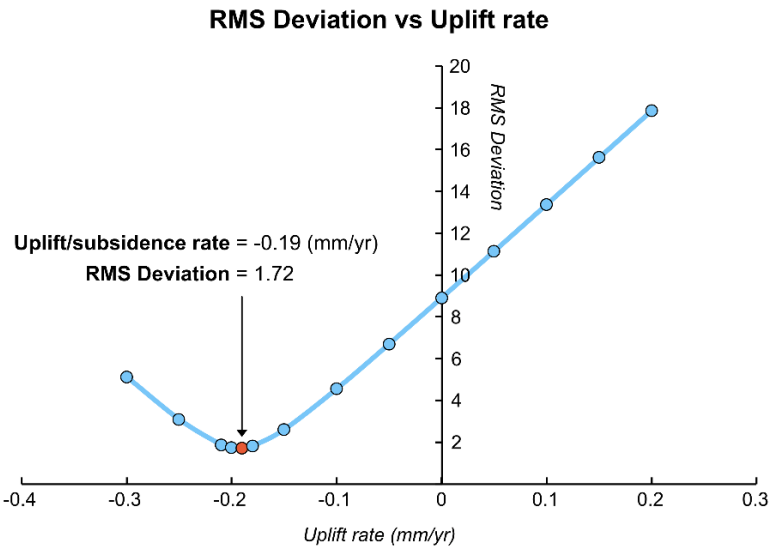

Figure 4. Root-Mean-Square (RMS) Deviation calculation. RMS deviation values for all the uplift/subsidence rate scenarios, from − 0.3 to 0.2 mm/yr at intervals of 0.05 mm/yr, are reported. This graph shows the best match between "measured" and "predicted" paleoshorelines elevations. By following previous investigations applying RMS deviation calculations (e.g. Robertson et al., 2019; Meschis et al., 2020), such values explain the misfit between measured and predicted paleoshoreline elevations during iteration of the uplift/subsidence rates, where the lowest RMS misfit is preferred. Note that details of these calculations are shown in Table SM 1.

This methodological framework ensured a systematic exploration of uplift/subsidence scenarios, allowing us to identify the rates that yielded the most accurate predictions in line with observed bathymetric data.

Results

Geomorphological evidence of paleoshorelines

The analysis of the DTM's histogram, slope gradient map, and contour map, specifically referencing contours from Varzi et al. (2023) used for identifying edges of structural scarps, unveiled the presence of terraced landforms, facilitating the mapping of potential paleoshorelines (Fig. 5). Initially, the histogram exhibits a peak in pixel abundance starting at 32 m water depth (w.d), reaching its summit at approximately 34 m w.d. (Fig. 5a). This marks the location of the first terraced area, defined by a paleoshoreline at 32 m w.d., consistent with prior investigations (e.g., Distefano et al., 2021b). The complexity observed over this flatter area is attributed to the occurrence of coralligenous bioconstructions, forming discrete columns/hybrid banks about 0.60 m high in this region (Bracchi et al., 2017; Varzi et al., 2023) (Fig. 5b). Further offshore, another peak emerges around 46 m w.d. (Fig. 5a), corresponding to the identification of a potential paleoshoreline at 45 m w.d., once again in agreement with Distefano et al. (2021a, b). The seafloor becomes less complex in this area, with smaller and sparsely distributed coralligenous buildups, sometimes associated with rhodolith beds (Varzi et al., 2023) (Fig. 5b). Moving further offshore, the pixel distribution shows a break at around 50 m w.d., indicating a sloping area marked by a paleochannel. However, the DTM's histogram does not show a distinct peak, leading us to abstain from marking any paleoshoreline in this region. Conversely, another peak is evident at a greater depth, approximately 72 m w.d. (Fig. 5a). The slope gradient map highlights a significant sloping area in this region, with an abrupt change in depth near the 70 m w.d. contour line, making it a plausible additional paleoshoreline for consideration in this study. Similarly, another terraced area is apparent at around 85 m w.d. (Fig. 5a), marked by a conspicuous depth change at 82 m w.d. (Fig. 5b). The morphological complexity intensifies in this deeper region, characterized by patchy massive coralligenous bioconstructions, <2 m high and typically clustered together (Varzi et al., 2023) (Fig. 5b). In the deeper portion of our investigated area, attention is drawn to another sloping area at

approximately 93/95 m w.d., hinting at the possibility of yet another flatter region. Unfortunately, the currently available bathymetric data is insufficient to confidently delineate another potential paleoshoreline in this zone. Further investigations and data collection efforts are essential to unveil additional insights and potentially identify another past eustatic reference in this area.

Estimation paleoshoreline ages and rates of crustal vertical movements

Up to four submerged paleoshorelines offshore of Marzamemi village in SE Sicily were detected for our study. Fig. 5c shows our attempt to correlate these mapped geomorphic features with past sea levels, using a well-known sea level curve describing the "MIS 5 - MIS 1 period" (Gowan et al., 2021). Our SCA is driven by an age control from a submerged paleoshoreline located offshore Syracuse town (Fig. 1) previously obtained (Table 1) (e.g. Dutton et al., 2009). Indeed, in the Siracusa offshore (Fig. 1) it has been shown that the paleoshoreline at −20 m belongs to MIS 5a (76.5 ka). By (i) using these bathymetric data together with an age control, and (ii) assuming a lateral continuity for the dated paleoshoreline (Table 1) southward, we iterated rates of uplift/subsidence for our correlation between multiple mapped and predicted paleoshoreline elevations/depths. We used an initial and simplest "constant rate over time" scenario aimed at finding the best match between the two datasets (mapped elevations and predicted past sea levels), following an approach used by previous geoscientists (Houghton et al., 2003; Roberts et al., 2009, 2013; Pedoja et al., 2018; Meschis et al., 2018, 2020, 2022a,b; Robertson et al., 2019, 2023, De Santis et al., 2021, 2023). We found our preferred constant uplift/subsidence rate through time of −0.19 mm/yr (Fig. 4) over the last 80 ka, which allows us to assign for the first time ages for our offshore mapped paleoshorelines. This is not surprising if we consider that rates of crustal deformation constant through time have already been proved a few tens kilometres north of the investigated onshore and offshore close to Siracusa (Meschis et al., 2020). The robustness of our correlation between measured and predicted paleoshoreline elevations is assessed by linear regression, where R2 exceeds 0.99 (Fig. 6).

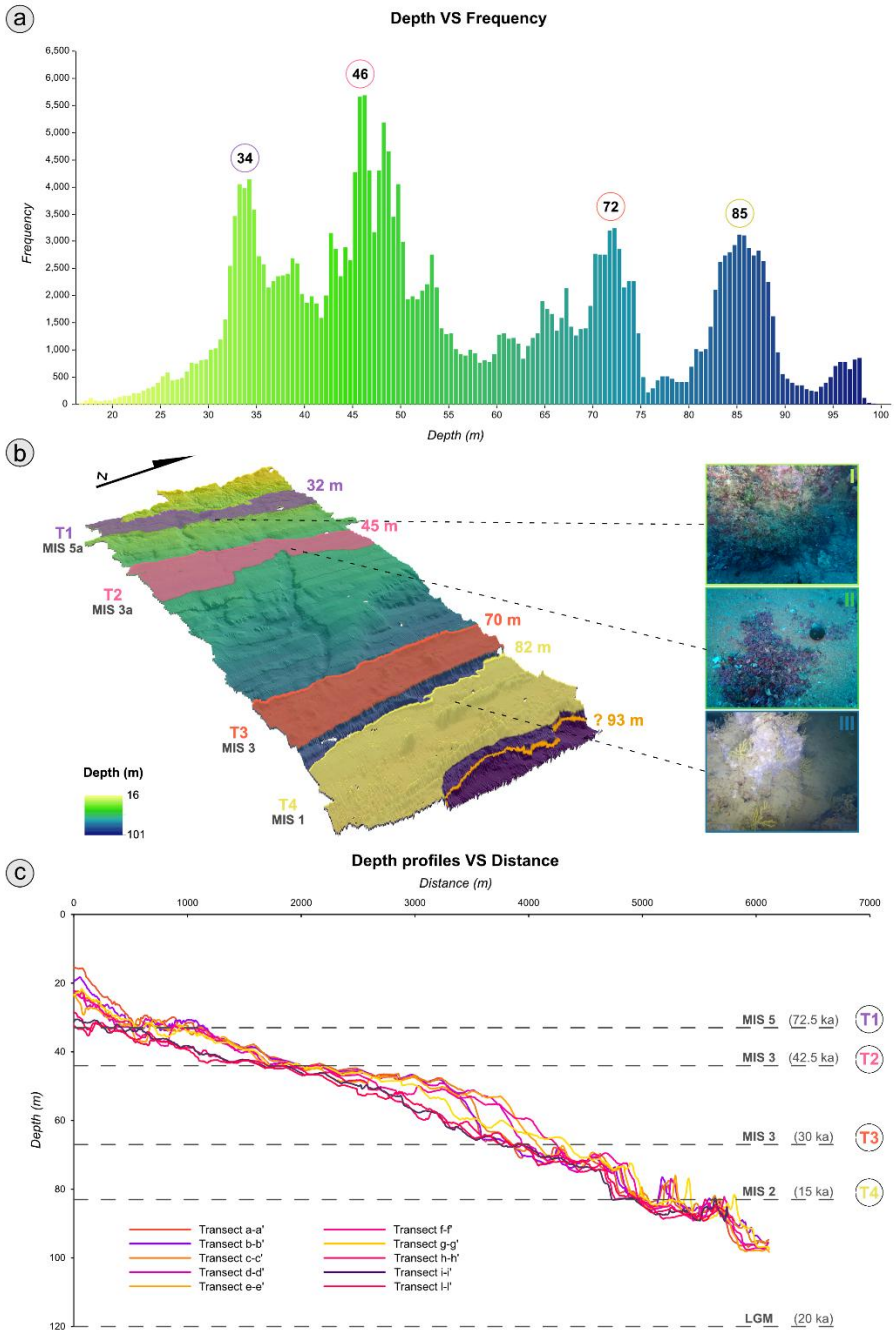

Figure 5. (a) Histogram showing bathymetric depth values distribution over distance; it reports the distribution of the image pixels along a depth gradient, easing the detection of larger areas at the same depth such as terraced areas. Main depths of 34 m (purple circle), 46 m (pink circle), 72 m (salmon circle), and 85 m (yellow circle) are highlighted in the graph as characterized by a peculiar abundance of pixels. (b) 3D representation of the study area showing the mapped potential submerged paleoshorelines at 32 m (purple line), 45 m (pink line), 70 m (salmon line), and 82 m (yellow line) w.d., with the associated submerged marine terraces (T1, T2, T3, and T4, respectively - faded polygons). The orange line at 93 m w.d. is represented with a "?" as the lack of sufficient bathymetric data do not allow the identification of another eustatic reference, yet perceivable. (c) Correlation between the potential submerged paleoshorelines and paleo-sea levels iterating uplift/ subsidence rate scenario, using Gowan et al. (2021) sea level curve describing the last 80 ka sea level changes at a global level. Colourful lines show the bathymetric transect extracted from the DTM (From transect a-a' to transect l-l' - see Fig. 3 for major information). Grey dashed lines indicate the iteratively calculated past sea levels driven by an age control shown in Table 1. (For interpretation of the references to colour in this figure legend, the reader is referred to the web version of this article.).

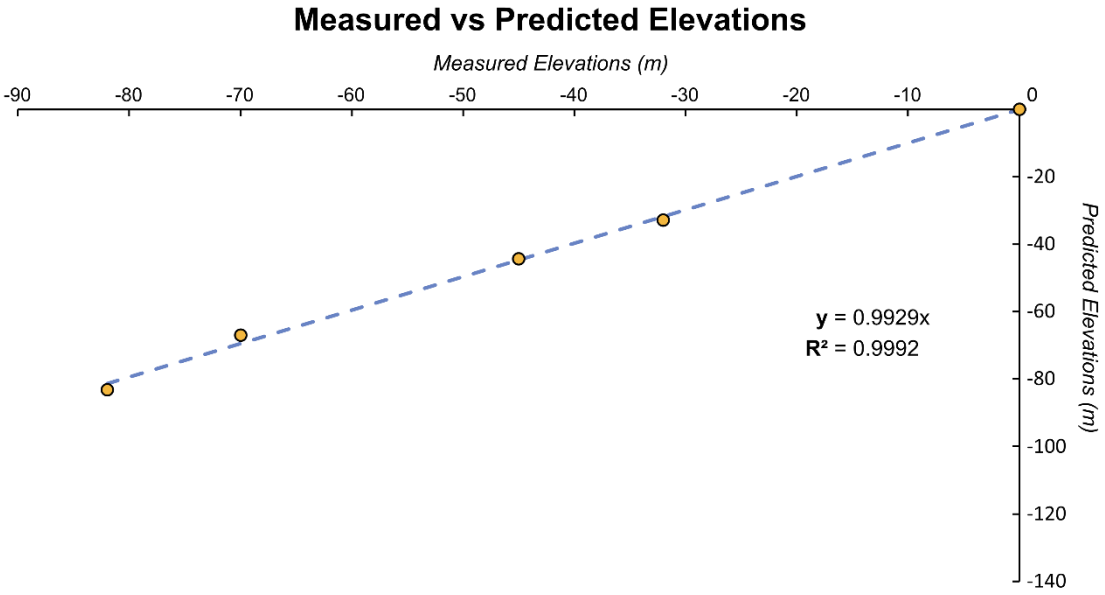

Figure 6. Coefficient of determination (R^2) calculation. The graph reports the linear regression analysis between measured and predicted paleoshoreline elevations. "Measured" elevations represent paleoshoreline elevations/depths mapped offshore using a Multibeam Echosounder system; "Predicted" elevations represent the synchronously calculated past-sea level elevations/depths, obtained by applying a constant subsidence rate through time. R^2 value has been calculated between these two datasets to assess the best fit for our offshore investigations, with a value >0.99.

Moreover, we calculated RMS deviation values to pinpoint the most accurate values of uplift/subsidence rates, as explained in the Method section. Estimation of RMS deviation (Fig. 4) and R2 values (Fig. 6) suggest that we obtained robust and reliable rates of crustal vertical movements for the investigated area, suggesting constancy over the past 80 ka. Furthermore, assuming a constant subsidence rate – 0.19 mm/yr over the last 80 ka we were able to assign ages to undated submerged paleoshorelines. Indeed, we assigned to the MIS 5 (72.5 ka), MIS 3 (42.5 ka), MIS 3 (30 ka), and MIS 2 (15 ka) the paleoshorelines at 32 m (T1), 45 m (T2), 70 m (T3), and 82 m (T4) w.d., respectively (Table 3 and Fig. 5). It is noteworthy that the paleoshoreline at 32 m w.d., assigned to the MIS 5, represents the coeval and lateral continuation southward of the one mapped at 20 m w.d. offshore Siracusa town (Table 1 and Fig. 2). This alignment is consistent with our findings suggesting a slight and likely local fault-related tectonic subsidence affecting the Marzamemi offshore, where T1 is mapped (Fig. 2 and Fig. 5). Finally, in the examination of the right part of the histogram (Fig. 5a), corresponding to the deeper section of the DTM

(Fig. 5b), another potential paleoshoreline at about 93 m w.d. becomes apparent, with a speculative age of 25 ka. This feature is also notable from the overlapping transects in that region (Fig. 5c). The sloping area at this depth seems to transition into a flatter region (Fig. 5b and c), indicative of another submerged marine terrace. However, the lack of consistent bathymetric data in this deeper region hinders its inclusion as a reference line in our modelling, restricting its use to speculative considerations.

Table 4. All mapped submarine terraces with their DEM-based elevations are shown. Furthermore, estimated ages assigned by using a synchronous correlation technique are proposed. Location of submarine terraces are in Figure 2 and 3. Note the T1 is starred to indicate the age control used in this work to drive our synchronous correlation technique.

Terrace Name	DEMs Measured Paleoshoreline Depth (m)	Predicted Sea Level Highstand Depth (m)	Our proposed Age (ka)	Marine Isotope Stage(MIS)
T1*	-32	-32	72.5	5a
T2	-45	-44	42.5	3a
T3	-70	-66	30	3
T4	-82	-83	15	1

Discussion

Late Pleistocene-Holocene limit

For our terrace modelling, we utilized a more detailed sea level curve spanning from MIS 5a to MIS 2, as proposed by Gowan et al. (2021). This choice was motivated by recent scrutiny and critical revaluation of sea levels during MIS 3 by geoscientists. Antonioli et al. (2021) and Gowan et al. (2021) investigated the possibility of a "higher" sea level during MIS 3 (61–29 ka) in comparison to established sea level curves (e.g. Rohling et al., 1998; Waelbroeck et al., 2002; Siddall et al., 2003; Grant et al., 2012). They suggested that the amount of melted ice during MIS 3 might have been underestimated, potentially resulting in a sea level that was approximately 20 m shallower, than present position as reported in PaleoMIST model (Gowan et al., 2021). Our findings align with these recent investigations, indicating that the sea level during MIS 3 was indeed about 20 m higher. The refined chronology for the mapped sequence of terraces appears to document the Late Pleistocene-

Holocene transition encompassing "MIS 5 – MIS 2," incorporating previously undated paleoshorelines likely corresponding to MIS 5 (72.5 ka), MIS 3 (42.5 ka), MIS 3 (30 ka), and MIS 2 (15 ka) (see Table 3). Our results are consistent with slower rates of sea level rise during the Late Pleistocene (ranging between 2.6 and 6 mm/yr - Thompson et al., 2011; Kopp et al., 2013) compared to the Holocene (values exceeding 10 mm/yr - Khan et al., 2015, 2017). Moreover, the identification of a paleo valley (Fig. 5b) formed by a river bedrock, where distinct (paleo)potholes were detected (Varzi et al., 2023), suggests bedrock erosion during a lowstand period, likely corresponding to the Last Glacial Maximum (LGM – 20 ka). Consequently, we discarded a potential scenario where all offshore paleoshorelines were shaped exclusively over the Holocene. Indeed, even if we tested the "Holocene" scenario, our results indicated a higher RMS deviation value and a lower R2 value (refer to Supplementary Material 1 – Table SM 1 – Terrace Calculator), supporting the recording of the "Late Pleistocene-Holocene limit". Additionally, relatively low uplift rates in the studied area may lead to the "re-occupation" of younger marine terraces, where sea level highstands identified by younger terraces overlap with and modify older ones. This phenomenon has been demonstrated in the Apulia region, where a younger paleoshoreline (MIS 7c) re-occupied an older one (MIS 5e) (De Santis et al., 2023). Consequently, if higher paleoshorelines correspond to older sea level highstands based solely on absolute dating may yield erroneous uplift rates and misleading tectonic implications, as highlighted by recent studies (Roberts et al., 2009, 2013; Pedoja et al., 2018; Meschis, et al., 2018, 2020; Robertson et al., 2019, 2023; De Santis et al., 2021, 2023).

In this region, only Distefano et al. (2021a) documented the presence of submerged paleoshorelines, revealing two distinct marine terraces at depths of −35 m and − 45 m w.d. According to our findings, these terraces can be attributed to MIS 5 and 3, respectively. The research also identified a paleoshoreline at −20 m w.d., which is not well visible in our study area, most likely due to the presence of the Posidonia meadow (Varzi et al., 2023). Nevertheless, based on our chronological scenario, a paleoshoreline at this depth would be indicative of an older Marine Isotope Stage. However, it is crucial to note that further

investigations are necessary to refine the dating of older marine terraces, some of which may even outcrop onshore. It is crucial to emphasize that the potential existence of paleo-sea levels persisting into the Holocene cannot be dismissed. This is particularly relevant as our estimation places the age of the mapped paleoshoreline at 82 m w.d. at approximately 15 ka. This finding aligns with previous research, wherein submerged paleoshorelines were employed to calculate rates of crustal vertical movements. In such studies, preserved marine terraces offshore have been identified with ages younger than 15 ka (e.g. Bilbao-Lasa et al., 2020). This consistency suggests that the presence of paleo-sea levels extending into the Holocene is a plausible scenario and warrants further investigation and verification. Finally we stress that results from this study may form a base as marine archive for future works on paleoclimate reconstructions within the Mediterranean realm, as proposed by some in the past (Montagna et al., 2008).

Speculative tectonic implications and future works for the investigated area

The paleoshorelines modelling here presented suggests the necessity to claim a constant subsidence rate of −0.19 mm/yr over the last 80 ka to achieve the best correlation between our submerged paleoshoreline depths and iteratively-calculated paleo-sea level elevations. This is in agreement with prior onshore investigations a few kilometres N of Marzamemi, near Vendicari village, where comparable values of subsidence rates over the Holocene were mapped (Spampinato et al., 2011; Scicchitano et al., 2018). Moreover, it is important to highlight that the investigated area is characterized by tectonic stability to relatively low uplift rates in terms of crustal vertical movement rates. Relatively low uplift rate values have indeed been proposed, ranging from 0.16 mm/yr close to Siracusa town (Meschis et al., 2020) to 0.07 mm/yr close to Pachino and Portopalo di Capo Passero villages (Fig. 2), where the MIS 5e (125 ka) is mapped at ~5–6 m above the sea level (e.g. Ferranti et al., 2006). One could argue that onshore of the investigated area the MIS 5e is recognized a few meters above the present sea level, suggesting tectonic stability to relatively low uplift process slightly in contrast with our results. However, active faulting is locally

controlling the evolution of the landscape close to and within the investigated area, as confirmed by the occurrence of historically damaging seismic events such as the "1908 Messina Earthquake (M 7.1)" (e.g. Aloisi et al., 2013; Barreca et al., 2021; Meschis et al., 2019) and the "1693 Val di Noto (M 7.4)" (Gambino et al., 2021; Scicchitano et al., 2022). For instance, previous investigations show that the NE-SW oriented SE-dipping normal fault system, here named "Avola Fault", is structurally controlling the topography and associated sedimentary processes of the coeval coastal plain with estimated throw-rates of 0.7–0.8 mm/yr (Monaco and Tortorici, 2000; Pavano et al., 2019) over the Middle-Late Pleistocene, likely suggesting faulting activity through time. Yet, there is no knowledge if rates of this faulting activity have remained constant through time since the MIS 5e. If not, it would be plausible speculating about a fluctuating fault-controlled uplift/subsidence rate over the Late Pleistocene where "local" tectonic subsidence would be affecting the relatively low "regional" uplift signal. However, we stress that this is beyond the scope of this paper, and more investigations are needed to refine the faulting activity of the Avola Fault. Furthermore, it is important to highlight that (i) the total length of the "Avola normal fault system" is >40 km, and (ii) the offshore investigated area (Fig. 2) lies close to the centre of the down-throw hanging wall (Fig. 1), where the likely maximum local tectonic subsidence is recorded. This would suggest that our mapped subsidence rates are locally counteracting the likely stable to slight regional uplift signal, a process already demonstrated elsewhere in the Mediterranean realm (e.g. Roberts et al., 2013; Meschis et al., 2018, 2022a,b; Robertson et al., 2019, 2023). Furthermore, the potential influence of the footwall uplift produced by the offshore active normal fault known as the "Western Fault" (Fig. 1b) (Bianca et al., 1999; Gambino et al., 2021; Scardino et al., 2022; Scicchitano et al., 2022), which has ruptured during the 1693 "Val di Noto Earthquake" (M 7.4), was considered. However, this scenario is ruled out as our mapped submerged marine terraces are located within an area situated over the southern fault tip of the fault (Fig. 1). Finally, we stress that even if more investigations are needed to better refine the crustal deformation rates of the "Avola fault system" (also named as "Ispica-Cassibile-Noto" fault system – Pavano et al., 2019) this

work may provide a base for future works assessing the long-term seismic hazard associated with the investigated area.

Bio-geomorphological implications

Marine terraces can form by either erosional or depositional processes (Rovere et al., 2016; Savini et al., 2021). If the area is subject to tectonic subsidence, the occurrence of depositional marine terraces associated with sedimentation is more likely to occur (Rovere et al., 2016) because of the sea level cycling. Nevertheless, as revealed by Distefano et al. (2021a, b) and confirmed by Varzi et al. (2023), the Marzamemi offshore is characterized by a hard bedrock (carved once in subaerial conditions) now dominated by variously spreading coralligenous outcrops (Fig. 2). Present-day coralligenous formations date back to the Holocene sea level rise, after the Late Glacial Maximum (LGM) regression (Ballesteros, 2006), and they are usually associated with climate warming (Basso et al., 2007; Bracchi et al., 2014, 2016). According to our results, we believe that the submerged marine terraces here analysed formed prior the Holocene period during a tectonically stable scenario, but it was only during the latter that coralligenous bioconstructions developed over the hard bedrock thanks to a low sedimentation rate coupled with a slight subsidence rate accommodating their accretion. Indeed, T1 (Fig. 5b) can be considered as a proper example of algal reef terrace (Rovere et al., 2016) resulting from the interaction between erosion and bioconstruction. The development of such a feature could have been possible only in a situation of sediment starvation, confirmed by the seismic analysis from Distefano et al. (2021a). In general, sediments would tend to accumulate beyond the shallower terrace occupied by coralligenous. This would explain why T2 and T3 (Fig. 5b) are not typified by the occurrence of large biogenic outcrops and are instead covered by a thin veneer of sediment. Similarly, T4 (Fig. 5b) is again characterized by biogenic buildups, suggesting slightly different environmental conditions but still optimal for the development of this habitat.

Conclusions

In this paper, we employed a Synchronous Correlation Approach (SCA) to enhance the chronology of submarine terraces mapped offshore the Marzamemi village in SE Sicily. Our aim was to refine the rates of crustal vertical movements over the "Late Pleistocene-Holocene limit" and provide new estimated ages for previously undated marine terraces. The results indicate a relatively stable tectonic activity in terms of crustal vertical movements rates, with modest and likely localized fault-related tectonic subsidence observed over the Late Pleistocene-Holocene boundary at a rate of −0.19 mm/yr. These findings not only contribute valuable insights into the faulting activity of the "Avola Fault System" but also lay the groundwork for future investigations aimed at assessing the associated long-term seismic hazard in the region. The integration of terrestrial and marine datasets underscores the importance of a comprehensive approach for geomorphological studies, climatic reconstructions, and geohazard assessments along coastal regions. Moreover, our results emphasize the significance of better defining the geomorphological characteristics of submerged marine terraces. Clarifying whether these features have a predominantly depositional or erosional origin becomes crucial in understanding the intricate interaction between crustal tectonic uplift and Quaternary sea-level changes. This connection gives rise to marine terraces uplifted on land during highstand periods and, in addition, leads to submerged marine terraces, whose nature, whether depositional or erosional, depends on the alignment or misalignment of the rate of crustal vertical movement with sea-level changes. This nuanced understanding adds depth to our interpretation of the geological history of the region and enhances our ability to decipher the complex interplay between tectonic and climatic forces.

Data availability

Bathymetric data from the Multibeam Echosounder system (MBES) survey used to derive paleoshoreline depths have been stored in https://www.pangaea.de/ (DOI: doi: https://doi.org/10.1594/PANGAEA.966517). Furthermore, results showing new uplift/subsidence rates can be re-produced using the "Terrace Calculator" uploaded as Supplementary Material.

Acknowledgment

This study benefited from ship-time and funding to DB, AS, VB, LF and AGV through the project "FISR2019_04543 CRESCIBLUREEF – Grown in the blue: new technologies for knowledge and conservation of Mediterranean reefs" and from geophysical equipment (MBES R2Sonic) provided by the Milano-Bicocca University infrastructure GEMMA (Geo-Environmental Measuring and Monitoring from multiple plAtforms). We are grateful to Captain Giuseppe Arena (ArenaSub s.r.l) and colleagues Giulia Galimberti and Petra Rybanska for their support during the acquisition of geophysical and ROV data on board the motorboat Valerio. The research was supported by the EU Erasmus+ project BridgET (Bridging the gap between the land and the sea in a virtual Environment for community involvement in the science of marine and coastal geohazards – Grant Agreement 2021-1-IT02-KA220-HED-000027612)" and by the Marine Cartography Lab (BluGLab) of the Dept. of Earth and Environmental Sciences (DISAT), University of Milano-Bicocca, which provided lab facilities and software licences for data acquisition, processing and analysis. AGV is funded through a PhD fellowship granted at the University of Milano Bicocca, DISAT.

References

Aloisi, M., Bruno, V., Cannavò, F., Ferranti, L., Mattia, M., Monaco, C., Palano, M., 2013. Are the source models of the M 7.1 1908 Messina Straits earthquake reliable? Insights from a novel inversion and a sensitivity analysis of levelling data. Geophys. J. Int. 192, 1025–1041. https://doi.org/10.1093/gji/ggs062

Anderson, Densmore, Ellis, 1999. The generation and degradation of marine terraces. Basin Res. 11, 7–19. https://doi.org/10.1046/j.1365-2117.1999.00085.x

Antonioli, F., Calcagnile, L., Ferranti, L., Mastronuzzi, G., Monaco, C., Orrù, P., Quarta, G., Pepe, F., Scardino, G., Scicchitano, G., Stocchi, P., Taviani, M., 2021. New Evidence of MIS 3 Relative Sea Level Changes from the Messina Strait, Calabria (Italy). Water 13, 2647. https://doi.org/10.3390/w13192647

Argnani, A., Bonazzi, C., 2005. Malta Escarpment fault zone offshore eastern Sicily: Pliocene-Quaternary tectonic evolution based on new multichannel seismic data: OFFSHORE EASTERN SICILY. Tectonics 24, n/a-n/a. https://doi.org/10.1029/2004TC001656

Armijo, R., Meyer, B., King, G.C.P., Rigo, A., Papanastassiou, D., 1996. Quaternary evolution of the Corinth Rift and its implications for the Late Cenozoic evolution of the Aegean. Geophys. J. Int. 126, 11–53. https://doi.org/10.1111/j.1365-246X.1996.tb05264.x

Azzaro, R., Barbano, M.S., 2000. Analysis of the seismicity of Southeastern Sicily: a proposed tectonic interpretation. Ann. Geofis. 43, 171–188. http://hdl.handle.net/2122/1292

Barreca, G., Gross, F., Scarfì, L., Aloisi, M., Monaco, C., Krastel, S., 2021. The Strait of Messina: Seismotectonics and the source of the 1908 earthquake. Earth-Sci. Rev. 218, 103685. https://doi.org/10.1016/j.earscirev.2021.103685

Ben-Avraham, Z., Grasso, M., 1991. Crustal structure variations and transcurrent faulting at the eastern and western margins of the eastern Mediterranean. Tectonophysics 196, 269–277. https://doi.org/10.1016/0040-1951(91)90326-N

Bianca, M., Monaco, C., Tortorici, L., Cernobori, L., 1999. Quaternary normal faulting in southeastern Sicily (Italy): a seismic source for the 1693 large earthquake. Geophys. J. Int. 139, 370–394. https://doi.org/10.1046/j.1365-246x.1999.00942.x

Bilbao-Lasa, P., Jara-Muñoz, J., Pedoja, K., Álvarez, I., Aranburu, A., Iriarte, E., Galparsoro, I., 2020. Submerged Marine Terraces Identification and an Approach for Numerical Modeling the Sequence Formation in the Bay of Biscay (Northeastern Iberian Peninsula). Front. Earth Sci. 8, 1–20. https://doi.org/10.3389/feart.2020.00047

Bracchi, V.A., Basso, D., Marchese, F., Corselli, C., Savini, A., 2017. Coralligenous morphotypes on subhorizontal substrate: A new categorization. Cont. Shelf Res. 144, 10–20. https://doi.org/10.1016/j.csr.2017.06.005

Cultrera, F., Barreca, G., Scarfì, L., Monaco, C., 2015. Fault reactivation by stress pattern reorganization in the Hyblean foreland domain of SE Sicily (Italy) and seismotectonic implications. Tectonophysics 661, 215–228. https://doi.org/10.1016/j.tecto.2015.08.043

De Santis, V., Scardino, G., Meschis, M., Ortiz, J.E., Sánchez-Palencia, Y., Caldara, M., 2021. Refining the middle-late Pleistocene chronology of marine terraces and uplift history in a sector of the Apulian foreland (southern Italy) by applying a synchronous correlation technique and amino acid racemization to Patella spp. and Thetystrombus latus. Ital. J. Geosci. 140, 438–463. https://doi.org/10.3301/IJG.2021.05

De Santis, V., Scardino, G., Scicchitano, G., Meschis, M., Montagna, P., Pons-Branchu, E., Ortiz, J.E., Sánchez-Palencia, Y., Caldara, M., 2023. Middle-late Pleistocene chronology of palaeoshorelines and uplift history in the low-rising to stable Apulian foreland: Overprinting and reoccupation. Geomorphology 421, 108530. https://doi.org/10.1016/j.geomorph.2022.108530

Dewey, J.F., Helman, M.L., Knott, S.D., Turco, E., Hutton, D.H.W., 1989. Kinematics of the western Mediterranean. Geol. Soc. Lond. Spec. Publ. 45, 265–283. https://doi.org/10.1144/GSL.SP.1989.045.01.15

Di Geronimo, I., Di Geronimo, R., Rosso, A., Sanfilippo, R., 2002. Structural and taphonomic analysis of a columnar coralline algal build-up from SE Sicily. Geobios 35, 86–95. https://doi.org/10.1016/S0016-6995(02)00050-5

Distefano, S., Gamberi, F., Borzì, L., Di Stefano, A., 2021. Quaternary Coastal Landscape Evolution and Sea-Level Rise: An Example from South-East Sicily. Geosciences 11, 506. https://doi.org/10.3390/geosciences11120506

Durán, R., 2017. Continental Shelf Landforms, in: Submarine Geomorphology.

Dutton, A., Scicchitano, G., Monaco, C., Desmarchelier, J.M., Antonioli, F., Lambeck, K., Esat, T.M., Fifield, L.K., McCulloch, M.T., Mortimer, G., 2009. Uplift rates defined by U-series and 14C ages of serpulid-encrusted speleothems from submerged caves near Siracusa, Sicily (Italy). Quat. Geochronol. 4, 2–10. https://doi.org/10.1016/j.quageo.2008.06.003

Faccenna, C., Molin, P., Orecchio, B., Olivetti, V., Bellier, O., Funiciello, F., Minelli, L., Piromallo, C., Billi, A., 2011. Topography of the Calabria subduction zone (southern Italy): Clues for the origin of Mt. Etna. Tectonics 30, 1–20. https://doi.org/10.1029/2010TC002694

Ferranti, L., Antonioli, F., Mauz, B., Amorosi, A., Dai Pra, G., Mastronuzzi, G., Monaco, C., Orrù, P., Pappalardo, M., Radtke, U., Renda, P., Romano, P., Sansò, P., Verrubbi, V., 2006. Markers of the last interglacial sea-level high stand along the coast of Italy: Tectonic implications. Quat. Int. 145–146, 30–54. https://doi.org/10.1016/j.quaint.2005.07.009

Ferranti, L., Burrato, P., Sechi, D., Andreucci, S., Pepe, F., Pascucci, V., 2021. Late Quaternary coastal uplift of southwestern Sicily, central Mediterranean sea. Quat. Sci. Rev. 255, 106812. https://doi.org/10.1016/j.quascirev.2021.106812

Gambino, S., Barreca, G., Gross, F., Monaco, C., Krastel, S., Gutscher, M.-A., 2021. Deformation Pattern of the Northern Sector of the Malta Escarpment (Offshore SE Sicily, Italy): Fault Dimension, Slip Prediction, and Seismotectonic Implications. Front. Earth Sci. 8. https://doi.org/10.3389/feart.2020.594176

Gowan, E.J., Zhang, X., Khosravi, S., Rovere, A., Stocchi, P., Hughes, A.L.C., Gyllencreutz, R., Mangerud, J., Svendsen, J.-I., Lohmann, G., 2021. A new global ice sheet reconstruction for the past 80 000 years. Nat. Commun. 12, 1199. https://doi.org/10.1038/s41467-021-21469-w

Grant, K.M., Rohling, E.J., Bar-Matthews, M., Ayalon, A., Medina-Elizalde, M., Ramsey, C.B., Satow, C., Roberts, A.P., 2012. Rapid coupling between ice volume and polar temperature over the past 150,000 years. Nature 491, 744–747. https://doi.org/10.1038/nature11593

Grasso, M., Lentini, F., 1982. Sedimentary and tectonic evolution of the eastern Hyblean Plateau (southeastern Sicily) during late Cretaceous to Quaternary time. Palaeogeogr. Palaeoclimatol. Palaeoecol. 39, 261–280. https://doi.org/10.1016/0031-0182(82)90025-6

Gutscher, M.-A., Roger, J., Baptista, M.-A., Miranda, J.M., Tinti, S., 2006. Source of the 1693 Catania earthquake and tsunami (southern Italy): New evidence from tsunami modeling of a locked subduction fault plane. Geophys. Res. Lett. 33, L08309. https://doi.org/10.1029/2005GL025442

Houghton, S.L., Roberts, G.P., Papanikolaou, I.D., McArthur, J.M., 2003. New 234 U- 230 Th coral dates from the western Gulf of Corinth: Implications for extensional tectonics. Geophys. Res. Lett. 30, 2013. https://doi.org/10.1029/2003GL018112

International Hydrographic Organization (IHO), 2008. No Title, in: Standardization of Undersea Feature Names: Guidelines Proposal Form Terminology. Paris.

Jacques, E., Monaco, C., Tapponnier, P., Tortorici, L., Winter, T., 2001. Faulting and earthquake triggering during the 1783 Calabria seismic sequence. Geophys. J. Int. 147, 499–516. https://doi.org/10.1046/j.0956-540x.2001.01518.x

Jara-Muñoz, J., Melnick, D., Zambrano, P., Rietbrock, A., González, J., Argandoña, B., Strecker, M.R., 2017. Quantifying offshore fore-arc deformation and splay-fault slip using drowned Pleistocene shorelines, Arauco Bay, Chile. J. Geophys. Res. Solid Earth 122, 4529–4558. https://doi.org/10.1002/2016JB013339

Johnson, S.Y., Hartwell, S.R., Dartnell, P., 2014. Offset of Latest Pleistocene Shoreface Reveals Slip Rate on the Hosgri Strike-Slip Fault, Offshore Central California. Bull. Seismol. Soc. Am. 104, 1650–1662. https://doi.org/10.1785/0120130257

Khan, N.S., Ashe, E., Horton, B.P., Dutton, A., Kopp, R.E., Brocard, G., Engelhart, S.E., Hill, D.F., Peltier, W.R., Vane, C.H., Scatena, F.N., 2017. Drivers of Holocene sea-level change in the Caribbean. Quat. Sci. Rev. 155, 13–36. https://doi.org/10.1016/j.quascirev.2016.08.032

Khan, N.S., Ashe, E., Shaw, T.A., Vacchi, M., Walker, J., Peltier, W.R., Kopp, R.E., Horton, B.P., 2015. Holocene Relative Sea-Level Changes from Near-, Intermediate-, and Far-Field Locations. Curr. Clim. Change Rep. 1, 247–262. https://doi.org/10.1007/s40641-015-0029-z

Kopp, R.E., Simons, F.J., Mitrovica, J.X., Maloof, A.C., Oppenheimer, M., 2013. A probabilistic assessment of sea level variations within the last interglacial stage. Geophys. J. Int. 193, 711–716. https://doi.org/10.1093/gji/ggt029

Lajoie, K.R., 1986. Coastal Tectonics, in: Active Tectonics: Impact on Society. pp. 95–124.

Lavecchia, G., Ferrarini, F., de Nardis, R., Visini, F., Barbano, M.S., 2007. Active thrusting as a possible seismogenic source in Sicily (Southern Italy): Some insights from integrated structural–kinematic and seismological data. Tectonophysics 445, 145–167. https://doi.org/10.1016/j.tecto.2007.07.007

Lentini, F., Di Geronimo, I., Grasso, M., Carbone, S., Sciuto, F., Scamarda, G., Cugno, G., Iozzia, S., Bommarito, S., La Rosa, N., 1987. Carta geologica della Sicilia sud-orientale. Università di Catania, Istituto di Scienze della Terra, 1987.

Malinverno, A., Ryan, W.B.F., 1986. Extension in the Tyrrhenian Sea and shortening in the Apennines as result of arc migration driven by sinking of the lithosphere. Tectonics 5, 227–245. https://doi.org/10.1029/TC005i002p00227

Mattia, M., Bruno, V., Cannavò, F., Palano, M., 2012. Evidences of a contractional pattern along the northern rim of the Hyblean plateau (Sicily, Italy) from GPS data. Geol. Acta 10, 63–70. https://doi.org/10.1344/105.000001705

Meschis, M., Roberts, G.P., Mildon, Z.K., Robertson, J., Michetti, A.M., Faure Walker, J.P., 2019. Slip on a mapped normal fault for the 28 th December 1908 Messina earthquake (Mw 7.1) in Italy. Sci. Rep. 1–8. https://doi.org/10.1038/s41598-019-42915-2

Meschis, M., Roberts, G.P., Robertson, J., Briant, R.M., 2018. The Relationships Between Regional Quaternary Uplift, Deformation Across Active Normal Faults, and Historical Seismicity in the Upper Plate of Subduction Zones: The Capo D'Orlando Fault, NE Sicily. Tectonics 37, 1231–1255. https://doi.org/10.1029/2017TC004705

Meschis, M., Roberts, G.P., Robertson, J., Mildon, Z.K., Sahy, D., Goswami, R., Sgambato, C., Walker, J.F., Michetti, A.M., Iezzi, F., 2022a. Out of phase Quaternary uplift-rate changes reveal normal fault interaction, implied by deformed marine palaeoshorelines. Geomorphology 416, 108432. https://doi.org/10.1016/j.geomorph.2022.108432

Meschis, M., Scicchitano, G., Roberts, G.P., Robertson, J., Barreca, G., Monaco, C., Spampinato, C., Sahy, D., Antonioli, F., Mildon, Z.K., Scardino, G., 2020. Regional deformation and offshore crustal local faulting as combined processes to explain uplift through time constrained by investigating differentially-uplifted Late Quaternary palaeoshorelines: the foreland Hyblean Plateau, SE Sicily. Tectonics. https://doi.org/10.1029/2020TC006187

Meschis, M., Teza, G., Serpelloni, E., Elia, L., Lattanzi, G., Di Donato, M., Castellaro, S., 2022b. Refining Rates of Active Crustal Deformation in the Upper Plate of Subduction Zones, Implied by Geological and Geodetic Data: The E-Dipping West Crati Fault, Southern Italy. Remote Sens. 14, 5303. https://doi.org/10.3390/rs14215303

Monaco, C., Bianca, M., Catalano, S., De Guidi, Tortorici, L., 2002. Sudden change in the Late Quaternary tectonic regime in eastern Sicily : evidences from geological and geomorphological features. Boll. Della Soc. Geol. Ital. 1, 901–913.

Monaco, C., Tortorici, L., 2000. Active faulting in the Calabrian arc and eastern Sicily. J. Geodyn. 29, 407–424. https://doi.org/10.1016/S0264-3707(99)00052-6

Nanson, R., Arosio, R., Gafeira, J., McNeill, M., Dove, D., Bjarnadottir, L.R., Dolan, M.F.J., Guinan, J., Post, A., Webb, J., Nichol, S., 2020. A two-part Seabed Geomorphology classification scheme. https://doi.org/10.5281/zenodo.7804019

Nicolich, R., Laigle, M., Hirn, A., Cernobori, L., Gallart, J., 2000. Crustal structure of the Ionian margin of Sicily: Etna volcano in the frame of regional evolution. Tectonophysics 329, 121–139. https://doi.org/10.1016/S0040-1951(00)00192-X

Palano, M., Ferranti, L., Monaco, C., Mattia, M., Aloisi, M., Bruno, V., Cannav, F., Siligato, G., 2012. GPS velocity and strain fields in Sicily and southern Calabria, Italy: Updated geodetic constraints on tectonic block interaction in the central Mediterranean. J. Geophys. Res. Solid Earth 117, 1–12. https://doi.org/10.1029/2012JB009254

Passaro, S., Ferranti, L., de Alteriis, G., 2011. The use of high-resolution elevation histograms for mapping submerged terraces: Tests from the Eastern Tyrrhenian Sea and the Eastern Atlantic Ocean. Quat. Int. 232, 238–249. https://doi.org/10.1016/j.quaint.2010.04.030

Pavano, F., Romagnoli, G., Tortorici, G., Catalano, S., 2019. Morphometric evidences of recent tectonic deformation along the southeastern margin of the Hyblean Plateau (SE-Sicily, Italy). Geomorphology 342, 1–19. https://doi.org/10.1016/j.geomorph.2019.06.006

Pedoja, K., Jara-Muñoz, J., De Gelder, G., Robertson, J., Meschis, M., Fernandez-Blanco, D., Nexer, M., Poprawski, Y., Dugué, O., Delcaillau, B., Bessin, P., Benabdelouahed, M., Authemayou, C., Husson, L., Regard, V., Menier, D., Pinel, B., 2018. Neogene-Quaternary slow coastal uplift of Western Europe through the perspective of sequences of strandlines from the Cotentin Peninsula (Normandy, France). Geomorphology 303, 338–356. https://doi.org/10.1016/j.geomorph.2017.11.021

Piatanesi, A., Tinti, S., 1998. A revision of the 1693 eastern Sicily earthquake and tsunami. J. Geophys. Res. Solid Earth 103, 2749–2758. https://doi.org/10.1029/97JB03403

Pirazzoli, P.A., 2005. Marine Terraces, in: Encyclopedia of Coastal Science. Springer Dordrecht.

Prampolini, M., Savini, A., Foglini, F., Soldati, M., 2020. Seven Good Reasons for Integrating Terrestrial and Marine Spatial Datasets in Changing Environments. Water 12, 2221. https://doi.org/10.3390/w12082221

Ricchi, A., Quartau, R., Ramalho, R.S., Romagnoli, C., Casalbore, D., Ventura da Cruz, J., Fradique, C., Vinhas, A., 2018. Marine terrace development on reefless volcanic islands: New insights from high-resolution marine geophysical data offshore Santa Maria Island (Azores Archipelago). Mar. Geol. 406, 42–56. https://doi.org/10.1016/j.margeo.2018.09.002

Roberts, G.P., Houghton, S.L., Underwood, C., Papanikolaou, I., Cowie, P.A., Van Calsteren, P., Wigley, T., Cooper, F.J., McArthur, J.M., 2009. Localization of quaternary slip rates in an active rift in 105 years: An example from central Greece constrained by 234U- 230Th coral dates from uplifted paleoshorelines. J. Geophys. Res. Solid Earth 114, 1–26. https://doi.org/10.1029/2008JB005818

Roberts, G.P., Meschis, M., Houghton, S., Underwood, C., Briant, R.M., 2013. The implications of revised Quaternary palaeoshoreline chronologies for the rates of active extension and uplift in the upper plate of subduction zones. Quat. Sci. Rev. 78, 169–187. https://doi.org/10.1016/j.quascirev.2013.08.006

Robertson, J., Meschis, M., Roberts, G.P., Ganas, A., Gheorghiu, D.M., 2019. Temporally Constant Quaternary Uplift Rates and Their Relationship With Extensional Upper-Plate Faults in South Crete (Greece), Constrained With ^{36}Cl Cosmogenic Exposure Dating. Tectonics 38. https://doi.org/10.1029/2018TC005410

Robertson, J., Roberts, G.P., Ganas, A., Meschis, M., Gheorghiu, D.M., Shanks, R.P., 2023. Quaternary uplift of palaeoshorelines in southwestern Crete: the combined effect of extensional and compressional faulting. Quat. Sci. Rev. 316, 108240. https://doi.org/10.1016/j.quascirev.2023.108240

Robertson, J., Roberts, G.P., Iezzi, F., Meschis, M., Gheorghiu, D.M., Sahy, D., Bristow, C., Sgambato, C., 2020. Distributed normal faulting in the tip zone of the South Alkyonides Fault System, Gulf of Corinth, constrained using 36Cl exposure dating of late-Quaternary wave-cut platforms. J. Struct. Geol. 136, 104063. https://doi.org/10.1016/j.jsg.2020.104063

Rohling, E.J., Fenton, M., Jorissen, F.J., Bertrand, P., Ganssen, G., Caulet, J.P., 1998. Magnitudes of sea-level lowstands of the past 500,000 years. Nature 394, 162–165. https://doi.org/10.1038/28134

Rohling, E.J., Foster, G.L., Grant, K.M., Marino, G., Roberts, A.P., Tamisiea, M.E., Williams, F., 2014. Sea-level and deep-sea-temperature variability over the past 5.3 million years. Nature 508, 477–482. https://doi.org/10.1038/nature13230

Rovere, A., Stocchi, P., Vacchi, M., 2016. Eustatic and Relative Sea Level Changes. Curr. Clim. Change Rep. 2, 221–231. https://doi.org/10.1007/s40641-016-0045-7

Rovida, A., Locati, M., Camassi, R., Lolli, B., Gasperini, P., 2020. The Italian earthquake catalogue CPTI15. Bull. Earthq. Eng. 18, 2953–2984. https://doi.org/10.1007/s10518-020-00818-y

Savini, A., Bracchi, V.A., Cammarosano, A., Pennetta, M., Russo, F., 2021. Terraced Landforms Onshore and Offshore the Cilento Promontory (South-Eastern Tyrrhenian Margin) and Their Significance as Quaternary Records of Sea Level Changes. Water 13, 566. https://doi.org/10.3390/w13040566

Scicchitano, G., Gambino, S., Scardino, G., Barreca, G., Gross, F., Mastronuzzi, G., Monaco, C., 2022. The enigmatic 1693 AD tsunami in the eastern Mediterranean Sea: new insights on the triggering mechanisms and propagation dynamics. Sci. Rep. 12, 9573. https://doi.org/10.1038/s41598-022-13538-x

Scicchitano, G., Monaco, C., 2006. Grotte carsiche e linee di costa sommerse tra Capo Santa Panagia e Ognina (Siracusa, Sicilia Sud-Orientale). Il Quat. 19, 187–194.

Serpelloni, E., Anzidei, M., Baldi, P., Casula, G., Galvani, A., 2005. Crustal velocity and strain-rate fields in Italy and surrounding regions: new results from the analysis of permanent and non-permanent GPS networks. Geophys. J. Int. 161, 861–880. https://doi.org/10.1111/j.1365-246X.2005.02618.x

Serpelloni, E., Bürgmann, R., Anzidei, M., Baldi, P., Mastrolembo Ventura, B., Boschi, E., 2010. Strain accumulation across the Messina Straits and kinematics of Sicily and Calabria from GPS data and dislocation modeling. Earth Planet. Sci. Lett. 298, 347–360. https://doi.org/10.1016/j.epsl.2010.08.005

Siddall, M., Rohling, E.J., Almogi-Labin, A., Hemleben, C., Meischner, D., Schmelzer, I., Smeed, D.A., 2003. Sea-level fluctuations during the last glacial cycle. Nature 423, 853–858. https://doi.org/10.1038/nature01690

Soldati, M., Prampolini, M., Foglini, F., Savini, A., 2021. Landscapes and Landforms of Terrestrial and Marine Areas: A Way Forward. Water 13, 1201. https://doi.org/10.3390/w13091201

Spampinato, C.R., Costa, B., Di Stefano, A., Monaco, C., Scicchitano, G., 2011. The contribution of tectonics to relative sea-level change during the Holocene in coastal south-eastern Sicily: New data from boreholes. Quat. Int. 232, 214–227. https://doi.org/10.1016/j.quaint.2010.06.025

Thompson, W.G., Allen Curran, H., Wilson, M.A., White, B., 2011. Sea-level oscillations during the last interglacial highstand recorded by Bahamas corals. Nat. Geosci. 4, 684–687. https://doi.org/10.1038/ngeo1253

Varzi, A.G., Fallati, L., Savini, A., Bracchi, V.A., Bazzicalupo, P., Rosso, A., Sanfilippo, R., Bertolino, M., Muzzupappa, M., Basso, D., 2023. Geomorphology of coralligenous reefs offshore southeastern Sicily (Ionian Sea). J. Maps 1–13. https://doi.org/10.1080/17445647.2022.2161963

Waelbroeck, C., Labeyrie, L., Michel, E., Duplessy, J.C., McManus, J.F., Lambeck, K., Balbon, E., Labracherie, M., 2002. Sea-level and deep water temperature changes derived from benthic foraminifera isotopic records. Quat. Sci. Rev. 21, 295–305. https://doi.org/10.1016/S0277-3791(01)00101-9

Westaway, R., 1993. Quaternary uplift of southern Italy. J. Geophys. Res. 98, 741–772. https://doi.org/10.1029/93JB01566

BridgET Project

c) Bridging the Gap: Multi-Sensor Seamless Digital Elevation Model of the Lachea Islet and Cyclops Rocks

This work has been submitted to *Marine Geology*:

Varzi A. G., Fallati L., Marino L., Klusak, J., Carlson D.F., Krastel S., Bonali F., Corsaro R. A., Drummer C., Falsaperla S., Gross F., Havenith HB., Micallef A., Nomikou P., Panieri G., Reitano D., Teege, J., Vitello F., Savini A. (Submitted). Bridging the Gap: Multi-Sensor Seamless Digital Elevation Model of the Lachea Islet and Cyclops Rocks. *Marine Geology*

Abstract

The integration of terrestrial and marine datasets across the nearshore zone remains one of the most critical challenges in coastal geomorphology and geohazard studies, where differences in resolution, acquisition techniques, and referencing systems often prevent the construction of seamless Digital Surface Models (DSMs). This study presents a multi-sensor workflow designed to overcome this challenge in the volcanic coastal setting of Lachea Islet and the Cyclops Rocks, eastern Sicily, Italy. Multibeam Echosounder (MBES), Uncrewed Aerial System (UAS)-based Light Detection And Ranging (LiDAR) and photogrammetry datasets were acquired within a four-day interval and processed into a seamless centimetric-resolution DSM. The resulting model, extending from subaerial to submerged domains, enabled morphometric analyses and Object-Based Image Analysis (OBIA) classification, from which a new geological and geomorphological map was derived. Beyond geological reconstruction, the integrated DSM highlights the added value of seamless land-sea models for coastal hazard assessment, particularly by allowing the detection of slope instabilities and the mapping of tectonic lineaments that extend into the submerged domain. Although integration remains limited in the shallowest transition zone, the workflow demonstrates that under favourable geomorphological conditions, high-resolution, multi-sensor DSMs can be effectively applied to other volcanic coasts, representing a powerful tool for advancing both scientific understanding and sustainable coastal management.

Introduction

The seamless integration of terrestrial and marine geospatial datasets, especially across the nearshore zone, which poses the greatest challenges to continuous land–sea mapping, is increasingly recognized as a key objective for geomorphological and geohazard studies (Prampolini et al., 2020). When properly combined, these data enable the construction of continuous Digital Surface Models (DSMs) that bridge the land-sea boundary, providing an integrated and multiscale representation

of coastal systems. Nevertheless, methodological and technological challenges still hinder this process, particularly in tectonically active and dynamic volcanic settings, where rapid morphological change and complex terrain complicate both data acquisition and alignment. Differences in acquisition techniques, point density, referencing systems, and the physical properties of land versus seafloor substrates often result in misalignments or discontinuities that complicate the production of seamless models at a regional scale.

One of the major obstacles in integrating multi-sensor datasets is the varying spatial resolution and coverage of different sensors. Each modality has its own strengths and limitations: Uncrewed Aerial System (UAS)-based LiDAR and photogrammetry Point Clouds (PCs) deliver high resolution over exposed terrain, but struggle in water, while Multibeam Echosounder (MBES) surveys provide accurate bathymetric data but face challenges in the shallow water-land transition zone, mostly due to vessel navigation constraints and very limited coverage. Another common challenge is ensuring consistent georeferencing and vertical datum alignment among datasets collected at different times, with different platforms and sensors. Errors in positioning (GNSS/RTK), timing, and possibly sound velocity, in marine sensors, can all lead to misaligned PCs if not handled rigorously.

Volcanic coasts are shaped by the combined action of volcanic construction, tectonic deformation, and marine erosion, resulting in complex morphologies and high geohazard potential (Branca et al., 2014; Gross et al., 2016; Barreca et al., 2018; Urlaub et al., 2018, 2022). In these environments, accurate and seamless DSMs can provide the spatial continuity needed to identify active structures, map volcanic and sedimentary units, and evaluate slope instability in both terrestrial and marine settings. However, despite their importance, examples of seamless high-resolution datasets remain scarce (e.g. Bernard and Hoover, 2010; Leon et al., 2013; Westhead et al., 2015; Fregoso et al., 2017; Prampolini et al., 2017; Savini et al., 2021) due to persistent challenges in terrestrial-marine data integration.

Currently, no standardized workflow exists that is specifically tailored to geomorphological applications in volcanic coastal settings, where the demand for robust and continuous terrain models is particularly high due to the high geohazard potential of these environments. Addressing this gap is a central objective of the Erasmus+ BridgET project (2021-1-IT02-KA220-HED-000027612), a collaboration among nine European institutions that seeks to overcome the "white ribbon gap" in the integration of onshore and offshore geospatial datasets (bridget.unimib.it).

Within this framework, we present a methodological workflow specifically designed for integrating multi-source datasets in the volcanic coastal environment of Lachea Islet and the Cyclops Rocks, Sicily (Italy). This workflow enabled the construction of a seamless DSM which, combined with existing geological knowledge, supported the generation of a continuous geological and geomorphological map across the land-sea transition. The resulting seamless, high-resolution map not only offers a solid foundation for future structural and geohazard analyses of this volcanic coastal sector but also allows the identification and tracing of major lithostratigraphic units from land into the submarine domain. This capability demonstrates the power of integrative, high-resolution mapping for advancing our understanding of complex coastal volcanic systems.

Geological Background

Regional setting

The Lachea Islet and Cyclops Rocks, located off the eastern coast of Sicily near Aci Trezza (Figure 1), represent the earliest volcanic products of Mount Etna and belong to the Basal Tholeiitic Supersynthem (Branca et al., 2011). These formations were emplaced in a shallow-marine environment during the Middle-Late Pleistocene, when the present coastline lay farther west and the area was submerged. The oldest volcanic deposits, assigned to the Aci Trezza Synthem, were emplaced around 500 ka and consist mainly of basaltic pillow lavas and hyaloclastic breccias with tholeiitic to transitional affinity (Corsaro and Cristofolini, 1996; De Beni et al., 2011). These lavas were emplaced on clay-rich marine sediments of the seabed, producing peperitic textures (Corsaro and Mazzoleni, 2002) that testify to intense magma–sediment interaction typical of shallow submarine eruptions. Within this broader framework, Lachea Islet represents a shallow subvolcanic body (laccolith) emplaced within marly clays during the first phase of Etna magmatism (Basal Tholeiites, Branca et al., 2011). Columnar jointing is locally well developed, and stratigraphic contacts with overlying marine clays are still observable. Subsequent progressive uplift and faulting raised these submarine magmatic bodies above sea level, sculpting the present-day coastal morphology of Aci Trezza. The Cyclops Rocks, coastal

cliffs, and wave-cut platforms preserve clear evidence of the combined effects of tectonic uplift, volcanic activity, and marine erosion.

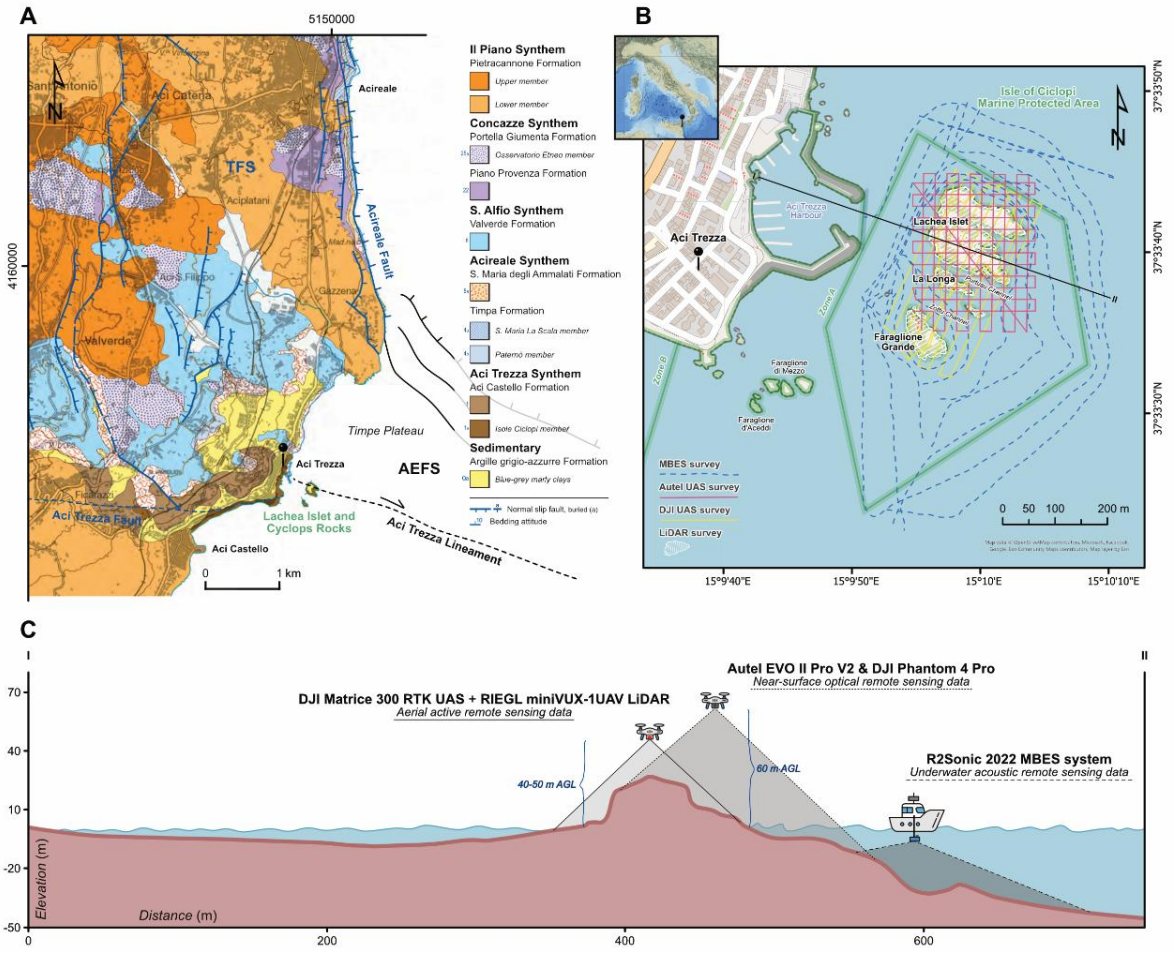

Figure 1. (A) Simplified structural and geological map of the southeastern sector of Mount Etna, focusing on the Aci Castello, Aci Trezza and Acireale area. Lithostratigraphic and synthemic units, as well as onshore tectonic elements, are adapted from Branca et al. (2011), while offshore tectonic features are based on Gambino et al. (2022). (B) Location map of the study area showing the MBES survey tracklines (blue), UAS-based photogrammetry trajectories from the Autel EVO II Pro V2 (pink) and DJI Phantom 4 Pro (yellow), and the area covered by the UAS-based RIEGL miniVUX-1UAV LiDAR survey (white dashed outline). Boundaries of the Isle of the Cyclops Marine Protected Area, including Zone A and Zone B, are shown in green. (C) Schematic cross-shore profile illustrating the spatial overlap of source datasets and the flight altitudes of the UAVs. The location of this profile is indicated in panel (B).

Today, the steep cliffs and fractured outcrops of the Lachea Islet and Cyclops Rocks are affected by ongoing instability and erosional processes, making the area perfect for studying the interplay between magmatism, tectonics, and coastal dynamics (Pappalardo et al., 2021). High-resolution MBES bathymetry and Remotely Operated

Vehicle (ROV) surveys further reveal that this coastal instability reflects the onshore expression of a larger continental margin instability affecting Etna's eastern flank. The submerged margin, cut by semicircular step-like scarps and fault-controlled depressions, aligns with deformation zones on land, indicating that Aci Trezza lies along the boundary of this mobile sector (Chiocci et al., 2011).

Geodynamic and tectonic context

Mount Etna is located at the transition between the collisional front of the Sicilian thrust system and the Hyblean foreland, within a geodynamic setting governed by Africa-Europe plate convergence and rollback of the Ionian slab beneath the Tyrrhenian lithosphere. This configuration produces a combination of NNW-SSE compression and E-W extension, resulting in a transtensional regime that strongly controls the volcano's evolution (Gambino et al., 2022). A major structural element of this system is the Alfeo-Etna Fault System (AEFS), a ~140 km-long dextral shear zone extending from the Ionian offshore to Etna's eastern flank. The AEFS accommodates differential motion between the Sicilian margin and the western Ionian Basin, generating releasing bends and pull-aparts that acted as magma ascent pathways during the early stages of Etnean volcanism (Firetto Carlino et al., 2019; Urlaub et al., 2022). The Aci Trezza area lies in the southern nearshore sector of the Timpe Plateau, which represents the southern portion of Mount Etna's offshore bulge. The plateau, interpreted as the seaward continuation of the Hyblean foreland (Argnani et al., 2013; Gross et al., 2016), is dissected by several strike-slip faults. Among these, the Aci Trezza Fault (ATF) links the onshore Timpe Fault System (TFS) with the offshore continuation of the AEFS, forming a key transfer zone within Etna's mobile eastern flank (Firetto Carlino et al., 2019). During the Middle-Late Pleistocene, transtensive deformation along the ATF favoured the emplacement of magmatic intrusions and fissure-type volcanism, giving rise to the Aci Trezza and Adrano Synthems. Later tectonic inversion generated transpressive push-ups that uplifted and exposed the subvolcanic complexes now visible at Lachea Islet and the Cyclops Rocks.

At present, the TFS represents one of Etna's most active tectonic belts, characterized by steep coastal scarps (up to 200 m), recurrent seismicity, and aseismic creep transferring deformation offshore. GNSS data indicate persistent transtension and eastward flank motion, with accelerations during eruptive phases, while uplifted Holocene paleo-shorelines near Acireale record vertical rates up to 3 mm/yr (Gambino et al., 2022). Offshore, marine geophysical surveys show that the ATF continues as the Ciclopi Fault System, where flower-structure geometries and dextral-transtensional kinematics affect the Lachea Islet laccolith (Chiocci et al., 2011). Displacement of 7.5 ka Chiancone fanglomerate deposits along semicircular coastal faults indicates vertical strain rates up to 8 mm/yr, far exceeding background uplift and confirming the exceptional tectonic activity of this margin. The Aci Trezza sector thus represents an actively deforming transition zone, where regional geodynamics, local faulting, and magmatic processes interact to shape the present morphology of Etna's eastern flank.

Material and Methods

The datasets used in this study were collected during the second summer school of the Erasmus+ BridgET project (2021-1-IT02-KA220-HED-000027612), held on Mt. Etna and in Aci Trezza, Sicily, Italy, from September 30 to October 11, 2023. The following sections present the acquired datasets along with the corresponding instruments and acquisition periods, followed by the processing steps and the procedures applied to assess data quality, consistency, and integration (Figure 2).

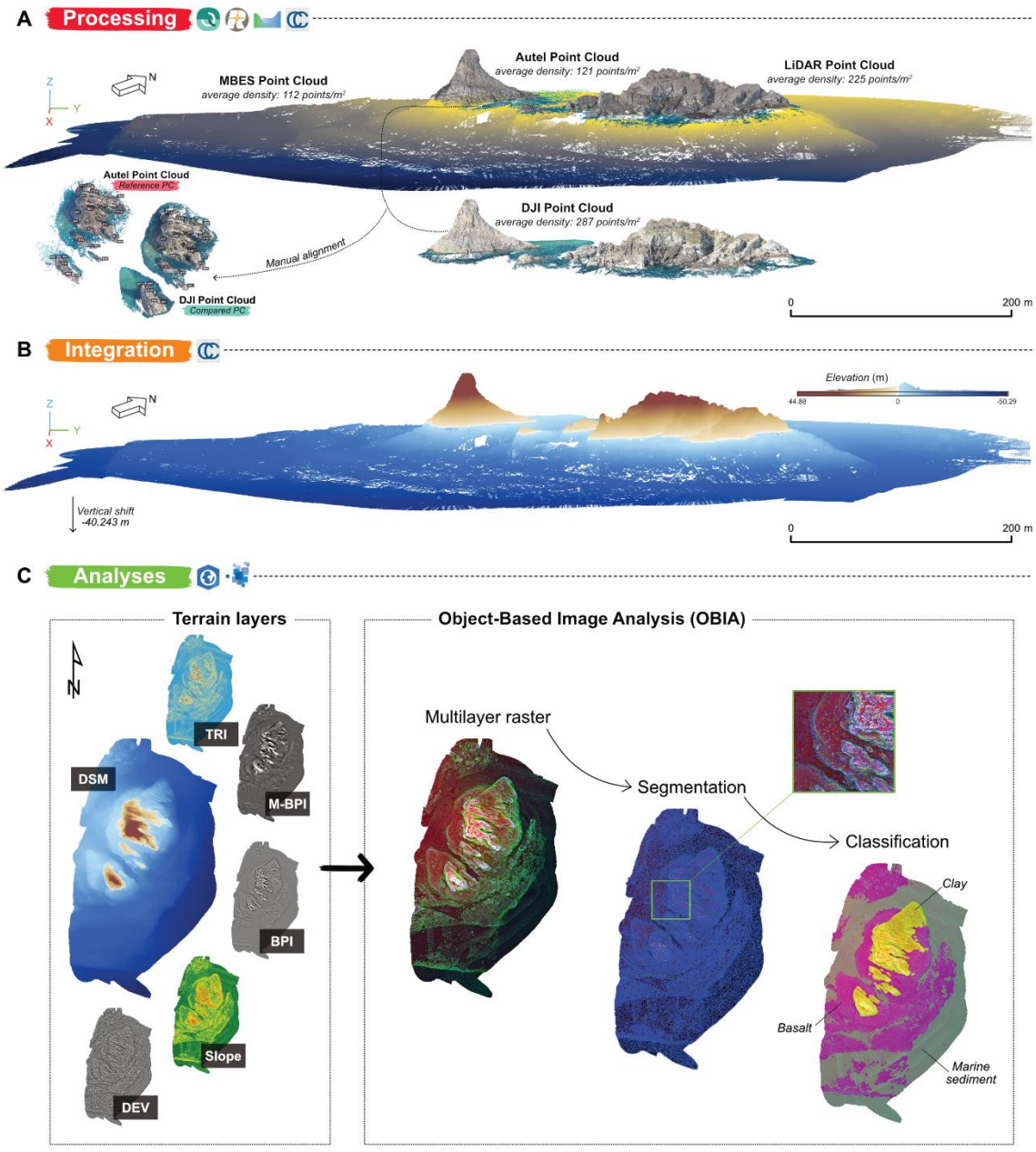

Figure 2. (A) Spatial distribution of the PCs derived from the processing of each dataset using dedicated software: QPS Qimera, Riegl RiProcess, Agisoft Metashape, and CloudCompare. The panel shows the already vertically aligned LiDAR PC, Autel PC, and MBES PC, together with the misaligned DJI PC. On the left, the manually selected tie points between the two UAS-derived PCs used for their manual alignment are visible. (B) Seamless PC obtained from the integration of the four datasets in CloudCompare. Brownish tones represent terrestrial areas, while bluish tones indicate submerged zones. (C) Workflow of the data analysis. On the left, the resulting seamless DSM derived from the integrated PC and the terrain layers produced in ArcGIS Pro. On the right, the sequence of steps performed in eCognition for the OBIA.

Datasets

Underwater acoustic remote sensing data were collected on October 5 using a pole-mounted integrated R2Sonic 2022 MBES system onboard the coastal hydrographic vessel *Neptune 1*, property of Geonautics srl. Data acquisition was performed using QPS Qinsy software. The sonar operated at a frequency of 400 kHz, emitting 1024 acoustic beams within a 130° swath. Surveys were conducted at an average speed of approximately 5 knots along closely spaced lines, ensuring at least 50% overlap (Figure 1B). Real-Time Kinematic (RTK) corrections were applied during acquisition via NTRIP to the GNSS Sicili@net network, to ensure accurate positioning. Data was collected around Lachea Islet, La Longa and Pitruda Rocks, which were surveyed jointly due to shallow waters preventing vessel passage between them, and around Faraglione Grande. Additional patch test lines were acquired following the standard guidelines, to be used for motion compensation. Due to an instrumental technical problem, the collection of Sound Velocity Profiles (SVPs) was not possible, and the sound velocity was measured only at the MBES head. In total, an area of approximately 0.33 km^2 was mapped, covering depths ranging from about 1 to 50 m.

Aerial active remote sensing data were acquired on October 6 by Orthodrone GmbH using a RIEGL miniVUX-1UAV LiDAR sensor mounted on a DJI Matrice 300 RTK UAS, flown at an altitude of 40-50 m Above Ground Level (AGL) to achieve a minimum point density of 50 points/m^2 in RTK mode, ensuring a georeferencing accuracy of approximately 2 cm (Figure 1 B,C).

Near-surface optical remote sensing data were acquired during two UAS-based photogrammetric surveys conducted on October 8. The first survey was carried out by Helmholtz-Zentrum Hereon using an Autel EVO II Pro V2, while the second was performed by a team from the University of Milano-Bicocca with a DJI Phantom 4 Pro. The Autel EVO was equipped with a 20 MP 1-inch CMOS sensor and an RTK antenna connected via NTRIP to the GNSS Sicili@net network. It collected 866 nadir and oblique images. Oblique images were acquired with camera pitch set to 45 degrees in a double-grid pattern with 80% forward overlap and 70% side overlap (Figure 1B) at an altitude of 60 m

AGL (Figure 1C). Flight paths were automated using the integrated ground station app. Similarly, the DJI Phantom 4 Pro, also equipped with a 20 MP 1-inch CMOS sensor and an electronic shutter, captured 481 nadir images at 50 m altitude (Figure 1C), using a predefined automated grid designed in the DJI GS app to maximize image overlap and optimize photogrammetric reconstruction (Figure 1B). Both flights were conducted at a low speed of 4 m/s to minimize distortion and motion blur, ensuring high-quality data acquisition for subsequent 3D model generation.

Data processing

Each dataset was processed using dedicated software to generate its corresponding point cloud (PC). All resulting PCs were then imported into Agisoft Metashape to calculate point density.

MBES bathymetric data were processed using QPS Qimera. Patch test calibration was carried out using the dedicated survey lines, allowing for the estimation and correction of roll, pitch, and heading offsets. Since in situ SVPs could not be collected during the survey, the TU Delft Sound Speed Inversion tool was applied to correct for refraction residuals (Beaudoin et al., 2018). Subsequent noise cleaning was carried out to eliminate imperfections in the dataset. Finally, each processed file was individually exported in LAS format to ensure that all processing steps were preserved. The resulting georeferenced PC achieved an average density of 112 points/m^2 (Figure 2A).

LiDAR data were processed using Applanix PosPAC, applying GNSS base station corrections from the EPOS HAGA base station. Flight trajectories were improved accordingly, and the raw PC was processed in RIEGL RiProcess, with trajectory refinement and accuracy enhancement performed in RIEGL RiPrecision. Subsequent cleaning and refinement of the PC were carried out in Agisoft Metashape and CloudCompare. A final georeferenced PC with an average density of 121 points/m^2 was generated (Figure 2A). This resulting PC has been exported in LAZ format.

UAS-based photogrammetric data were processed using Structure-from-Motion (SfM) algorithms in Agisoft Metashape, following a well-established photogrammetric workflow (e.g. Bonali et al., 2019; Fallati et al., 2020; Over et al., 2021). All raw images were first inspected for focus, exposure, and composition. Blurry or over-exposed images, as well as those containing only water, thus lacking stationary features for matching, were manually discarded. Image alignment was performed with the high accuracy setting to ensure maximum geometric precision, which was essential given the absence of Ground Control Points (GCPs) due to the remote island locations. Tie points generated during alignment were refined through an iterative process of gradual selection and camera calibration (Over et al., 2021). Thresholds for reconstruction uncertainty, projection accuracy, and reprojection error were incrementally adjusted to remove low-quality points. The filtered tie points were then used to generate the dense PC. For both datasets, dense PC computation was carried out with high accuracy and mild depth filtering. The DJI Phantom 4 Pro dataset produced a georeferenced PC with a density of 287 points/m^2, while the Autel EVO II Pro V2 dataset yielded 225 points/m^2 (Figure 2A). Both outputs were exported as LAZ files.

Data integration

The integration of multi-sensor datasets was carried out in CloudCompare. MBES and LiDAR data, together with the Autel SfM dataset corrected with RTK, showed consistent horizontal (XY) and vertical (Z) georeferencing. In contrast, the DJI SfM dataset, although horizontally accurate, was characterised by vertical inaccuracies (Figure 2A). To address this issue, both automatic and manual alignment with the Autel SfM dataset were tested. Automatic alignment using CloudCompare's fine registration tool did not achieve satisfactory results, likely due to differing water penetration effects between the two UAS platforms, which hindered accurate correspondence despite both acquisitions being conducted on the same morning. Manual alignment was therefore performed by selecting 20 point pairs exclusively in the terrestrial area, considered the most reliable region for this

operation (Figure 2A). All PCs were subsequently merged into a single seamless dataset (Figure 2B). A vertical shift of -40.243 m, derived from the difference between the reference ellipsoid and the geoid at the INGV Catania Geodetic Station, was applied to ensure accurate vertical positioning. The final PC was exported in .las format for GIS applications.

Dataset integration accuracy was evaluated using the Cloud/Cloud Dist (C2C) tool, which provided color-coded distance maps and statistical measures, including Mean distance, Standard deviation, and Root Mean Square (RMS). Given that all datasets were collected within a four-day period, we assumed that the analysis reflects alignment accuracy rather than environmental changes. Analyses were conducted on full spatial extents and then refined to the only overlapping regions, as defined by the dominant peak of value distributions.

Data analyses

The merged PC was imported into the ArcGIS Pro environment to enable statistical and spatial analyses (Figure 2C). A DSM with a spatial resolution of 75 cm was generated using the *Interpolate From Point Cloud* tool. Subsequent analyses with the Spatial Analyst Tools allowed for the derivation of several terrain parameters, including Slope and Terrain Ruggedness Index (TRI). The Data Preparation Tools of the Comma Toolbox (Arosio et al., 2024) were further applied to calculate the Mean and Median Local Topographic Position (LTP), which included the Bathymetric Position Index (BPI), the Deviation (DEV) from the mean elevation, and the Median BPI (M-BPI) (for details, see Arosio et al., 2024). Parameter testing indicated that the most reliable results for BPI and DEV were obtained with an inner radius of 2 and an outer radius of 8, while optimal M-BPI results were achieved with values of 10 and 25, respectively. These morphometric layers, together with the DSM, were then used as inputs for Object-Based Image Analysis (OBIA), a classification approach that groups pixels into homogeneous image-objects based on their spectral and spatial properties, improving thematic accuracy with respect to pixel by pixel image analysis (Blaschke, 2010). The objective was to identify and map the main

geological formations of the study area, particularly the Isole Ciclopi Member and the Argille Grigio-Azzurre Formation, the principal lithostratigraphic units of the Lachea Islet and the Cyclops Rocks. In eCognition, a multi-resolution segmentation was first applied using a scale factor of 20, a shape parameter of 0.1, and a compactness value of 0.5, which determined the size, geometry, and internal consistency of the image-objects. A supervised classification was then performed with a decision tree algorithm, which provided the most reliable results for this dataset. As TRI provided redundant information, it was excluded from this step, while the remaining variables effectively supported the identification of three distinct morpho-acoustic facies: *Marine Sediment*, *Basalt*, and *Clay* (Figure 2C). The classification results highlighted consistent differences in the morphometric parameters among these facies, allowing for their unambiguous discrimination. Average feature values for each class are summarized in Table 1.

Table 1. Mean values of the terrain parameters associated with the three morpho-acoustic facies.

	Mean DEV	*Mean BPI*	*Mean M-BPI*	*Mean Slope*
Marine sediment	-0.129294462	-0.085798305	-0.159009819	7.041942214
Clay	0.06057725	0.137752747	1.476128509	40.74694109
Basalt	0.01894905	-0.027624912	0.073538215	24.72085971

Notes: Values represent the average of the parameter ranges used to discriminate among the facies.

The resulting classification shapefile was imported into ArcGIS Pro together with the multilayer raster. Targeted manual edits were then performed to refine the automated classification, primarily to correct the misinterpretation of the *Basalt-Clay* boundary at the land-sea interface on Lachea Island and, more broadly, across the Faraglione Grande. Finally, major structural elements were delineated, such as fault lineaments, on-land geological contacts, and prominent escarpments, as well as finer-scale morphological descriptors within the identified geological classes.

Results

Point Clouds integration and derived seamless Digital Elevation Model

The C2C distance tool shows a generally good agreement among the aerial datasets, with the LiDAR and SfM Autel displaying close correspondence. Even smaller discrepancies were measured between the two UAS surveys, confirming a close match. Larger deviations were recorded in the overlap between the DJI SfM and MBES datasets (Figure 3). These statistics indicate that the aerial PCs are internally consistent at decimetric to sub-decimetric levels, while the integration with bathymetric data yields comparatively larger discrepancies, though still within acceptable limits for seamless DSM construction.

The final seamless DSM, with a resolution of 0.75 m, provides a continuous representation of both terrestrial and submerged surfaces (Figure 4A). Overall, the model covers an area of approximately 0.39 km^2, of which 0.02 km^2 corresponds to emerging land and 0.37 km^2 to the seabed, yielding a ratio of emerging to submerged surfaces of 5.4%**.** The minimum elevation in the DSM is -50.29 m water depth (wd), and the maximum elevation is 44.88 m wd. Hence the total relief range is 95.17 m. The hypsometric distribution derived from the elevation histogram shows that the DSM is strongly dominated by the submerged portion, with 62.2% of the surface area lying deeper than -20 m wd. An additional 31.7% of the area is located between -20 m and sea level, while only 6.1% corresponds to the emerging land above 0 m. Within the submerged domain, the largest frequencies of cells occur between -30 m and -5 m, highlighting the prevalence of gently sloping and relatively flat seabed areas. The terrestrial topography is therefore a minor but steeper component of the model, while the seabed dominates with smoother and more homogeneous surfaces**.** These results emphasize the asymmetric nature of the hypsometric curve and the distinct morphological contrasts between land and seafloor. To further characterize these differences, indices of surface roughness such as Slope, TRI, or Curvatures were computed, confirming that steeper gradients and sharper relief features are associated with the terrestrial portion, whereas the submerged terrain is defined by broader, low-relief surfaces.

It is important to outline that within the 30 m wd it is still possible to witness morphological complexity in continuity and surrounding the Lachea Islet and rocks.

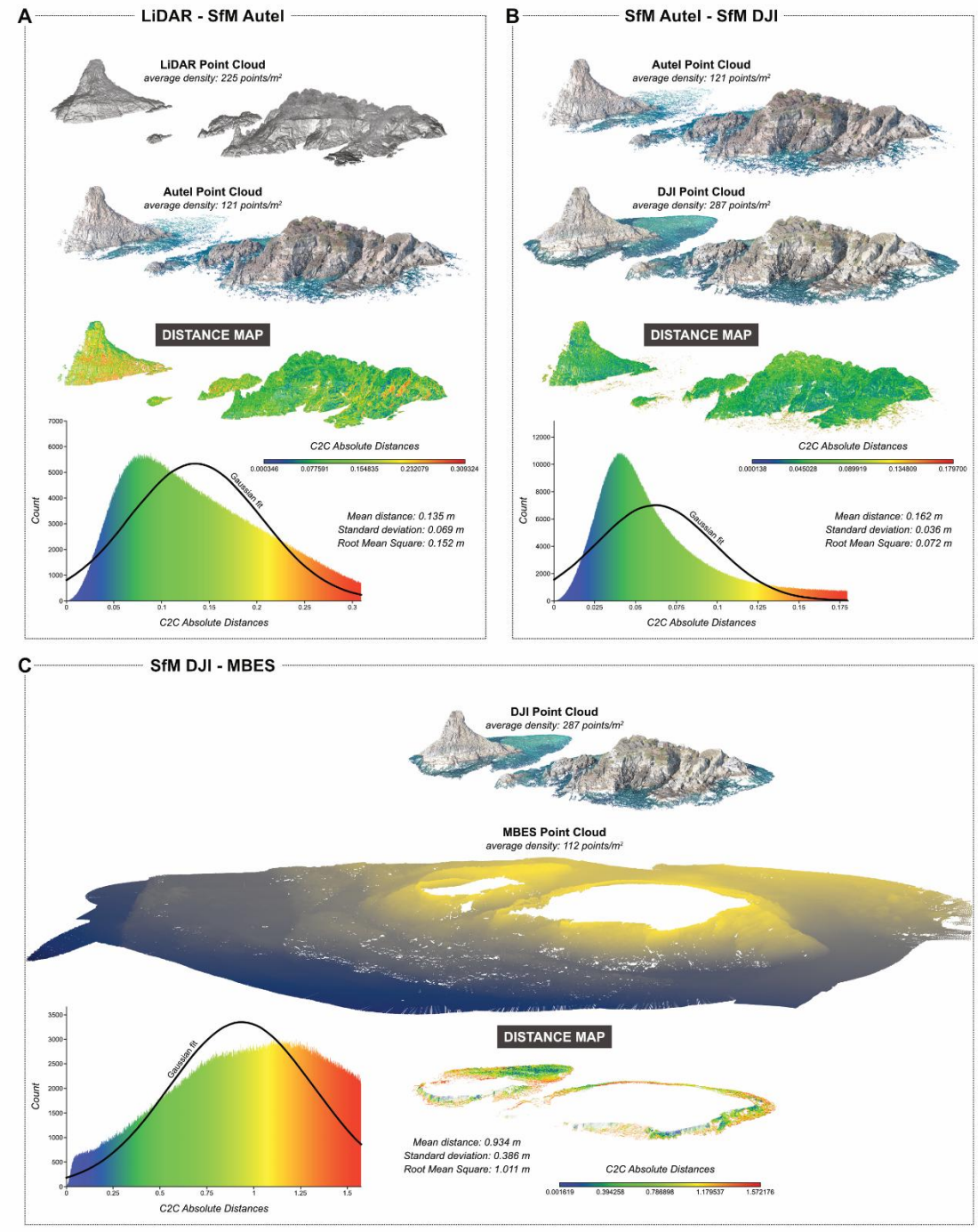

Figure 3. Dataset integration accuracy assessment using the Cloud-to-Cloud (C2C) distance tool in CloudCompare. (A) Comparison between the LiDAR and Autel PCs; (B) comparison between the Autel and DJI PCs; (C) comparison between the DJI and MBES PCs. The color-coded distance maps range from blue (minimal distance between points) to red (greater distance between points). Accompanying histograms display the distribution of point-to-point distances, with the corresponding Gaussian fit overlaid. Statistical parameters (Mean distance, Standard Deviation, and Root Mean Square) are reported for each comparison.

Geological and geomorphological map

The integration of DSM-derived morphometric parameters, OBIA, and pre-existing geological knowledge enabled the production of a new geological and geomorphological map of the study area (Figure 4B).

OBIA classification identified three main morpho-acoustic classes: Marine sediment, Basalt, and Clay, which together represent the principal geological units exposed onshore and offshore. The Marine sediment class is confined to the submerged domain and corresponds to unconsolidated Holocene marine deposits draping the seafloor along areas of lower slope. The Basalt class encompasses magmatic products emplaced during the Middle-Late Pleistocene and represents the dominant lithology of the area, as it corresponds to the Isole Ciclopi member. This unit occurs both on land and at sea, though the geomorphological expression differs between the two environments. Onshore, the basalts are characterized by extensive columnar jointing, typically forming sub-hexagonal patterns. This structure reflects the cooling of subvolcanic bodies intruded into marine sediments, which were later uplifted above sea level. One of the most striking examples of this feature is observed on Faraglione Grande, where the columns are exceptionally well preserved and visually prominent. Offshore, the same basaltic formations are still recognizable but appear more subdued. While traces of columnar jointing can be detected from the roughness of the DSM, they are less sharply expressed than on land, likely due to the smoothing effects of prolonged marine erosion. Finally, the Clay class corresponds to the Argille grigio-azzurre Formation, thus marly clay deposits laid down in a shallow-marine environment prior to the emplacement of the basaltic intrusions. Unlike the sharply jointed volcanic outcrops, the clays are highly erodible and form gentler, elongated morphologies both onshore and offshore. Their subdued topographic expression contrasts with the rugged relief of the basalts, and their recognition in the submarine setting was only made possible through the high-resolution DSM derived from the integrated multi-source PC.

In addition to lithological classes, the map also records the major structural elements that characterize the area. The well-known fault lineament cutting the

northeastern part of Lachea Islet is clearly indicated, together with the stratigraphic contact between the Argille grigio-azzurre Formation and the Isole Ciclopi member, which can be traced on land at the top and along the flanks of Lachea Islet and at the top of Faraglione Grande. Offshore, the morphological contrast between clays and basalts remains evident, especially by looking at the OBIA multilayer raster (see Figure 2C), but the absence of ground-truthing data precludes delineating a definitive contact between the two units. Prominent escarpments were also mapped, including the steep slopes that extend from Lachea Islet and the Cyclops Rocks into their offshore prolongations, as well as two additional offshore scarps that bound the study area towards deeper sectors. These mapped structures are consistent with the regional deformation framework, linking the onshore continuation of the Alfeo–Etna Fault System with offshore scarps and fault-controlled depressions. Overall, this structural architecture conditions the distribution and morphology of lithological units and underscores the strong interplay between volcanic emplacement, tectonic activity, and subsequent erosion.

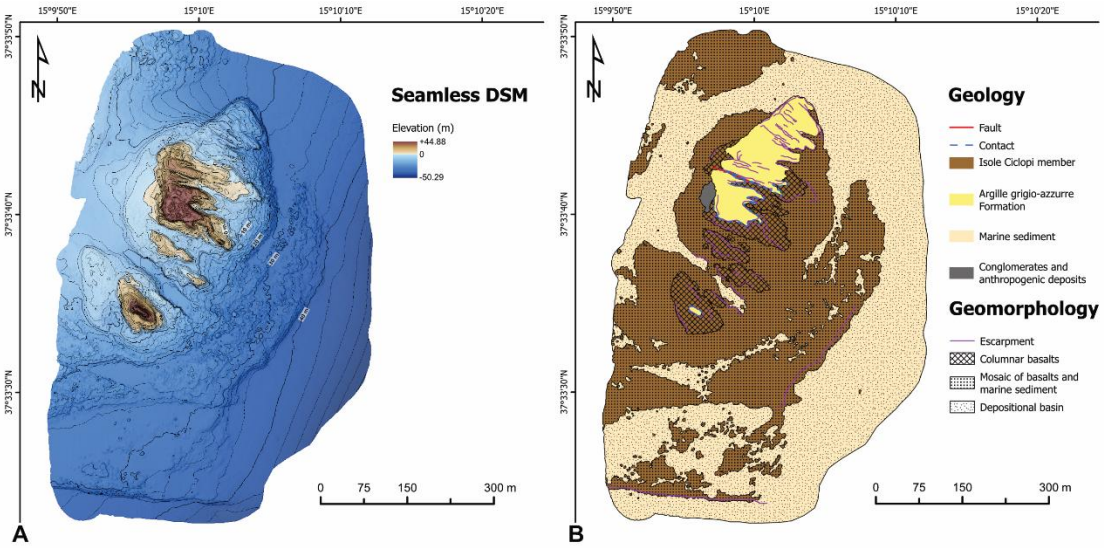

Figure 4. (A) Seamless DSM generated from the integrated PC. Brownish tones represent terrestrial areas, whereas bluish tones indicate submerged zones. Major contour lines are labeled at 10 m intervals, and minor contours are spaced every 2 m. (B) Geological and geomorphological map of the study area derived from OBIA and existing geological data. The Isole Ciclopi Member and Argille grigio-azzurre Formation are defined following Branca et al. (2011), while Conglomerates and anthropogenic deposits are mapped in accordance with Pappalardo et al. (2021). Marine sediment classification was performed in this study to identify unconsolidated Holocene marine deposits draping the seafloor in areas of lower slope.

Discussion

Producing seamless, high-resolution topographic and bathymetric datasets across the land-sea boundary remains a significant challenge in coastal geomorphology. Achieving centimetric continuity is far from trivial, as coastal environments often present bathymetric and geomorphological conditions that severely limit overlap between terrestrial and marine datasets (Savini et al., 2025). On sandy or low-gradient coasts, for instance, extensive shallow zones and unconsolidated deposits hinder full integration, as MBES cannot adequately cover very shallow waters. In addition to these morphological constraints, acquiring high-quality aerial imagery for SfM at the land-sea interface presents its own set of difficulties. The abrupt change in surface reflectance, where land surfaces appear much brighter than submerged features due to the rapid absorption of light by seawater, makes image composition highly variable. Sun glint, surface roughness, and changing illumination angles further degrade image quality, demanding careful flight planning to minimise their effects (Mount, 2005). SfM across the land–sea interface is therefore a challenge in itself, and producing a truly seamless product that integrates SfM, LiDAR, and MBES is even more demanding. Against this background, the Lachea Islet and Cyclops Rocks case study demonstrates that, under favourable environmental conditions, a carefully designed multi-sensor workflow can effectively overcome many of these limitations. The Cyclops coastal sector provides particularly advantageous conditions: rocky shorelines, limited sediment cover, and steep bathymetric gradients reduce the gap between the operational ranges of different sensors, enabling the integration of MBES surveys with SfM and LiDAR data for detailed geomorphological mapping and preliminary hazard assessment. Consistency among aerial datasets was excellent, particularly between LiDAR and the Autel SfM survey (Figure 3A), with only minor deviations observed between the two UAS acquisitions (Figure 3B). By contrast, discrepancies in the overlap between the DJI SfM and MBES datasets underscore the persistent difficulties of the nearshore zone (Figure 3C), where shallow depths, refraction effects, and limited overlap continue to complicate integration

(Mount, 2005; Prampolini et al., 2020). Crucially, the near-simultaneous acquisition of all datasets within four days minimized environmental variability and proved essential in achieving consistency. This highlights a broader methodological point: temporal alignment of datasets is decisive in multi-sensor workflows, as even short acquisition delays can introduce mismatches driven not by sensor error but by genuine geomorphological change in dynamic coastal systems.

Achieving consistency across the land-sea interface substantially enhances the interpretative potential of the resulting dataset. The seamless DSM obtained here provides clear added value for both geomorphological and tectonic interpretation, making it possible to recognize continuous structures that may appear fragmented when datasets are analyzed in isolation. Indeed, a significant outcome of this study is the ability to distinguish lithological units solely from their geomorphological expression, even in the submerged sector. The geological and geomorphological map derived from this DSM reveals the offshore continuity of basalt and clay formations, consistent with magmatic intrusions into marine sediments, followed by uplift and deformation (Branca et al., 2011; Corsaro and Cristofolini, 2000). This was possible due to the high-resolution detail of the DSM, which enabled the recognition of the gentler elongated morphologies that characterise marly clays in contrast with the distinctive columnar structures of basaltic outcrops. Although this classification is based purely on morphology, it carries implications well beyond geological mapping, since substrate type and rugosity are also key parameters for habitat mapping and coastal management, particularly in Marine Protected Areas (MPAs) such as the Lachea Islet and Cyclops Rocks. Furthermore, fault lineaments, lithological contacts, and escarpments could be traced continuously across the shoreline, improving the delineation of unstable slopes and tectonic features. Offshore scarps and fault-bounded depressions complement their onshore counterparts, reinforcing the interpretation of Pappalardo et al. (2021) that this coastal sector records the combined influence of magmatism, tectonics, and erosion on pre-existing volcanic bodies. From a tectonic perspective, the mapped lineaments and scarps align with transtensional structures associated with the Alfeo-Etna

Fault System. Their offshore expression fits into the broader framework of instability along Etna's eastern flank (Chiocci et al., 2011; Gambino et al., 2022; Urlaub et al, 2022), suggesting that flank sliding, uplift, and coastal instability are interconnected processes within a single geodynamic system extending from the subaerial edifice to the continental margin. This continuity underscores the value of seamless DSMs not only for reconstructing geological evolution, but also for coastal hazard assessment, by enabling a more comprehensive evaluation of slope instability, active faults, and mechanically weak lithological zones across the land–sea transition.

Nonetheless, the transition zone between terrestrial and marine datasets remains the weakest link in the integration process. Vertical misalignments are primarily driven by refraction effects, SVPs uncertainties, and a scarcity of reliable tie points in very shallow waters. To overcome these limitations, future work should increase overlap in nearshore survey, adopt rigorous vertical datum corrections, use underwater GCPs, and explore the integration of new technologies such as bathymetric LiDAR. Furthermore, the absence of offshore ground-truthing currently restricts lithological interpretation, underscoring the need for complementary geophysical surveys and sampling campaigns to validate remote-sensing results.

Conclusion

This study developed and implemented a multi-sensor workflow designed to generate a seamless, centimetric-resolution DSM across the land-sea interface of Lachea Islet and the Cyclops Rocks. The workflow combined MBES bathymetry, UAS-based LiDAR, and SfM photogrammetry, all acquired within a four-day interval to ensure temporal consistency. Each dataset underwent dedicated processing, calibration, and alignment, followed by georeferencing correction and cross-sensor integration, to produce a unified PC evaluated through quantitative accuracy assessment. The resulting DSM successfully bridged the terrestrial and submerged domains, overcoming the *white ribbon gap* at the

land-sea transition. The model enabled morphometric and OBIA classification, leading to the construction of a new geological and geomorphological map of the investigated area. This map reveals the offshore continuation of basaltic and clay formations, the geomorphic discrimination of lithologies based solely on morphology, and the tracing of tectonic lineaments and scarps across the shoreline, refining the structural interpretation of Etna's eastern flank. While integration performance strongly depends on local geomorphological conditions, the approach demonstrated here provides a replicable and adaptable workflow for other volcanic coastal settings, particularly where steep morphologies and limited sediment cover favour sensor overlap. The study confirms that high-resolution, seamless DSMs, derived from coordinated multi-sensor workflows, are powerful tools for advancing geomorphological and tectonic research, as well as for improving coastal hazard assessment and sustainable management of dynamic coastal systems.

Acknowledgment

This research was supported by the EU Erasmus+ project BridgET (*Bridging the gap between the land and the sea in a virtual Environment for innovative Teaching and community involvement in the science of climate-change-induced marine and coastal geohazards*; www.unimib.bridget.it), coordinated by the University of Milano-Bicocca. Data acquisition was conducted during the Mt. Etna Summer School, organised within the framework of the project. The authors are grateful to all the students and staff involved for their enthusiasm and commitment.

We also acknowledge the International Lithosphere Program (ILP) Task Force "LithoMar", which provided the collaborative framework underpinning the BridgET initiative.

AGV is funded through a PhD fellowship granted by the University of Milano-Bicocca, DISAT. LM is funded through a PhD fellowship granted by the University of Milano-Bicocca, DISAT, and PNRR MUSA (ex D.M. 118/2023). LF's work is funded by

the research project 2021- RTDAPON-149 (RTDa PON 'ricerca e innovazione' 2014–2020). This research was also supported by the Marine Cartography Lab (BluGLab) of the Department of Earth and Environmental Sciences (DISAT), University of Milano-Bicocca, which provided lab facilities and software licenses for data acquisition, processing, and analysis.

DC acknowledges support from the Optical Oceanography Group at Helmholtz-Zentrum Hereon and funding from the Helmholtz Association through the program Polar Regions and Coasts in the Changing Earth System (PACES II).

The authors also express their sincere gratitude to the staff and management of the Area Marina Protetta Isole Ciclopi in Aci Trezza, particularly Director Dott. Riccardo Strada, for their invaluable support, research permits, and logistical assistance during the BridgET Mt. Etna Summer School.

Finally, the authors wish to thank Geonautics srl for their operational and logistical support during data collection.

References

Argnani, A., Mazzarini, F., Bonazzi, C., Bisson, M., & Isola, I. (2013). The deformation offshore of Mount Etna as imaged by multichannel seismic reflection profiles. *Journal of Volcanology and Geothermal Research*, *251*, 50–64. https://doi.org/10.1016/J.JVOLGEORES.2012.04.016

Arosio, R., Gafeira, J., de Clippele, L. H., Wheeler, A. J., Huvenne, V. A. I., Sacchetti, F., Conti, L. A., & Lim, A. (2024). CoMMa: A GIS geomorphometry toolbox to map and measure confined landforms. *Geomorphology*, *458*, 109227. https://doi.org/10.1016/J.GEOMORPH.2024.109227

Barnard, P.L., and Hoover, D., 2010, A seamless, high-resolution coastal digital elevation model (DEM) for southern California. U.S. Geological Survey Data Series 487, 8 p. https://pubs.usgs.gov/ds/487/ds487_text.pdf

Barreca, G., Corradino, M., Monaco, C., & Pepe, F. (2018). Active Tectonics along the South East Offshore Margin of Mt. Etna: New Insights from High-Resolution Seismic Profiles. *Geosciences 2018, Vol. 8, Page 62*, *8*(2), 62. https://doi.org/10.3390/GEOSCIENCES8020062

Beaudoin, J., Renoud, W., Haji Mohammadloo, T., & Snellen, M. (2018). Automated Correction of Refraction Residuals. In HYDRO18 Conference: 30 October – 1 November 2018, Sydney, Australia

Blaschke, T. (2010). Object based image analysis for remote sensing. *ISPRS Journal of Photogrammetry and Remote Sensing*, *65*(1), 2–16. https://doi.org/10.1016/J.ISPRSJPRS.2009.06.004

Bonali, F. L., Tibaldi, A., Marchese, F., Fallati, L., Russo, E., Corselli, C., & Savini, A. (2019). UAV-based surveying in volcano-tectonics: An example from the Iceland rift. *Journal of Structural Geology*, *121*, 46–64. https://doi.org/10.1016/J.JSG.2019.02.004

Branca, S., Coltelli, M., & Groppelli, G. (2011). Geological evolution of a complex basaltic stratovolcano: Mount Etna, Italy. *Italian Journal of Geosciences*, *Vol. 130, n. 3*, 306–317. https://doi.org/10.3301/IJG.2011.13

Branca, S., de Guidi, G., Lanzafame, G., & Monaco, C. (2014). Holocene vertical deformation along the coastal sector of Mt. Etna volcano (eastern Sicily, Italy): Implications on the time–space constrains of the volcano lateral sliding. *Journal of Geodynamics*, *82*, 194–203. https://doi.org/10.1016/J.JOG.2014.07.006

Chiocci, F. L., Coltelli, M., Bosman, A., & Cavallaro, D. (2011). Continental margin large-scale instability controlling the flank sliding of Etna volcano. *Earth and Planetary Science Letters*, *305*(1–2), 57–64. https://doi.org/10.1016/j.epsl.2011.02.040

Corsaro, R. A., & Cristofolini, R. (1996). Origin and differentiation of recent basaltic magmas from Mount Etna. *Mineralogy and Petrology*, *57*(1), 1–21. https://doi.org/10.1007/BF01161619/METRICS

Corsaro, R. A., & Cristofolini, R. (2000). Subaqueous volcanism in the Etnean area: evidence for hydromagmatic activity and regional uplift inferred from the Castle Rock of Acicastello. In *Journal of Volcanology and Geothermal Research* (Vol. 95). www.elsevier.comrlocaterjvolgeores

Corsaro, R. A., & Mazzoleni, P. (2002). Textural evidence of peperites inside pillow lavas at Acicastello Castle Rock (Mt. Etna, Sicily). *Journal of Volcanology and Geothermal Research*, *114*(1–2), 219–229. https://doi.org/10.1016/S0377-0273(01)00290-6

De Beni, E., Branca, S., Coltelli, M., Groppelli, G., & Wijbrans, J. R. (2011). 40Ar/39Ar isotopic dating of Etna volcanic succession. *Italian Journal of Geosciences*, *130*(3), 292–305. https://doi.org/10.3301/IJG.2011.14

Fallati, L., Saponari, L., Savini, A., Marchese, F., Corselli, C., & Galli, P. (2020). Multi-Temporal UAV Data and Object-Based Image Analysis (OBIA) for Estimation of Substrate Changes in a Post-Bleaching Scenario on a Maldivian Reef. *Remote Sensing 2020, Vol. 12, Page 2093*, *12*(13), 2093. https://doi.org/10.3390/RS12132093

Finocchiaro, C., Coccato, A., Barone, G., Bersani, D., Culka, A., Fornasini, L., Mazzoleni, P., Jehlička, J., Rousaki, A., & Vandenabeele, P. (2022). In situ and micro-Raman spectroscopy for the identification of natural Sicilian zeolites. *Journal of Raman Spectroscopy*, *53*(3), 525–539. https://doi.org/10.1002/jrs.6278

Firetto Carlino, M., Cavallaro, D., Coltelli, M., Cocchi, L., Zgur, F., & Patanè, D. (2019). Time and space scattered volcanism of Mt. Etna driven by strike-slip tectonics. *Scientific Reports*, *9*(1). https://doi.org/10.1038/s41598-019-48550-1

Fregoso, T.A., Wang, R-F. T., Ateljevich, E.S., and Jaffe, B.E., 2017, A new seamless, high-resolution digital elevation model of the San Francisco Bay-Delta Estuary, California: U.S. Geological Survey Open-File Report 2017–1067, 27 p. https://doi.org/10.3133/ofr20171067

Gambino, S., Barreca, G., Bruno, V., de Guidi, G., Ferlito, C., Gross, F., Mattia, M., Scarfì, L., & Monaco, C. (2022). Transtension at the Northern Termination of the Alfeo-Etna Fault System (Western Ionian Sea, Italy): Seismotectonic Implications and Relation with Mt. Etna Volcanism. *Geosciences (Switzerland)*, *12*(3). https://doi.org/10.3390/geosciences12030128

Gross, F., Krastel, S., Geersen, J., Behrmann, J. H., Ridente, D., Chiocci, F. L., Bialas, J., Papenberg, C., Cukur, D., Urlaub, M., & Micallef, A. (2016a). The limits of seaward spreading and slope instability at the continental margin offshore Mt Etna, imaged by high-resolution 2D seismic data. *Tectonophysics*, *667*, 63–76. https://doi.org/10.1016/j.tecto.2015.11.011

Leon, J. X., Phinn, S. R., Hamylton, S., & Saunders, M. I. (2013). Filling the "white ribbon" - a multisource seamless digital elevation model for Lizard Island, northern Great Barrier Reef. *International Journal of Remote Sensing*, *34*(18), 6337–6354. https://doi.org/10.1080/01431161.2013.800659

Mount, R. (2005). Acquisition of Through-water Aerial Survey Images. *Photogrammetric Engineering & Remote Sensing*, *71*(12), 1407–1415. https://doi.org/10.14358/PERS.71.12.1407

Over, J.R., Ritchie, A.C., Kranenburg, C.J., Brown, J.A., Buscombe, D., Noble, T., Sherwood, C.R., Warrick, J.A., and Wernette, P.A., 2021, Processing coastal imagery with Agisoft Metashape Professional Edition, version 1.6—Structure from motion workflow documentation: U.S. Geological Survey Open-File Report 2021–1039, 46 p. https://doi.org/10.3133/ofr20211039

Pappalardo, G., Mineo, S., Carbone, S., Monaco, C., Catalano, D., & Signorello, G. (2021). Preliminary recognition of geohazards at the natural reserve “lachea islet and cyclop rocks” (Southern italy). *Sustainability (Switzerland)*, *13*(3), 1–14. https://doi.org/10.3390/su13031082

Prampolini, M., Foglini, F., Biolchi, S., Devoto, S., Angelini, S., & Soldati, M. (2017). Geomorphological mapping of terrestrial and marine areas, northern Malta and comino (Central mediterranean sea). *Journal of Maps*, *13*(2), 457–469. https://doi.org/10.1080/17445647.2017.1327507

Prampolini, M., Savini, A., Foglini, F., & Soldati, M. (2020). Seven good reasons for integrating terrestrial and marine spatial datasets in changing environments. In *Water (Switzerland)* (Vol. 12, Issue 8). MDPI AG. https://doi.org/10.3390/w12082221

Savini, A., Antoniou, V., Bonali, F. L., Drummer, C., Fallati, L., Falsaperla, S., Gauci, A., Gross, F., Havenith, H.-B., Klusak, J., Krastel, S., Martens, I., Micallef, A., Nomikou, P., Panieri, G., Reitano, D., Teege, J., Tibaldi, A., Varzi, A. G., and Vitello, F. and the EU Erasmus+ BridgET team: Bridging the Gap Between Land and Sea: Integrating Technological Innovation with Geomorphological Contexts for Seamless Coastal Models, EGU General Assembly 2025, Vienna, Austria, 27 Apr–2 May 2025, EGU25-21531, https://doi.org/10.5194/egusphere-egu25-21531, 2025.

Savini, A., Bracchi, V. A., Cammarosano, A., Pennetta, M., & Russo, F. (2021). Terraced Landforms Onshore and Offshore the Cilento Promontory (South-Eastern Tyrrhenian Margin) and Their Significance as Quaternary Records of Sea Level Changes. *Water 2021, Vol. 13, Page 566*, *13*(4), 566. https://doi.org/10.3390/W13040566

Urlaub, M., Geersen, J., Petersen, F., Gross, F., Bonforte, A., Krastel, S., & Kopp, H. (2022). The Submarine Boundaries of Mount Etna’s Unstable Southeastern Flank. *Frontiers in Earth Science*, *10*. https://doi.org/10.3389/feart.2022.810790

Urlaub, M., Petersen, F., Gross, F., Bonforte, A., Puglisi, G., Guglielmino, F., Krastel, S., Lange, D., & Kopp, H. (2018). Gravitational collapse of Mount Etna’s southeastern flank. *Science Advances*, *4*(10), 9700. https://doi.org/10.1126/SCIADV.AAT9700;PAGE:STRING:ARTICLE/CHAPTER

Westhead, K., Smith, K., Campbell, E., Colenutt, A., & McVey, S. (2015). Pushing the boundaries: Integration of multi-source digital elevation model data for seamless geological mapping of the UK’s coastal zone. *Earth and Environmental Science Transactions of the Royal Society of Edinburgh*, *105*(4), 263–271. https://doi.org/10.1017/S1755691015000134

Methane Seep Hunting Project

d) Stratigraphic and Structural Controls on Fluid Seepage and Pockmark Formation in the Sinú Offshore Basin, Colombian Caribbean

This work has been submitted to *Marine Geology* after revision:

Varzi A. G., Galimberti G., Ramírez Florez S., Savini A., Micallef A., Zapata-Ramírez P. A. (Submitted). Stratigraphic and Structural Controls on Fluid Seepage and Pockmark Formation in the Sinú Offshore Basin, Colombian Caribbean. *Marine Geology*

Abstract

Cold seep systems on continental shelves reflect the interaction between fluid overpressure, stratigraphic architecture, and tectonic deformation, yet their distribution and controls remain poorly constrained in the Colombian Caribbean.

This study investigates seep-related seafloor morphologies and their subsurface controls in the Sinú Offshore Basin, southwestern Colombian Caribbean, by integrating high-resolution Multibeam Echosounder (MBES) data, 2D seismic reflection profiles, and ROV observations. The survey covered approximately 247 km² of the continental shelf, revealing an extensive field of small-scale crater-like depressions and a few positive-relief features. Morphometric analysis identifies a total of 5,271 pockmarks characterized by low vertical relief (<5 m), clustered along major structural lineaments and within Pliocene piggyback basins, and 7 dome-like features occurring preferentially along structural lineaments. Seismic interpretation reveals a network of listric reverse faults, diapiric intrusions, and fracture systems within Paleogene–Neogene mud-rich sequences, which likely serve as conduits for episodic fluid migration. Acoustic anomalies correlate with mapped depressions, suggesting a connection between subsurface gas accumulations and seepage expressions at the seabed. The spatial correspondence between these seismic anomalies and the pockmark clusters suggest that seepage is primarily structurally focused, while stratigraphic contrasts modulate fluid trapping and release. The subdued relief of most pockmarks and the limited number of active water column flares suggest weak or episodic seepage. These results highlight the combined influence of faulting, diapirism, and stratigraphic architecture in controlling fluid migration and shaping the seabed.

Introduction

Cold seeps, commonly located on continental margins (Sibuet & Olu, 1998; Cruaud et al., 2017) and petroleum basins (Sun et al., 2020), are characterized by the migration of low-temperature, hydrocarbon-rich fluids from the subseafloor to the seabed. These processes give rise to a variety of distinctive seafloor morphologies and sustain unique biogeochemical systems (Judd & Hovland, 2007; Ceramicola et al., 2018). Methane, a predominant gas in these environments, can originate from either thermogenic (Clayton, 1991) or microbial processes (Rice and Claypool, 1981). Its migration and expulsion often result in crater-like depressions, or pockmarks, which display wide variability in size, shape, and genesis (King & MacLean, 1970; Hovland & Judd, 1988; Hovland et al., 2002; Gafeira et al., 2018; Spatola et al., 2025). While shallow biogenic gas or gas hydrate dissociation can explain the presence of many pockmarks fields (Judd & Hovland, 1992; Rollet et al., 2009; Roelofse et al., 2020), more complex and larger features are often associated with thermogenic gas migration along active plumbing systems (Marcon et al., 2014; Waage et al., 2020). Positive seafloor features such as mud volcanoes may result from the expulsion of overpressured mud and gas-rich fluids (Milkov, 2000; Kopf, 2002; Dimitrov, 2002; Mazzini & Etiope, 2017), giving rise to a variety of features variable in size, dimension, and configuration (Savini et al., 2009; Savini et al., 2018; Bialik et al. 2022; Fallati et al., 2023, Napoli et al., 2025 among others) that can also release large amounts of methane into the water column and possibly, when present at shelfal depths, the atmosphere (Milkov et al., 2003; Etiope & Milkov, 2004; Etiope, 2005; Napoli et al., 2025; Joung et al., 2025). When this ductile material deforms but does not breach the seafloor, mud diapirs form (Milkov, 2000; Zhong et al., 2021), altering local bathymetry and often inducing faulting, fracturing, or collapse (Palomino et al., 2016).

The distribution, morphology, and activity of seep-related landforms are shaped by the interaction of tectonic structures and stratigraphic architecture. Faults have been widely recognised as critical elements since they can either promote fluid migration by acting as

conduits or inhibit it by acting as barriers, thus influencing both the location and nature of fluid-related seafloor features (Hooper, 1991; Bense and Person, 2006; Savini et al., 2018; Micallef et al., 2019). Meanwhile, the stratigraphic framework, through controls on permeability, lithological layering, and sedimentary architecture, exerts a primary influence on how fluids accumulate and migrate, and how seepage is expressed on the seafloor (Hovland & Judd, 1988). While many seep-related studies have emphasized structural controls, the combined role of stratigraphy and structure remains less well constrained, particularly in shelf settings with high sedimentation rates and complex depositional histories. This lack of integrated understanding limits our ability to predict where and how fluids reach the seafloor, and how those expressions evolve morphologically over time. Specifically, how variations in sediment type, permeability, and depositional architecture interact with faults and diapirs to localize seepage and shape features like pockmarks or mud domes remains an open question. Furthermore, the episodic nature of seepage and its connection to basin evolution, overpressure development, and tectonic forcing is still poorly constrained.

The southwestern Colombian Caribbean continental shelf hosts diverse fluid flow systems including mud volcanoes, diapirs, and methane seeps (Sánchez & Permanyer, 2006; Gracia et al., 2012; Cortés et al., 2018). Shaped by the complex interplay of Caribbean-South American plate interactions and a thick, heterogeneous siliciclastic stratigraphy (Rodríguez et al., 2021), this setting offers a chance to explore how geological architecture controls fluid dynamics. Despite being recognized as a gas-rich basin since the 1970s (Hatfield et al., 1975; Katz et al., 2003), in which methane is thought to be produced by both microbial and thermogenic processes (Katz et al., 2003; Gonzalez-Penagos et al., 2019), this area lacks comprehensive high-resolution seabed mapping and seismic stratigraphy (Osorio-Granada et al., 2023).

The Colombian project "Methane Seep Hunting (MSH): A Multi-Scale and Multi-Method Approach" seeks to address key knowledge gaps in the understanding of methane seep dynamics in the Colombian Caribbean, with a focus on the Sinú offshore basin. The

selection of this study area was guided by Hernández-Hamón et al. (2023), whose detection and mapping of natural methane seepage at the sea surface identified this region as a promising target for further investigation. Barragán and Bernal (2024) subsequently presented a preliminary view of the newly acquired bathymetric data and previously collected seismic data, using them primarily as contextual background rather than discussing their broader significance. In the present work, we deliver a high-resolution Digital Terrain Model (DTM) that enables detailed geomorphological characterization of the region. By integrating this dataset with the interpretation of a seismic profile crossing the study area, we provide a comprehensive assessment of the geological and geomorphological framework of the area. This combined analysis underscores the critical influence of tectonic structures, sediment properties, and subsurface fluid migration in shaping seep-related seafloor morphologies.

Geological Background

Colombia contains 23 sedimentary basins, and the Caribbean region falls within the northern Central and Western tectonic domains (ANH, 2007). The study area is located offshore the Gulf of Morrosquillo, in the Moñitos region of Córdoba, within the southwestern Colombian Caribbean Sea (Figure 1). It lies within the Sinú Offshore Basin, the submerged continuation of the Sinú-San Jacinto Fold Belt and part of the Southern Caribbean Deformed Belt (Duque-Caro, 1979; Flinch, 2003; Arismendy et al., 2020). Regionally, this portion of the margin reflects the long-term interaction between the Caribbean and South American plates, where convergent and transpressive forces have shaped a complex system of fold belts, basins, and deformation fronts extending from onshore Colombia to the continental shelf (Pindell & Barrett, 1991; Mann, 1999; James, 2009). The stratigraphy of the region records a transition from Cretaceous oceanic and deep-marine environments to Neogene-Quaternary deltaic and shelfal conditions influenced by Andean uplift and sediment delivery from major river systems. Modern

seafloor morphology is dominated by fine-grained sediments and a variety of tectonically controlled features such as ridges, seabed depressions, and mud-related structures. Together, these characteristics define the Sinú Offshore Basin as a rapidly evolving margin where sedimentation, deformation, and fluid flow interact across multiple spatial and temporal scales.

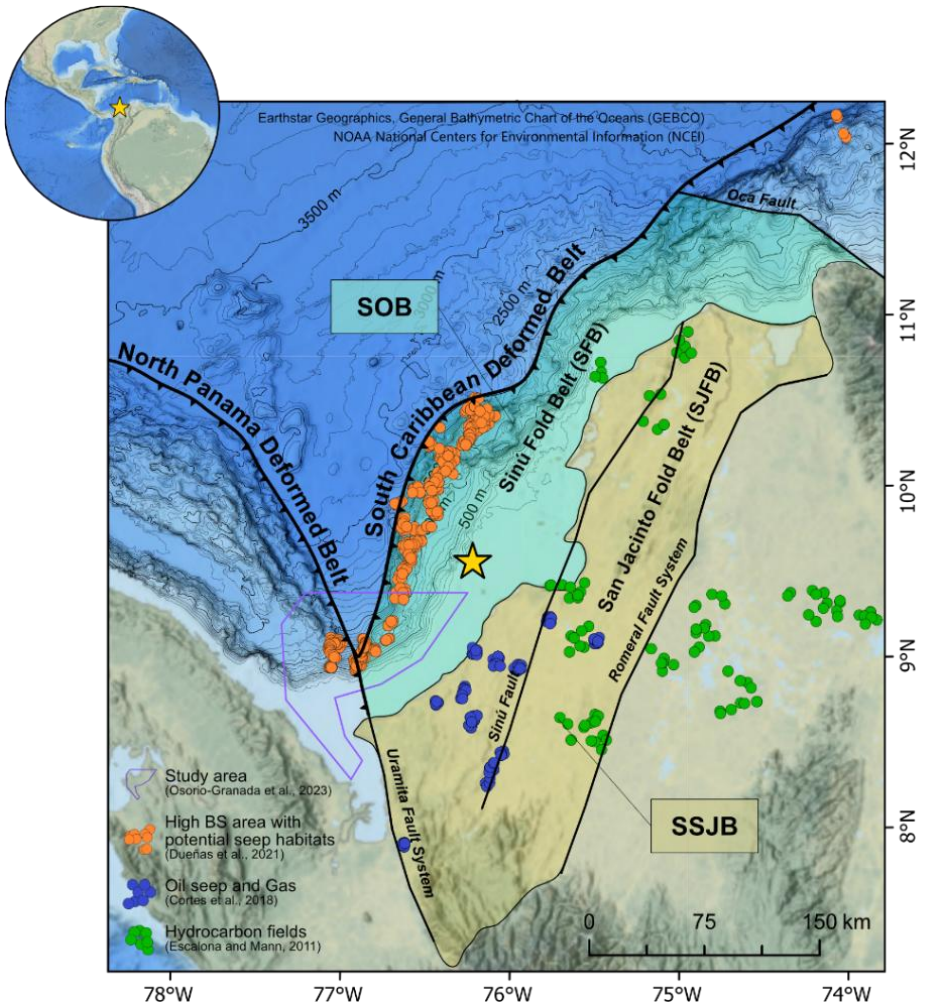

Figure 1. Simplified tectonic map of the Caribbean-Colombian region highlighting key geological features. The North Panama Deformed Belt and South Caribbean Deformed Belt are indicated. Black labels mark the positions of the San Jacinto Fold Belt (SJFB) and the Sinú Fold Belt (SFB). Brown and green shaded areas represent the extents of the Sinú-San Jacinto Basin (SSJB) and the Sinú Offshore Basin (SOB), respectively. Major hydrocarbon provinces in the region are indicated: green dots represent hydrocarbon fields (based on Escalona & Mann, 2011; blue dots show oil seeps and gas locations in the SSJB (based on Cortés et al., 2018); orange dots mark offshore potential seep locations (based on Dueñas et al., 2021); finally, violet polygon represent methane-dominated basin area studied by Osorio-Granada et al. (2023). The yellow star marks the location of the study area. The ocean basemap is from GEBCO, with major bathymetric contours spaced at 500 m intervals.

Geodynamic and Tectonic Framework

The southwestern Colombian Caribbean margin forms part of a complex convergent boundary where the Caribbean Plate moves eastward relative to the South American Plate at rates of ~15-20 mm/yr (Escalona & Mann, 2011; Rodríguez et al., 2021). This oblique convergence generates a transpressional regime characterized by NW-SE shortening and right-lateral shear, producing a system of fold belts, thrusts, strike-slip faults, and diapiric structures that extend from onshore Colombia toward the continental shelf and slope. Within this margin, the Sinú-San Jacinto orogenic system represents an accretionary-forearc complex composed of progressively younger deformational domains (Duque-Caro, 1979; Flinch, 2003; Galindo & Lonergan, 2013; Rodríguez et al., 2021). Onshore, the San Jacinto Fold Belt (SJFB) and the Sinú-San Jacinto Basin (SSJB) contains the oldest contractional structures, whereas its offshore continuation, the Sinú Offshore Basin (SOB) and Sinú Fold Belt (SFB), records younger deformation as the accretionary wedge migrated basinward (Figure 1 - Duque-Caro, 1979; Flinch, 2003; Galindo & Lonergan, 2013; Rodríguez et al., 2021). The South Caribbean Deformed Belt (SCDB) marks the outer structural boundary (Figure 1) separating the SOB from the Colombian Basin (Rodríguez et al., 2021; Rincón-Martínez et al., 2022). High sedimentation rates derived from Andean uplift, together with the presence of mechanically weak Cretaceous-Paleogene shales, have strongly influenced margin deformation (Alfaro & Holz, 2014). Rapid burial promotes undercompaction and overpressure development, reducing shale strength and facilitating detachment folding and shale mobilization (Pindell & Barrett, 1991; Mann, 1999; James, 2009). These processes contribute to the widespread formation of mud diapirs, diapiric ridges, and fault-propagation folds observed across the continental shelf and slope (Duque-Caro, 1984; Flinch, 2003; Cortés et al., 2018; López Ramos et al., 2022). Seismic and bathymetric data reveal antiformal ridges, piggyback basins, thrust-bound blocks, and diapiric domes, reflecting the interplay between contractional tectonics and gravitational processes (Cortés et al., 2018; López Ramos et al., 2022). The deformation front of the SFB is marked by active diapirs and thrusts that breach the seabed, forming

major conduits for fluid migration from overpressured strata in the SOB and SFB. Numerous studies document mud volcanism, gas venting, and pockmark fields along this segment of the margin (e.g. Escalona and Mann, 2011; Cortés et al., 2018; Dueñas et al., 2021; Osorio-Granada et al., 2023), underscoring the dynamic coupling among compression, shale mobility, and fluid expulsion.

Stratigraphic Framework

The stratigraphic evolution of the Sinú-San Jacinto system records the transition from a Mesozoic rifted margin to a Neogene-Quaternary forearc and accretionary wedge (Alfaro & Holz, 2014). The sedimentary succession spans from the Cretaceous to the Quaternary and comprises six major tectono-stratigraphic sequences that reflect shifts in tectonic regime, sediment supply, and depositional environment (Arismendy et al., 2020). The basal units consist of Cretaceous-Paleogene deep marine shales deposited under subsiding passive margin conditions (Duque-Caro, 1979; Alfaro & Holz, 2014; Rodríguez et al., 2021). These fine-grained, low-permeability strata form regionally extensive detachment levels that promote detachment folding, shale mobility, and overpressure accumulation during Neogene-Quaternary compression. Their mechanical weakness contributes to widespread diapirism and provides reservoirs for fluid overpressure (Rodríguez et al., 2021; Osorio-Granada et al., 2023). Overlying Paleogene successions include hemipelagic muds, turbidites, and mass-transport deposits influenced by early deformation and slope instability (Alfaro & Holz, 2014). These grade into Neogene sequences dominated by siliciclastic influx from the uplifted Andes, particularly the Magdalena, Atrato, Mulatos, and Sinú river systems (Castaño et al., 2002; Naranjo-Vesga et al., 2020; Osorio-Granada et al., 2023). During the Miocene-Pliocene, increased sediment flux drove progradation of slope, shelf, and deltaic systems, producing thick clinoformal packages and enhanced accommodation space in the

offshore basin (Arismendy et al., 2020). Finally, Neogene-Quaternary deposits show abundant evidence of syntectonic sedimentation, including growth strata, onlaps, stratigraphic discontinuities, and chaotic seismic facies associated with turbidites and debris flows (Rodríguez et al., 2021). Sediment thickness increases seaward from ~2 km on the outer shelf to more than 4-6 km near the deformation front, reflecting the combined effects of rapid sedimentation and ongoing tectonic loading (Duque-Caro, 1979; Rodríguez et al., 2021).

Stratigraphy exerts a strong control on fluid migration: thick Paleogene shales act as overpressured sources, while sandier Neogene units provide lateral pathways for fluid transport. Vertical migration is focused along faults, diapirs, and fracture corridors, producing seismic indicators such as acoustic blanking and gas-charged reflectors (Rodríguez et al., 2021; Osorio-Granada et al., 2023). At the seabed, fine-grained muddy sediments derived from regional river systems accumulate under low-energy marine conditions (Castaño et al., 2002; Naranjo-Vesga et al., 2020), forming a soft substrate prone to deformation by active diapirism and fluid escape.

Material and Methods

Datasets

The datasets used in this study (Figure 2.1) include a seismic reflection profile provided by the Colombian National Hydrocarbons Agency (ANH) and newly acquired Multibeam Echosounder (MBES) data collected within the framework of the MSH Project. Ground-truth observations from 27 Remotely Operated Vehicle (ROV) stations were also integrated to confirm active fluid seepage and validate sediment composition (Figure 2.2, see panels) at selected sites (for more details about sedimentological analysis, see Barragán & Bernal, 2024).

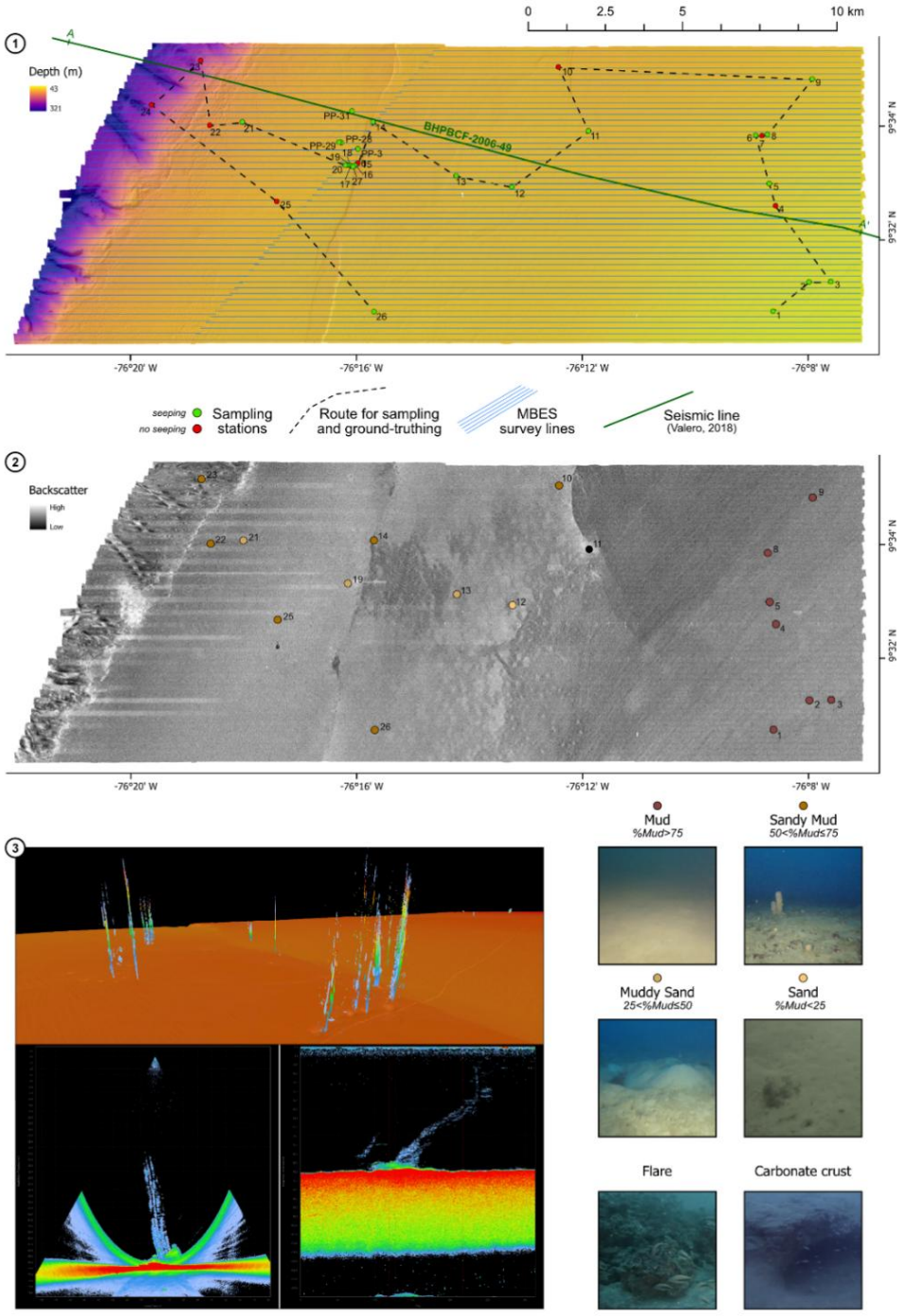

Figure 2. Datasets collected during two surveys conducted aboard the DP1 SEAWORKER vessel operated by GeoMares S.A.S. (1) Digital Terrain Model (DTM) resulted from the MBES data acquisition (survey lines are shown in blue). The seismic reflection line is in green. Numbered dots show the location of the 27 sampling stations and ground-truthing ROV dives, which selection has been based on the detection of MBES acoustic anomalies in the water column data during the acquisition phase (see Barragán & Bernal, 2024); green dots represent locations where the seeping was detected (PP locations were detected in the post-processing phase), while red dots are locations without anomalies. (2) Backscatter mosaic resulted from the MBES data acquisition; black areas represent a lower intensity (softer sediments), white areas indicate higher intensity (harder substrate). Numbered dots mark the locations of the 18 sampled stations used to run the granulometric analysis, with colours corresponding to the derived sediment classification (see Barragán & Bernal, 2024); on the bottom right, insets show ROV-derived images showing the sediment composition, a carbonate crust and a flare. (3) Water column data resulted from the MBES data acquisition.

I. Seismic Reflection Data

The seismic reflection dataset analyzed in this study forms part of the extensive 2D seismic coverage acquired across the Colombian Caribbean margin, totaling 103,571 km of 2D seismic lines from 54 exploration programs conducted between the 1970s and 2010s (ANH, 2016). Within this framework, the SOB, where the study area is located, includes approximately 29,835 km of 2D seismic data, which were interpreted in detail during the "Integración Sismoestratigráfica Caribe" project carried out by the ANH (2016). That regional interpretation provided an integrated understanding of the generation of accommodation space, sedimentation patterns, and deformation styles along the SOB and adjacent provinces (Guajira Offshore, Urabá Basin, and Colombia Basin). The results of that campaign served as a geological and structural foundation for the present study, guiding the interpretation of the seismic lines analyzed here.

The seismic data used in this work were originally acquired during marine surveys conducted by Compagnie Générale de Géophysique-Veritas (CGG) in 2006 and DIGICON Geophysical in 1993, under exploration operations by Broken Hill Proprietary (BHP) and British Petroleum (BP) (Valero, 2018). Data acquisition employed airgun arrays as energy sources and hydrophone streamers as receivers. Only profiles overlapping the study area were selected for detailed interpretation. In this work, we present the interpretation of line BHPBCF-2006-49 (see location in Figure 1).

II. MBES data

Data acquisition was conducted aboard the DP1 Seaworker Vessel of the GeoMares S.A.S. The pole-mounted MBES survey was performed using a Teledyne RESON SeaBat® T50-R. The MBES was set in equidistant beam mode at a frequency of 200 kHz, with an angular range between 30° and 85°. Positioning data and motion compensation were managed using the MV-POSView system. For differential correction, the MARINESTAR G2+ satellite system was used, guaranteeing spatial precision (XYZ) of less than 30 cm. To correct for speed of sound errors, several Sound Velocity Profiles (SVPs) were collected

throughout the survey area using a Valeport Monitor CTD. All lines had an E-W orientation, and the chosen spacing ensured an overlap of at least 20%; a total of about 247 km^2 of the seafloor was mapped, ranging from about 43 to 320 m water depth (wd). The MBES survey allowed for the collection of bathymetry, backscatter, and water column data.

Seismic Reflection Data Interpretation

The seismic dataset used in this study had been previously processed using a Pre-Stack Time Migration (PSTM) workflow following standard industry practices, resulting in improved signal-to-noise ratio and structural imaging quality. Interpretation was performed using Kingdom® software, incorporating seismic attribute analysis, manual fault picking, and horizon correlation to delineate the main structural and stratigraphic elements along the seismic line. The interpretation workflow was constrained by the regional tectono-stratigraphic framework developed by the Integración Sismoestratigráfica Caribe project (UT Offshore - ANH, 2016), which provided seismic-to-well ties with wells Cartagena-2 and Barranquilla-1. These correlations enabled calibration of key stratigraphic units and the identification of regionally significant reflectors that define the major tectono-stratigraphic sequences. Based on this framework, reflections were evaluated using parameters such as amplitude strength, continuity, frequency attenuation, polarity, and impedance contrast. These criteria guided the classification of reflection patterns and the recognition of structural or stratigraphic anomalies. Attributes including amplitude extraction, coherency, semblance, and variance were applied to enhance reflector definition, highlight discontinuities, and support the identification of fluid-related features.

MBES Data Processing

Bathymetric data were processed using QPS Qimera, following a workflow that included noise removal, sound velocity corrections based on collected SVPs, and tidal corrections, to improve vertical accuracy. The resulting Digital Terrain Model (DTM) of

the survey area was generated at a 2 m resolution (Figure 2.1). After cleaning the raw acquisition lines, .gsf files were exported to produce a backscatter mosaic with a 0.65 m cell size using QPS FMGT software (Figure 2.2). Finally, water column data were visualized in QPS FMMidwater to identify acoustic anomalies associated with potential seafloor seepage (Figure 2.3).

Morphological Mapping and Morphometric Analysis

Spatial analysis to derive seep-related landforms was performed within the ArcGIS Pro environment using the CoMMa Toolbox, which provides tools for pre-processing, landform delineation, and detailed description of morphometric parameters, texture, and volume (Arosio et al., 2024). Basic statistical analyses were then carried out to derive key terrain parameters. To enhance visualization of the morphologies, we also computed the positive and negative Openness (RVT for ArcGIS Pro - Novak et al., 2023). Furthermore, Maximum and Minimum Median Local Topographic Position (LTP) metrics were calculated using the Data Preparation Toolbox from CoMMa. For semi-automatic landform delineation, we adopted a standardized approach using the Boundary-based tool (CoMMA Delineation). After the initial mapping phase (Delineation - Table 1), the delineation was refined by excluding features with a Vertical Relief (VR) of 0, those incorrectly delineated, and those with a Width-to-Length (W/L) ratio of less than 0.3 (Refinement n.1 - Table 1). Manual edits were then applied to remove any remaining visible errors, mainly related to noise artifacts in the bathymetric data. A second refinement was carried out to exclude morphologies with a VR of less than 0.1 m, as these small features were deemed unsuitable for statistical analysis. This comprehensive approach enabled us to accurately map both positive and negative morphologies across the study area. By utilizing the Basic Descriptors, Texture Descriptors, and Volume Descriptors tools, we further refined the delineation, particularly in terms of VR, and derived essential statistical parameters related to their morphology, texture, and volume. Notably, the Polsby-Popper (PP) test for circularity (Cox, 1927; Arosio et al., 2024) allowed us to assess the circularity

of these landforms, while the Dissection Index, calculated as the ratio of maximum relative relief to maximum absolute relief, helped determine whether they exhibited a U- or V-shape. Detailed information about the attributes provided by each of these tools is presented in Table 3 of Arosio et al. (2024).

Table 1. Overview of the feature mapping workflow using the CoMMA Toolbox.

Negative features	**Positive features**
Delineation	
V Cutoff: 0.1	V Cutoff: 0.1
Min VR: 0.1	Min VR: 0.1
Min W: 5	Min W: 5
Min W/L: 0	Min W/L: 0
Buffer: 1	Buffer: 1
48,688 features	**35,370 features**
Refinement 1	
VR = 0	
W/L < 0.3	
28,025 features	**14,820 features**
Manual edit	
25,133 features	**12 features**
Refinement 2	
VR < 0.1	
Optim_R < 0.1	
8,944 features	**7 features**

Notes: the workflow integrates automated and manual procedures for feature identification. The Delineation stage summarizes the parameters used for automated detection of both positive and negative features, the selected parameter values, and the resulting number of features delineated. Refinement 1 presents the initial filtering criteria applied to remove major errors, along with the number of features remaining after filtering. Manual Edit reports the number of features retained following expert-based manual cleaning. Refinement 2 describes the final filtering conditions applied to complete the delineation process. Parameters considered include V Cutoff (Vertical Cutoff), Min VR (Minimum Vertical Relief), Min W (Minimum Width), Min W/L (Minimum Width/Length Ratio), Buffer (Buffer Distance), VR (Vertical Relief), and Optim_R (Optimal Vertical Relief).
For further details, see Arosio et al. (2024).

Results

Subsurface Observations

Several seismic anomalies were identified along seismic line BHPBCF-2006-49 (Figure 3.1). Their spatial distribution, geometry, and seismic expression were systematically mapped to assess their relationships with the underlying structural framework and stratigraphic architecture. Bright Spots (BS) are identified as localized high-amplitude reflections with negative polarity. Gas Chimneys (GC) are expressed as vertically aligned zones of disrupted or blanked reflections with amplitude attenuation and localized pull-down effects. Discontinuous Reflectors (DR) are as well visible, occurring as reflector terminations, offsets, and localized disruptions associated with structural discontinuities, together with Enhanced Reflections (ER), consisting of strong, laterally coherent high-amplitude events with sharp impedance contrasts. Other reflection patterns include Folded and Chaotic Reflectors (FCR), which show internally disturbed or contorted geometries that interrupt the surrounding stratigraphy. Finally, Bottom-Simulating Reflectors (BSR) are present as negative-polarity reflections that mimic seafloor morphology at shallow subsurface depths.

The interpreted seismic line (Figure 3.2) reveals a structurally complex margin characterized by thrust-related deformation and variable reflector continuity across the SOB. The profile shows a clear stratigraphic organization from the Late Oligocene to the Quaternary, with distinct reflector packages corresponding to the main regional tectono-stratigraphic sequences established by the ANH (2016) framework. Below the Late Miocene top, the seismic data display a succession of well-stratified Miocene reflectors with distinct characteristics. Early Miocene reflectors are strong, continuous, and display high-impedance contrasts, which are interpreted as fine-grained basin-fill deposits and calcareous-sandstone packages accumulated over basement paleo-highs. Middle Miocene reflectors are mainly continuous, high-amplitude, and subparallel, whereas Late Miocene

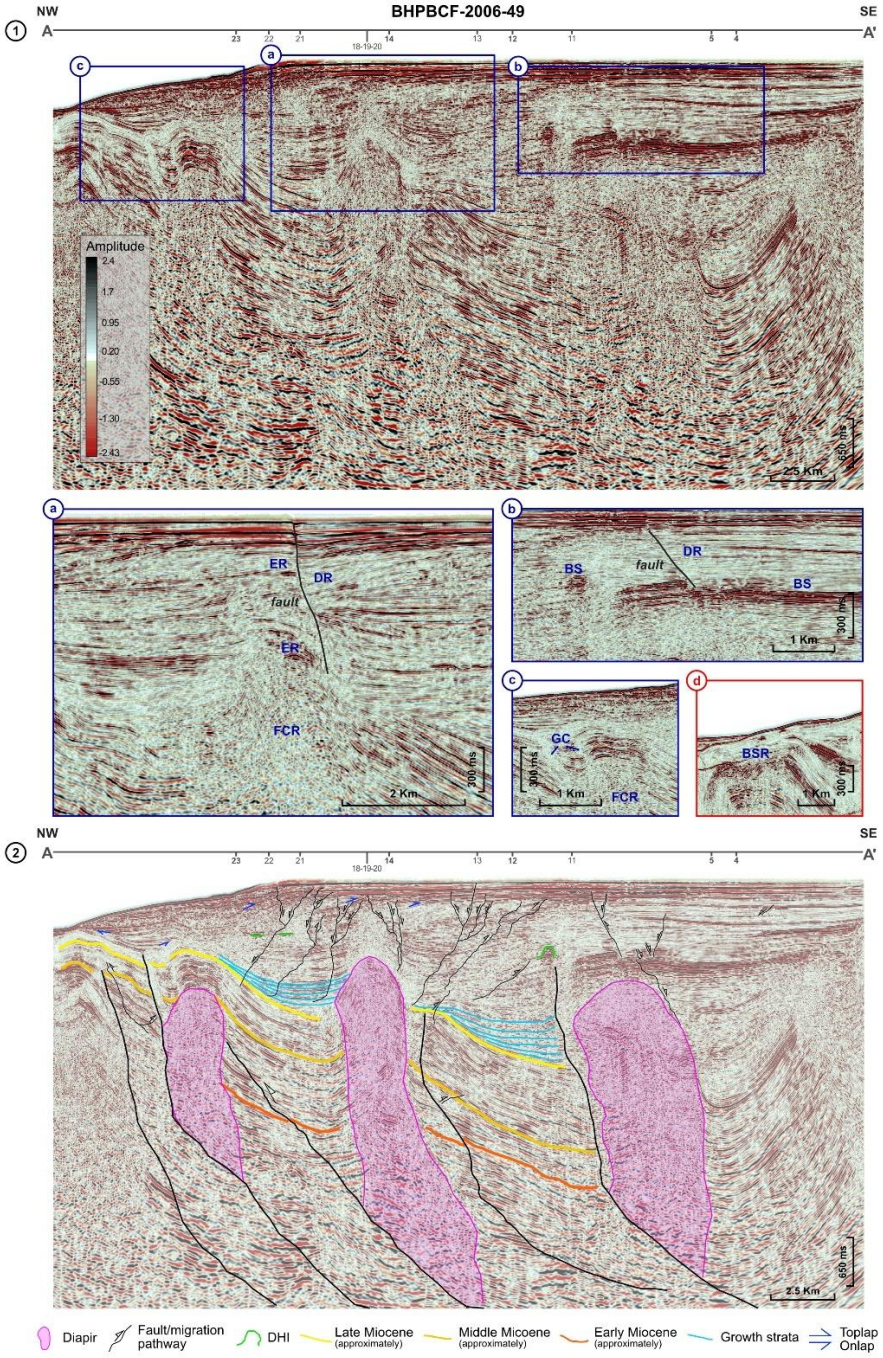

Figure 3. Subsurface observations. (1) Seismic reflection line BHPBCF-2006-49, presented in the time domain, is correlated along profile A–A' with nearby sampling and ground-truthing stations (Barragán & Bernal, 2024). Panels a, b, and c display several key seismic anomalies, including Bright Spots (BS), Gas Chimneys (GC), Discontinuous Reflectors (DR), Enhanced Reflections (ER), and Folded and Chaotic Reflectors (FCR). In contrast, panel d, located west of the study area along the same seismic line, reveals the presence of Bottom Simulating Reflectors (BSR). (2) The final interpretation of the seismic line indicates intense diapiric activity, accompanied by significant folding and fracturing within the sedimentary layers. The Late, Middle, and Early Miocene horizons were approximately delineated based on multiple stratigraphic and structural sources (Ramírez, 1969; Duque-Caro, 1979, 1984; Vernette, 1986; Briceño & Vernette, 1992; Vernette et al., 1992; Ruiz et al., 2000; Arismendy, 2020). Refer to Figure 1 for the location and orientation of the seismic line.
Data provided by ANH - Banco de Información Petrolera.

with deltaic foreset and bottomset deposits related to progradational geometries. These Miocene successions exhibit laterally persistent reflectors that serve as regional correlation markers. Above this interval, Pliocene to Quaternary deposits display moderate to low continuity and medium to high amplitudes. They show wedge-shaped and syn-tectonic geometries, recording sediment accumulation associated with ongoing compression and thrust propagation. Their internal architecture indicates gravitational and tectonically controlled sedimentation over an actively deforming substrate. The seismic line also reveals several structural features. Fault systems with detachments occur within Oligocene shales, forming ductile horizons associated with reflector disruptions and changes in reflector dip which may facilitate the upward migration of mud and fluids. In fact, the faults connecting to these strata provide preferential pathways for vertical displacement and diapir ascent. Moreover, chaotic and low-frequency reflection zones occur in multiple locations and extend upward across Miocene and Pliocene units, consistent with diapiric bodies. These features locally disturb surrounding reflections and are associated with vertical zones of reduced continuity.

Seafloor Morphologies

The semi-automatic delineation process resulted in the identification of 8,944 negative relief landforms and 7 positive relief ones (Table 1). All details of the morphometric analysis are summarized in Table 2.

Focusing on the negative relief landforms, these depressions are predominantly concentrated within a depth range of approximately 70-100 m wd; they are more densely distributed in the central part of the study area, particularly near the major lineaments characterizing the area (Figure 4.B), as well as in the southwestern sector near the slope, where the depressions also exhibit a more elongated shape (Figure 4.A). Despite the overall little relief, individual features occasionally reach elevations between 1 and 3 m, and the most prominent depression measures 4.68 m (Figure 5.1). The PP test for circularity (Figure 5.3) shows a general high degree of circularity while the dissection index (Figure 5.4) infers

a slightly V shape of the landforms (Figure 5.5). In terms of their texture, we classify all the morphologies into five categories of backscatter intensity; most features exhibit moderate to high values (Figure 5.2).

Table 2. Results of the morphometric analysis.

Attribute	***Field name***	**Negative landforms** n. 8,944	**Pockmarks** n. 5,271	**Positive landforms** n. 7
Area	*Shape_Area*	197,31	255,92	134,79
Lenght	*Shape_Leng*	50,81	59,32	41,93
Perimeter	*Perimeter*	50,81	59,32	41,96
Minimum Bounding Geometry (MBG) width, lenght, width/lenght, orientation	*MBG_Width*	12,83	14,74	11,23
	MBG_Length	18,97	22,16	16,54
	MBG_W_L	0,73	0,72	0,75
	MBG_Orient	54,29	57,21	62,50
Relief	*VRelief*	0,52	0,66	0,39
Minimum, mean and maximum slope	*Slope_MIN*	0,91	1,08	0,90
	Slope_MEAN	3,62	4,50	3,14
	Slope_MAX	5,88	7,43	4,59
Mean and maximum Local Deviation from Global (LDfG) median	*LDfG_MEAN*	11,42	16,30	-14,70
	LDfG_MAX	11,58	16,54	-14,58
Minimum, mean and maximum depth	*Depth_MIN*	-82,76	-87,76	-56,38
	Depth_MEAN	-82,50	-87,40	-56,20
	Depth_MAX	-82,20	-86,98	-56,02

Polsby–Popper test for circularity	*PP_Score*	0,91	0,89	0,92
Convex hull area	*Area_CH*	209,29	275,45	138,92
Convex hull-object area ratio	*CH_Score*	0,99	0,98	0,98
Dissection index	*Dissect*	0,77	0,60	0,91
Depth range	*Depth_RAN*	0,56	0,77	0,36
Variance of LDfG	*LDfG_VAR*	648,91	932,99	127,38
Confined relief	*Conf_VR*	0,15	0,22	0,11
Minimum, mean and maximum ruggedness index	*Rugg_MIN*	0,0001	0,0002	0,0001
	Rugg_MEAN	0,0006	0,0008	0,0005
	Rugg_MAX	0,0019	0,0027	0,0013
Minimum, mean and maximum Aspect Variability Index (AVI)	*Avi_MIN*	1,95	2,26	2,17
	Avi_MEAN	3,34	4,14	2,90
	Avi_MAX	4,82	6,10	3,66
Minimum, mean and maximum backscatter	*Bsc_MIN*	46,29	40,74	54,43
	Bsc_MEAN	138,13	136,84	161,18
	Bsc_MAX	223,21	227,42	221,14
Optimum R	*Optim_R*	0,34	0,47	0,25
Volume	*Volume*	25,16	40,02	9,90

Notes: summary of the morphometric analysis of both positive and negative relief landforms, with particular emphasis on pockmarks. The first column lists the calculated morphometric attributes, while the second column provides their corresponding shapefile field names. Detailed definitions and calculation methods for each attribute are available in Table 3 of Arosio et al. (2024). The reported values represent the mean values for all mapped morphological features.

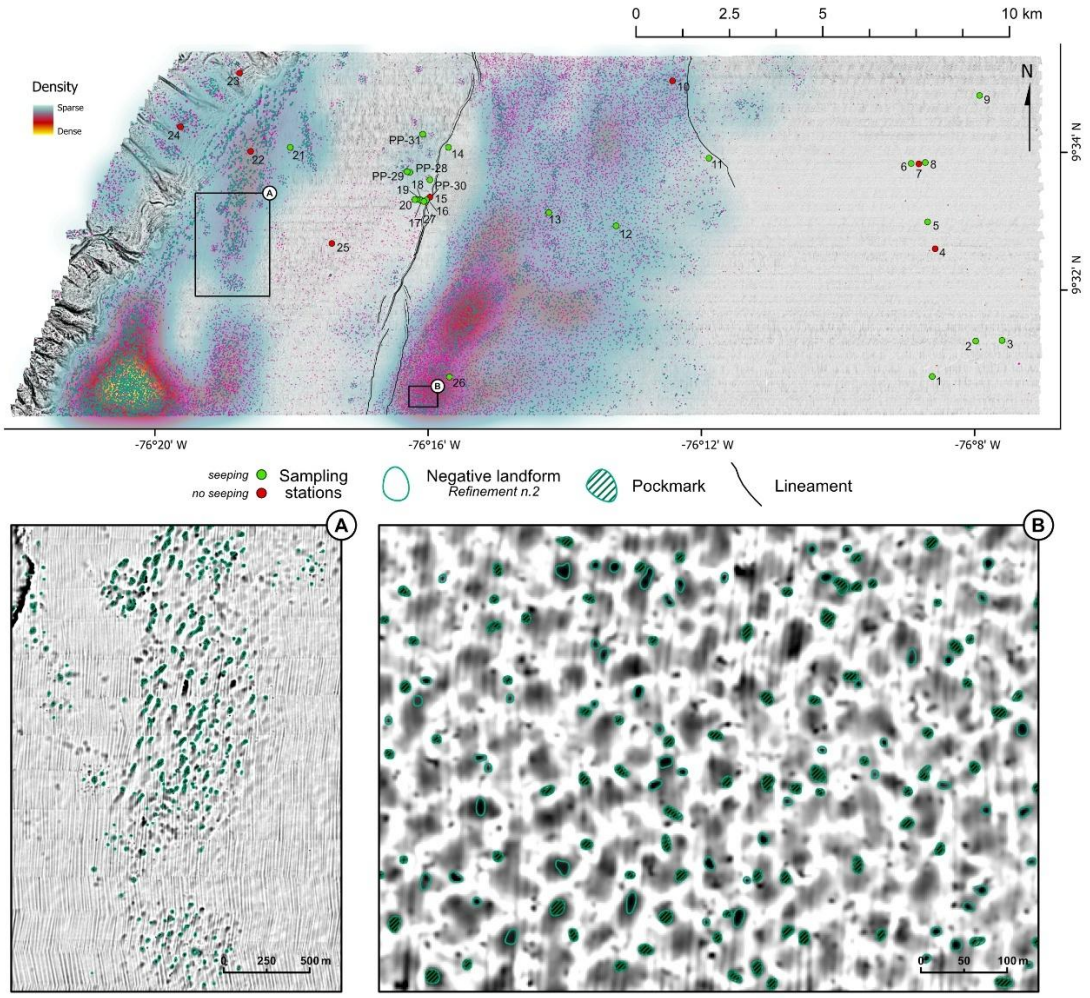

Figure 4. Results of the morphological mapping. Numbered dots show the location where seeping activity was (green dots) or was not (red dots) detected via the water column data analysis. Green polygons represent negative-relief features remaining after Refinement 2 (see Table 1); striped ones highlight those morphologies classified as pockmarks based on specific criteria (see Discussion). The grayscale background layer shows the positive Openness, which enhances the visualization of circular-rounded concave features (Novak et al., 2023). Kernel Density layer permits to better appreciate the sparse-dense distribution of the landforms. Inset (A) provides a zoomed view of the morphologies before the continental slope, while inset (B) of those characterising the central portion of the study area.

About the seven positive landforms, they are as well notably rounded. Five of these landforms are in the shallower depths of the investigated areas, at about 50 m wd, where the sediment is finer (Barragán & Bernal, 2024), while the other two are in proximity of two major lineaments characterizing the area. Of the two most prominent features, one is in proximity of the major lineament, at 74 m wd (Figure 5.5), while the other is in the shallower region at 48 m wd; both are characterized by high backscatter.

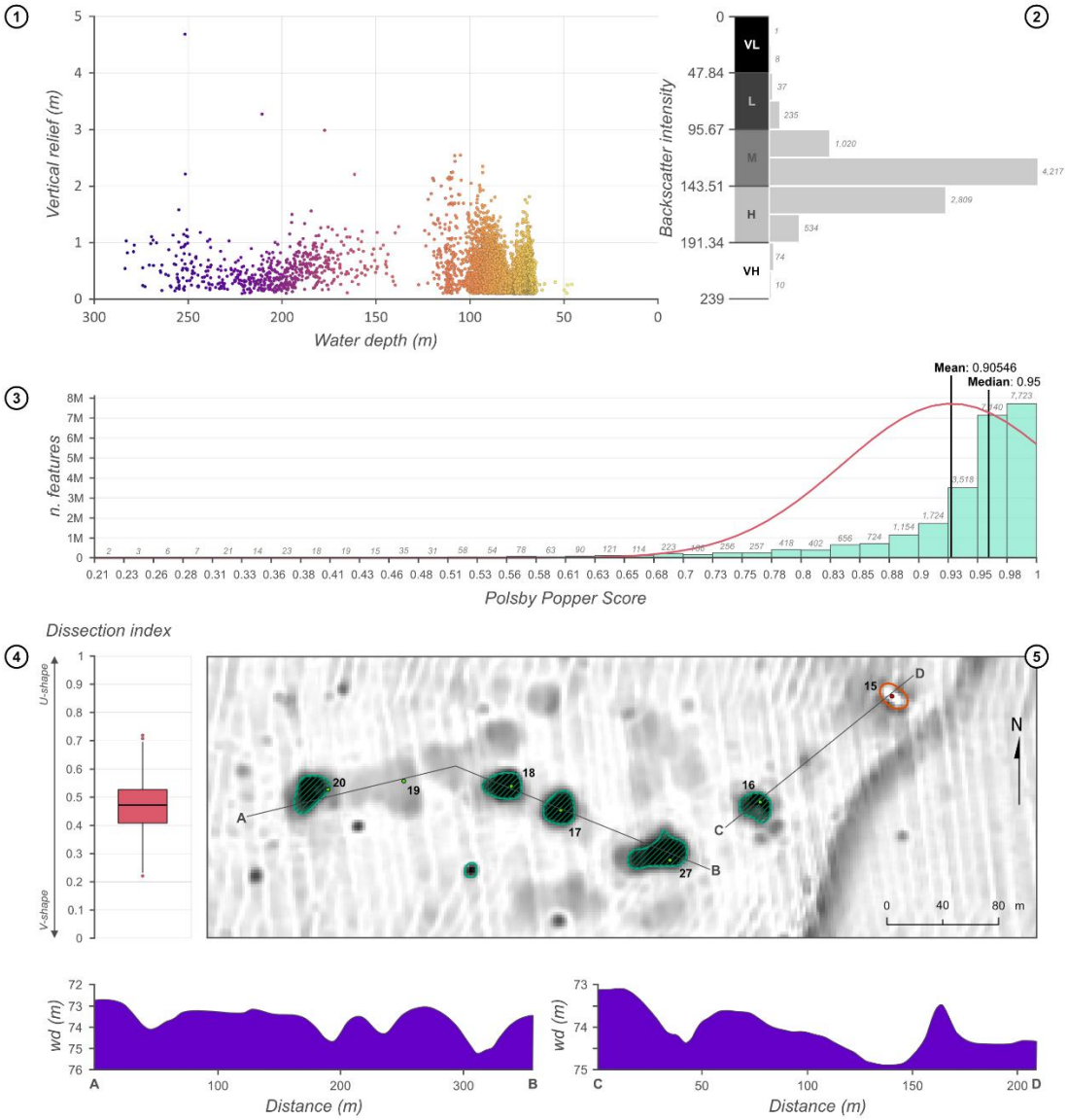

Figure 5. Results of the morphometric analysis. (1) Scatter plot illustrating the relationship between vertical relief and water depth for the negative-relief features. (2) Horizontal bar graph showing their categorisation according to the backscatter intensity: VL = Very Low; L = Low; M = Moderate; H = High; and VH = Very High. (3) Trend of the Polsby-Popper test for circularity. (4) Box-and-whisker plot of the Dissection Index. (5) Zoomed view of negative and positive-relief morphologies located between stations 16 and 27 (see Figure 4 for location), along with two cross-sectional profiles (A-B and C-D) of the selected landforms.

Discussion

The integrated interpretation of seismic reflection data and high-resolution seafloor morphology indicates a strong coupling between the structural-stratigraphic framework of the SOB and the spatial distribution of fluid seepage at the seafloor (Figure 6).

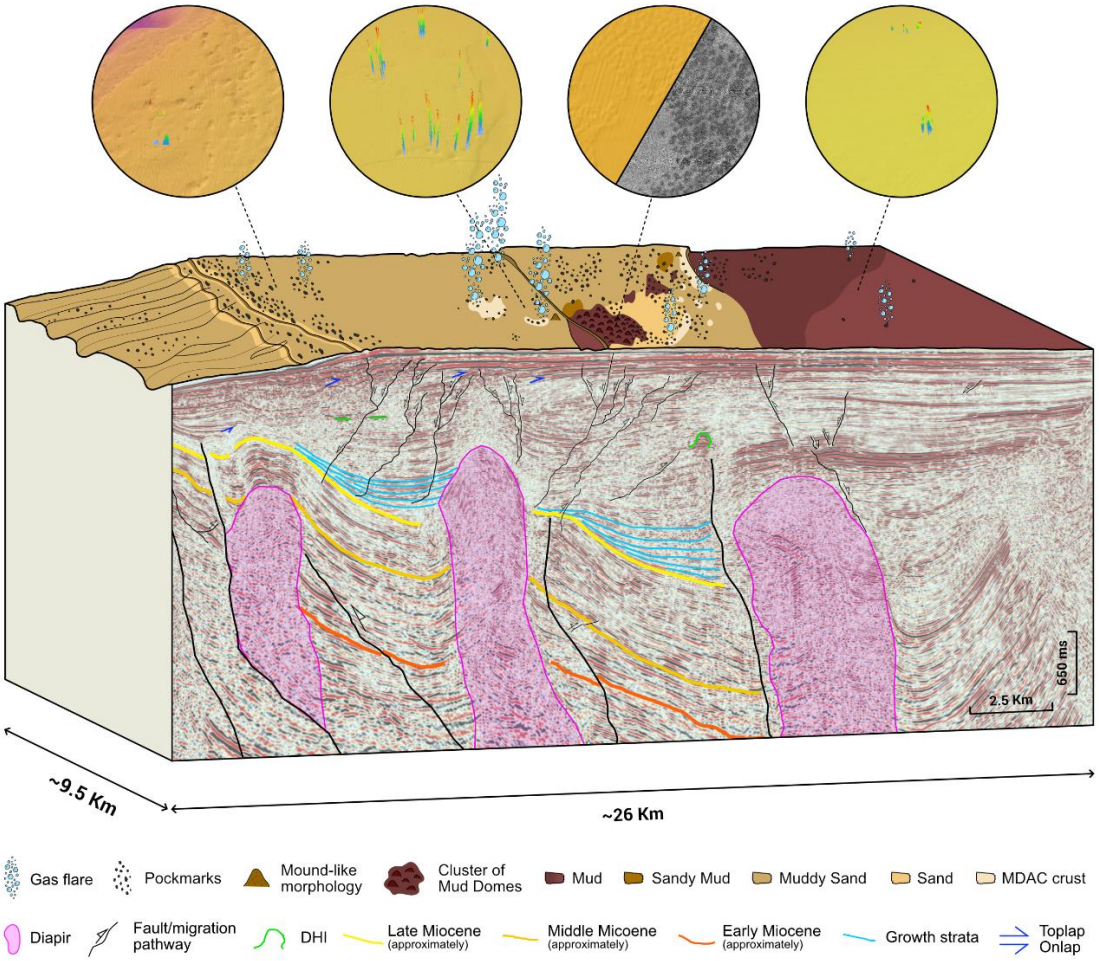

Figure 6. Schematic sketch showing the spatial relationships between seafloor morphologies and sub-seafloor structures across the study area. The bathymetric surface is colour-coded based on the interpretation of backscatter intensity, informed by sedimentological samples from Barragán & Bernal (2024), to highlight substrate variability. Interpreted geomorphological features, including pockmarks, mound-like morphologies, and clusters of mud domes, are mapped throughout the area. Circular insets provide zoomed 3D bathymetric views of selected locations, illustrating characteristic morphologies and the principal site where flares were detected analysing the water column data. The model highlights how pockmarks cluster within structurally controlled piggyback basins and along faulted margins, where faults and doming likely enable vertical fluid migration. In contrast, diapir crests show few morphological features, indicating different seepage dynamics.

Seismic line BHPBCF-2006-49 reveals a complex network of listric reverse faults, diapiric intrusions, and subsidiary fractures developed within Paleogene-Neogene mud-rich sequences. These ductile intervals, deposited during the post-rift phase and subsequently shortened during Pliocene-Quaternary compression, likely serve as overpressure-prone layers and potential conduits for vertical fluid ascent. The diapiric bodies that pierce Miocene to Pliocene strata record the upward mobility of undercompacted or overpressured shales driven by differential loading and contraction, consistent with regional models of mud diapirism across the SOB and SFB (Flinch, 2003; Alfaro & Holz, 2014; Rodríguez et al., 2021). The growth strata draping over these structures support ongoing deformation concurrent with sedimentation. Faults and fractures along diapir flanks coincide with zones of acoustic attenuation and reflection distortions in the upper Miocene to Quaternary interval, suggesting that these structures act as preferential pathways for fluid migration. This structural configuration likely enhances vertical permeability contrasts, facilitating the ascent of gas-charged fluids toward the seabed. Multiple types of seismic anomalies were identified along the profile, each providing information about potential fluid accumulations, migration pathways, or shallow geohazards. BS appear as localized high-amplitude, negative-polarity reflections, typically associated with gas-charged sandy intervals overlain by fine-grained seals. Their distribution suggests trapped pockets of free gas within Miocene and Pliocene units. Gas chimneys are expressed as vertically disrupted reflection zones with amplitude attenuation and pull-down effects, consistent with acoustic scattering in gas-saturated media. Their vertical alignment above deeper fault zones and diapir flanks supports the interpretation of upward fluid migration through structurally weakened or fractured zones. DR and reflection terminations coincide with shallow faulting and minor deformation, indicating zones where local fault permeability may enhance fluid leakage. ER, characterized by strong amplitude contrasts, likely represent accumulations of free gas at lithological boundaries or within high-porosity units. FCR, often associated with diapiric structures, mark zones of disturbed or ductile deformation where focused flow may also occur. The BSR is more

plausibly explained as a high-amplitude gas-related reflection at a permeability boundary, rather than a true hydrate base. Hydrate stability at the observed water depth and temperature offshore Colombia is unlikely (López & Ojeda, 2006), aligning with interpretations of gas accumulations at the base of fine-grained layers elsewhere (Løseth et al., 2009; Cartwright & Santamarina, 2015). Together, these anomalies depict a vertically integrated system linking deeper overpressured shales with upper sediment layers and, in many cases, with seafloor seepage structures.

The high-resolution bathymetric mapping revealed an extensive field of crater-like depressions on the seafloor. Based on their morphological characteristics, and in some cases supported by direct evidence of fluid seepage detected through MBES water column data and video footage from ROV surveys (Figure 2), these negative landforms were interpreted as pockmarks (Figure 4), indicators of potential past and ongoing seepage activity in the area. In the literature, there is not a specific minimum vertical threshold to determine whether a feature can or cannot be considered as a pockmark, and it is common rule to set it between 0.2-0.5 m - mostly depending on the spatial and vertical resolution of the mapping systems (Gafeira et al., 2018; Nanson et al., 2023). In our classification, all the features having an optimal VR lower than 0.2 m were not considered, resulting in a total of 5,271 pockmarks over the total 8,944 mapped negative relief morphologies. Bathymetric data revealed that pockmark morphology and density vary laterally across the region. Most observed pockmarks are small in scale and can be classified as *unit pockmarks* (Hovland et al., 2002; Nanson et al., 2023). These minor features typically form by the focused, episodic release of gas, predominantly methane, resulting in localized sediment displacement and collapse (Hovland & Judd, 1988; Hovland et al., 2002). Backscatter data also allowed for the identification of *eyed pockmarks*, which are characterized by high acoustic reflectivity, likely associated with authigenic carbonate precipitation and microbial activity and suggesting potential localised ongoing fluid seepage (Hovland et al., 2002; Nanson et al., 2023). Near the slope break, *elongated pockmarks* were identified, typical of sloping environments where strong bottom currents influence their shape (Hovland et al., 2002).

In addition to pockmarks, positive clustered morphologies resembling mud domes (Kopf, 2002; Nanson et al., 2023) were observed near the major lineament, possibly indicative of the extrusion of overpressured muds and gas. These spatial patterns support the interpretation that fluid expulsion in the area is structurally focused.

The spatial coincidence between seismic anomalies and the dense pockmark field mapped on the seafloor suggests a structural influence on seep distribution, and an interplay between tectonic deformation, stratigraphic architecture, and sedimentary processes (Figure 6). Comparable relationships between shallow faulting, diapirism, and pockmark occurrence have been documented in other compressional and mud-rich margins (Palomino et al., 2016; Savini et al., 2018; Osorio-Granada et al., 2023). Since direct fault traces are not always clearly visible in the bathymetric data, it is possible that fault control operates primarily at shallow sub-seafloor depths rather than through distinct surface scarps, or that subtle surface expressions are buried by recent sediments. Nevertheless, the spatial density of the pockmarks, which are the dominant seep-related features in the study area, peaks in the central part of the study area, near the two visible major faults and within Pliocene piggyback basins, where structural accommodation likely enhances vertical permeability contrasts. Their relative scarcity atop diapir crests, compared with their prevalence along flanks, suggests that seepage preferentially occurs where brittle deformation dominates over ductile behavior-conditions more favorable for the development of conduits. Sedimentological variability across the shelf likely influences seepage intensity and pockmark morphology. Siliciclastic muds supplied by the Atrato, Sinú, and Magdalena rivers (Castaño et al., 2002; Naranjo-Vesga et al., 2020; Osorio-Granada et al., 2023) create low-permeability caps that trap fluids and promote pressurization. Localized breaches induced by faulting, differential compaction, or subtle lithological contrasts facilitate focused venting and pockmark formation. The small vertical relief and overall shallow depth of the mapped pockmarks raise questions about their longevity in a relatively dynamic shelf setting. Intermittent seepage may explain their preservation, with episodic venting maintaining or reactivating depressions. This could be

the reason why, despite the huge number of features detected, only a few seepage sites were spotted. Similar episodic cycles linked to pressure fluctuations, fault reactivation, or minor seismicity have been described elsewhere (Andresen & Huuse, 2011; Lundsten et al., 2024), though their time scales remain unknown for this region and deserve further investigations. Post-formational processes may further shape pockmark morphology and perhaps be responsible for their preservation. Rapid sedimentation on the inner shelf may infill older features, while stronger bottom currents near the shelf break may erode infill or re-expose previously buried depressions. Such a balance between burial and erosion may explain why the observed pockmarks do not show a marked vertical relief, but still, they are morphologically discernible. The coexistence of negative-relief pockmarks and positive-relief features, interpreted as mounds or mud domes, could suggest a difference of fluid expulsion intensity. While the smaller, circular pockmarks likely reflect low discharge rates, the few positive-relief features may represent higher overpressure areas associated with minor mud extrusion (Kopf, 2002; Mazzini & Etiope, 2017). Yet, these interpretations remain tentative in the absence of direct sedimentological or geochemical evidence.

Although the dataset is limited to a single 2D seismic line and bathymetric coverage confined to the continental shelf, the results provide valuable insights into the shallow subsurface architecture and its influence on seepage processes in the region. Even if the interpretation is constrained by the intrinsic limitations of 2D seismic data, and the restricted spatial coverage hampers the reconstruction of the three-dimensional geometry of the structural elements and stratigraphic units, this work offers an initial framework for understanding the interactions between deformation, stratigraphy, and seepage processes in the SOB.

Conclusion

This study examines the relationship between subsurface structures, stratigraphic architecture, and seep-related seafloor morphologies offshore the Gulf of Morrosquillo, in

the Sinú Offshore Basin, Colombian Caribbean. By integrating MBES data with seismic reflection profiles, we identified a complex system of seep-related landforms whose spatial distribution appears to be influenced by local tectonics and basin evolution. Morphological mapping revealed a total of 5,271 small-scale pockmarks, predominantly clustered on major structural trends. The fine-grained, low-permeability nature of the shelf sediments likely favors fluid retention and overpressure buildup, while localized faulting and compaction may facilitate vertical venting. The limited number of active seeps detected in the water column data, together with the subdued relief of most depressions, suggests that seepage is currently weak or intermittent.

This work provides an initial framework for linking stratigraphic and structural controls to seep-related morphologies in the study area. The results point to the combined influence of faulting, diapirism, and stratigraphic architecture in focusing fluid migration and shaping the seabed. While additional geochemical data would further refine the nature of the emitted fluids, interpretations are grounded on the coherent spatial and stratigraphic relationships observed in the seismic and bathymetric datasets, and the proposed model highlights the first-order role of diapir-related deformation and fractures in controlling fluid migration and seafloor expression. Further investigations, incorporating additional high-resolution seismic profiles and temporal monitoring, will be necessary to verify the inferred connections between subsurface structures and seafloor expressions, and to better understand the dynamics of fluid escape on this sector of the Colombian Caribbean margin.

Acknowledgment

We acknowledge Ministerio de Ciencia, Tecnología e Innovación (MinCiencias) - Colombia, and Agencia Nacional de Hidrocarburos - Colombia (ANH) for their financial support through the project "*Methane Seep Hunting: A Multi-Scale and Multi-Method Approach*" (785/668–2019). Special recognition goes to the crew of the DP1 Seaworker

Vessel - Santiago Urdaneta, Dario Robledo, John Urrecheaga, Leonardo Rincon, David Herrera, and Ricardo Flórez - for their support during the field campaign and their contributions to geophysical and hydrographic data collection. We would also like to thank Rubén Arismendy and Sebastian Krastel for their valuable support and guidance during the interpretation of seismic reflection data.

AGV is funded through a PhD fellowship granted by the University of Milano-Bicocca, DISAT. GG is funded through a PhD fellowship granted by project TECLA - MIUR "Dipartimenti di Eccellenza" 2023-2027, University of Milano-Bicocca, DISAT. AM was supported by the David and Lucile Packard Foundation. This research was also supported by the Marine Cartography Lab (BluGLab) of the Department of Earth and Environmental Sciences (DISAT), University of Milano-Bicocca.

References

Alfaro, E., & Holz, M. (2014). Review of the chronostratigraphic charts in the Sinú-San Jacinto basin based on new seismic stratigraphic interpretations. *Journal of South American Earth Sciences*, *56*, 139–169. https://doi.org/10.1016/J.JSAMES.2014.09.004

ANH. (2007). *Colombian Sedimentary Basins: Nomenclature, boundaries and petroleum geology, a New Proposal.* Agencia Nacional de Hidrocarburos.

ANH. (2016). *Informe de gestión - 2016*. Agencia Nacional de Hidrocarburos. www.anh.gov.co

Arismendy, R., Kairuz, E., Osorno, J., & Rey, C. (2020). Tectonic Evolution & Structural Provinces of the Colombian Caribbean Offshore. *AAPG - Virtual Research Symposium Latin America y Caribbean Region – Southwest Caribbean Basins*. https://www.aapg.org/videos/webinar/lacr/articleid/57774/tectonic-evolution-and-structural-provinces-of-the-colombian-caribbean-offshore

Arosio, R., Gafeira, J., de Clippele, L. H., Wheeler, A. J., Huvenne, V. A. I., Sacchetti, F., Conti, L. A., & Lim, A. (2024). CoMMa: A GIS geomorphometry toolbox to map and measure confined landforms. *Geomorphology*, *458*. https://doi.org/10.1016/j.geomorph.2024.109227

Barragán, C., & Bernal, G. (2024). Benthic foraminifera as bioindicators of gas seep intensity in the offshore zone of the Sinú fold belt. *Journal of South American Earth Sciences*, *148*. https://doi.org/10.1016/j.jsames.2024.105103

Bense, V. F., & Person, M. A. (2006). Faults as conduit-barrier systems to fluid flow in siliciclastic sedimentary aquifers. *Water Resources Research*, *42*(5). https://doi.org/https://doi.org/10.1029/2005WR004480

Bialik, O. M., Varzi, A. G., Durán, R., le Bas, T., Gauci, A., Savini, A., & Micallef, A. (2022). Mesophotic Depth Biogenic Accumulations ("Biogenic Mounds") Offshore the Maltese Islands, Central Mediterranean Sea. *Frontiers in Marine Science*, *9*. https://doi.org/10.3389/fmars.2022.803687

Cartwright, J., & Santamarina, C. (2015). Seismic characteristics of fluid escape pipes in sedimentary basins: Implications for pipe genesis. *Marine and Petroleum Geology*, *65*, 126–140. https://doi.org/10.1016/J.MARPETGEO.2015.03.023

Castaño, C. (2002). *Golfos y bahías de Colombia*. Banco de Occidente Credencial.

Ceramicola, S., Dupré, S., Somoza, L., & Woodside, J. (2018). Cold Seep Systems. In A. Micallef, S. Krastel, & A. Savini (Eds.), *Submarine Geomorphology* (pp. 367–387). Springer International Publishing. https://doi.org/10.1007/978-3-319-57852-1_19

Clayton, C. (1991). Carbon isotope fractionation during natural gas generation from kerogen. *Marine and Petroleum Geology*, *8*(2), 232–240. https://doi.org/10.1016/0264-8172(91)90010-X

Cortes, J. E., Aguilera, R., Wilches, O., Osorno, J. F., & Cortes, S. I. (2018). Organic geochemical insights from oil seeps, tars, rocks, and mud volcanoes on the petroleum systems of the Sinú-San Jacinto basin,

Northwestern, Colombia. *Journal of South American Earth Sciences*, *86*, 318–341. https://doi.org/10.1016/j.jsames.2018.06.007

Cox, E. P. (1927). A Method of Assigning Numerical and Percentage Values to the Degree of Roundness of Sand Grains. *Journal of Paleontology*, *1*(3), 179–183. http://www.jstor.org/stable/1298056

Cruaud, P., Vigneron, A., Pignet, P., Caprais, J. C., Lesongeur, F., Toffin, L., Godfroy, A., & Cambon-Bonavita, M. A. (2017). Comparative study of Guaymas Basin microbiomes: Cold seeps vs. hydrothermal vents sediments. *Frontiers in Marine Science*, *4*(DEC). https://doi.org/10.3389/fmars.2017.00417

Dimitrov, L. I. (2002). Mud volcanoes—the most important pathway for degassing deeply buried sediments. *Earth-Science Reviews*, *59*(1–4), 49–76. https://doi.org/10.1016/S0012-8252(02)00069-7

Dueñas, L. F., Puentes, V., León, J., & Herrera, S. (2021). Fauna associated with cold seeps in the deep Colombian Caribbean. *Deep-Sea Research Part I: Oceanographic Research Papers*, *173*. https://doi.org/10.1016/j.dsr.2021.103552

Duque-Caro, H. (1979). Major Structural Elements and Evolution of Northwestern Colombia. In J. S. Watkins, L. Montadert, & P. W. Dickerson (Eds.), *Geological and Geophysical Investigations of Continental Margins* (Vol. 29, pp. 329–351). American Association of Petroleum Geologists. https://doi.org/10.1306/M29405C22

Duque-Caro, H. (1984). Structural style, diapirism, and accretionary episodes of the Sinú-San Jacinto terrane, southwestern Caribbean borderland. In W. E. Bonini, R. B. Hargraves, & R. Shagam (Eds.), *The Caribbean-South American Plate Boundary and Regional Tectonics* (p. 0). Geological Society of America. https://doi.org/10.1130/MEM162-p303

Escalona, A., & Mann, P. (2011). Tectonics, basin subsidence mechanisms, and paleogeography of the Caribbean-South American plate boundary zone. *Marine and Petroleum Geology*, *28*(1), 8–39. https://doi.org/10.1016/j.marpetgeo.2010.01.016

Etiope, G. (2005). Mud Volcanoes and Microseepage: The Forgotten Geophysical Components of Atmospheric Methane Budget. *Annals of Geophysics*, *48*(1). https://repository.geologyscience.ru/handle/123456789/42341

Etiope, G., & Milkov, A. v. (2004). A new estimate of global methane flux from onshore and shallow submarine mud volcanoes to the atmosphere. *Environmental Geology*, *46*(8), 997–1002. https://doi.org/10.1007/s00254-004-1085-1

Fallati, L., Panieri, G., Argentino, C., Varzi, A. G., Bünz, S., & Savini, A. (2023). Characterizing Håkon Mosby Mud Volcano (Barents Sea) cold seep systems by combining ROV-based acoustic data and underwater photogrammetry. *Frontiers in Marine Science*, *10*. https://doi.org/10.3389/fmars.2023.1269197

Flinch, J. F. (2003). Structural Evolution of the Sinu-Lower Magdalena Area (Northern Colombia). *AAPG Memoir*, *79*, 141–143. https://doi.org/10.1306/M79877C35

Gafeira, J., Dolan, M. F. J., & Monteys, X. (2018). Geomorphometric characterization of pockmarks by using a GIS-based semi-automated toolbox. *Geosciences (Switzerland)*, *8*(5). https://doi.org/10.3390/geosciences8050154

Galindo, P., & Lonergan, L. (2013). *Evolution of the Bahia Basin: Evidence for Vertical-Axis Block Rotation and Basin Inversion at the Caribbean Plate Margin Offshore Northern Colombia**.

Gonzalez-Penagos, F., Milkov, A., Lopez, E., & Duarte, L. (2019). Microbial and Thermogenic Petroleum Systems in the Colombian offshore Caribbean—New Geochemical Insights in an Emerging Basin. *2019 AAPG Annual Convention and Exhibition*.

Gracia, A., Rangel-Buitrago, N., & Sellanes, J. (2012). Methane seep molluscs from the Sinú-San Jacinto fold belt in the Caribbean Sea of Colombia. *Journal of the Marine Biological Association of the United Kingdom*, *92*(6), 1367–1377. https://doi.org/10.1017/S0025315411001421

Hatfield, L. E., Tator, B. A., & Neff, C. H. (1975). Petroleum developments in South America, Central America, and Caribbean area in 1974. *Am. Assoc. Pet. Geol. Bull.*, *59*(10), 1756–1813.

Hernández-Hamón, H., Ramírez, P. Z., Zaraza, M., & Micallef, A. (2023). Google Earth Engine app using Sentinel 1 SAR and deep learning for ocean seep methane detection and monitoring. *Remote Sensing Applications: Society and Environment*, *32*. https://doi.org/10.1016/j.rsase.2023.101036

Hooper, E. C. D. (1991). Fluid migration along growth faults in compacting sediments. *Journal of Petroleum Geology*, *14*(S1), 161–180. https://doi.org/https://doi.org/10.1111/j.1747-5457.1991.tb00360.x

Hovland, M., Gardner, J. v., & Judd, A. G. (2002). The significance of pockmarks to understanding fluid flow processes and geohazards. *Geofluids*, *2*(2), 127–136. https://doi.org/10.1046/j.1468-8123.2002.00028.x

Hovland, M., & Judd, A. (1988). Seabed Pockmarks and Seepages. Impact on Geology, Biology and the Marine Environment. *Graham & Trotman*.

James, K. H. (2009). Evolution of Middle America and the *in situ* Caribbean Plate model. *Geological Society, London, Special Publications*, *328*(1), 127–138. https://doi.org/10.1144/SP328.4

Joung, D. J., Weber, T., Gregory, K., Dugan, J., & Kessler, J. (2025). Deep Gulf of Mexico seeps are not a significant source of methane to the atmosphere. *Communications Earth & Environment 2025 6:1*, *6*(1), 999-. https://doi.org/10.1038/s43247-025-03027-0

Judd, A. G., & Hovland, M. (1992). The evidence of shallow gas in marine sediments. *Continental Shelf Research*, *12*(10), 1081–1095. https://doi.org/10.1016/0278-4343(92)90070-Z

Judd, A., & Hovland, M. (2007). Seabed fluid flow: The impact on geology, biology, and the marine environment. In *Seabed Fluid Flow: The Impact on Geology, Biology, and the Marine Environment*. https://doi.org/10.1017/CBO9780511535918

Katz, B., & Williams, K. (2003). Biogenic Gas Potential Offshore Guajira Peninsula, Colombia. In C. Bartolini, R. T. Buffler, & J. F. Blickwede (Eds.), *The Circum-Gulf of Mexico and the Caribbean<subtitle>Hydrocarbon Habitats, Basin Formation and Plate Tectonics</subtitle>*. American Association of Petroleum Geologists Memoir. https://doi.org/10.1306/M79877C43

King, L. H., & MacLean, B. (1970). Pockmarks on the Scotian Shelf. *GSA Bulletin*, *81*(10), 3141–3148. https://doi.org/10.1130/0016-7606(1970)81[3141:POTSS]2.0.CO;2

Kopf, A. J. (2002). SIGNIFICANCE OF MUD VOLCANISM. *Reviews of Geophysics*, *40*(2). https://doi.org/10.1029/2000RG000093

López, C., & Ojeda, G. Y. (2006). Heat flow in the Colombian Caribbean from the bottom simulating reflector (BSR). *CT&F - Ciencia, Tecnología y Futuro*, *3*(2), 29–39. http://www.scielo.org.co/scielo.php?script=sci_arttext&pid=S0122-53832006000200002&lng=en&nrm=iso&tlng=en

López- Ramos, E., González Penagos, F., Rincón Martínez, D. A., & Moreno Gómez, N. R. (2022). Detachment levels of Colombian caribbean mud volcanoes. *CT&F - Ciencia, Tecnología y Futuro*, *12*(2), 49–77. https://doi.org/10.29047/01225383.401

Løseth, H., Gading, M., & Wensaas, L. (2009). Hydrocarbon leakage interpreted on seismic data. *Marine and Petroleum Geology*, *26*(7), 1304–1319. https://doi.org/10.1016/J.MARPETGEO.2008.09.008

Lundsten, E., Paull, C. K., Gwiazda, R., Dobbs, S., Caress, D. W., Kuhnz, L. A., Walton, M., Nieminski, N., McGann, M., Lorenson, T., Cochrane, G., & Addison, J. (2024). Pockmarks Offshore Big Sur, California Provide Evidence for Recurrent, Regional, and Unconfined Sediment Gravity Flows. *Journal of Geophysical Research: Earth Surface*, *129*(5). https://doi.org/10.1029/2023JF007374

Mann, P. (1999). Chapter 1 Caribbean sedimentary basins: classification and tectonic setting from jurassic to present. *Sedimentary Basins of the World*, *4*(C), 3–31. https://doi.org/10.1016/S1874-5997(99)80035-5

Marcon, Y., Ondréas, H., Sahling, H., Bohrmann, G., & Olu, K. (2014). Fluid flow regimes and growth of a giant pockmark. *Geology*, *42*(1), 63–66. https://doi.org/10.1130/G34801.1

Mazzini, A., & Etiope, G. (2017). Mud volcanism: An updated review. *Earth-Science Reviews*, *168*, 81–112. https://doi.org/10.1016/J.EARSCIREV.2017.03.001

Micallef, A., Camerlenghi, A., Georgiopoulou, A., Garcia-Castellanos, D., Gutscher, M. A., lo Iacono, C., Huvenne, V. A. I., Mountjoy, J. J., Paull, C. K., le Bas, T., Spatola, D., Facchin, L., & Accettella, D. (2019). Geomorphic evolution of the Malta Escarpment and implications for the Messinian evaporative drawdown in the eastern Mediterranean Sea. *Geomorphology*, *327*, 264–283. https://doi.org/10.1016/j.geomorph.2018.11.012

Milkov, A. v. (2000). Worldwide distribution of submarine mud volcanoes and associated gas hydrates. *Marine Geology*, *167*(1–2), 29–42. https://doi.org/10.1016/S0025-3227(00)00022-0

Milkov, A. v., Sassen, R., Apanasovich, T. v., & Dadashev, F. G. (2003). Global gas flux from mud volcanoes: A significant source of fossil methane in the atmosphere and the ocean. *Geophysical Research Letters*, *30*(2). https://doi.org/10.1029/2002GL016358

Nanson, R., Arosio, R., Gafeira, J., McNeil, M., Dove, D., Bjarnadóttir, L., Dolan, M., Guinan, J., Post, A., Webb, J., & Nichol, S. (2023). A two-part seabed geomorphology classification scheme. Part 2:

Geomorphology classification framework and glossary - Version 1.0. *Zenodo*, 90pp. https://doi.org/10.5281/zenodo.7804019

Napoli, S., Spatola, D., Casalbore, D., Lombardo, L., Tanyas, H., & Chiocci, F. L. (2025). Comprehensive global inventory of submarine mud volcanoes. *Scientific Data*, *12*(1). https://doi.org/10.1038/s41597-025-04726-1

Naranjo-Vesga, J., Ortiz-Karpf, A., Wood, L., Jobe, Z., Paniagua-Arroyave, J. F., Shumaker, L., Mateus-Tarazona, D., & Galindo, P. (2020). Regional controls in the distribution and morphometry of deep-water gravitational deposits along a convergent tectonic margin. Southern Caribbean of Colombia. *Marine and Petroleum Geology*, *121*, 104639. https://doi.org/10.1016/J.MARPETGEO.2020.104639

Novak, A., Poglajen, S., & Vrabec, M. (2023). Not another hillshade: alternatives which improve visualizations of bathymetric data. *Frontiers in Marine Science*, *10*. https://doi.org/10.3389/fmars.2023.1266364

Osorio-Granada, A. M., Jigena-Antelo, B., Vidal-Perez, J., Zambianchi, E., Osorio-Granada, E. G., Torrecillas, C., Romero-Cozar, J., Leon-Rincón, H., Oviedo-Prada, K., & Muñoz-Perez, J. J. (2023). Acoustic Evidence of Shallow Gas Occurrences in the Offshore Sinú Fold Belt, Colombian Caribbean Sea. *Journal of Marine Science and Engineering*, *11*(11). https://doi.org/10.3390/jmse11112121

Palomino, D., López-González, N., Vázquez, J. T., Fernández-Salas, L. M., Rueda, J. L., Sánchez-Leal, R., & Díaz-del-Río, V. (2016). Multidisciplinary study of mud volcanoes and diapirs and their relationship to seepages and bottom currents in the Gulf of Cádiz continental slope (northeastern sector). *Marine Geology*, *378*, 196–212. https://doi.org/10.1016/J.MARGEO.2015.10.001

Pindell, J. L., & Barrett, S. F. (1991). Geological evolution of the Caribbean region; A plate-tectonic perspective. *The Caribbean Region*, 405–432. https://doi.org/10.1130/DNAG-GNA-H.405

Rice, D. D., & Claypool, G. E. (1981). Generation, Accumulation, and Resource Potential of Biogenic Gas. *AAPG Bulletin*, *65*(1), 5–25. https://doi.org/10.1306/2F919765-16CE-11D7-8645000102C1865D

Rincón-Martínez, D., Ruge, S. M., & Silva Arias, A. (2022). Seismic analysis of the geological occurrence of gas hydrate in the Colombian Caribbean offshore. *Journal of South American Earth Sciences*, *116*, 103800. https://doi.org/10.1016/j.jsames.2022.103800

Rodríguez, I., Bulnes, M., Poblet, J., Masini, M., & Flinch, J. (2021). Structural style and evolution of the offshore portion of the Sinu Fold Belt (South Caribbean Deformed Belt) and adjacent part of the Colombian Basin. *Marine and Petroleum Geology*, *125*, 104862. https://doi.org/10.1016/J.MARPETGEO.2020.104862

Roelofse, C., Alves, T. M., & Gafeira, J. (2020). Structural controls on shallow fluid flow and associated pockmark fields in the East Breaks area, northern Gulf of Mexico. *Marine and Petroleum Geology*, *112*. https://doi.org/10.1016/j.marpetgeo.2019.104074

Rollet, N., Logan, G. A., Ryan, G., Judd, A. G., Totterdell, J. M., Glenn, K., Jones, A. T., Kroh, F., Struckmeyer, H. I. M., Kennard, J. M., & Earl, K. L. (2009). Shallow gas and fluid migration in the northern

Arafura Sea (offshore Northern Australia). *Marine and Petroleum Geology*, *26*(1), 129–147. https://doi.org/10.1016/j.marpetgeo.2007.07.010

Sánchez, C., & Permanyer, A. (2006). Origin and alteration of oils and oil seeps from the Sinú-San Jacinto Basin, Colombia. *Organic Geochemistry*, *37*(12), 1831–1845. https://doi.org/10.1016/j.orggeochem.2006.07.012

Savini, A., Malinverno, E., Etiope, G., Tessarolo, C., & Corselli, C. (2009). Shallow seep-related seafloor features along the Malta plateau (Sicily channel – Mediterranean Sea): Morphologies and geo-environmental control of their distribution. *Marine and Petroleum Geology*, *26*(9), 1831–1848. https://doi.org/https://doi.org/10.1016/j.marpetgeo.2009.04.003

Savini, A., Pinson, S., Bistacchi, A., Etiope, G., & Holland, C. W. (2018). Imaging shallow gas migration pathways in a mud-volcano province using an autonomous underwater vehicle (Malta Plateau, Mediterranean Sea). *Near Surface Geophysics*, *16*(6), 681–699. https://doi.org/10.1002/nsg.12017

Sibuet, M., & Olu, K. (1998). Biogeography, biodiversity and fluid dependence of deep-sea cold-seep communities at active and passive margins. *Deep Sea Research Part II: Topical Studies in Oceanography*, *45*(1–3), 517–567. https://doi.org/10.1016/S0967-0645(97)00074-X

Spatola, D., Dahal, A., Lombardo, L., Casalbore, D., & Chiocci, F. L. (2025). First Pockmark susceptibility map of the Italian continental margins. *Marine and Petroleum Geology*, *176*, 107337. https://doi.org/10.1016/J.MARPETGEO.2025.107337

Sun, Y., Gong, S., Li, N., Peckmann, J., Jin, M., Roberts, H. H., Chen, D., & Feng, D. (2020). A new approach to discern the hydrocarbon sources (oil vs. methane) of authigenic carbonates forming at marine seeps. *Marine and Petroleum Geology*, *114*. https://doi.org/10.1016/j.marpetgeo.2020.104230

Valero Pinzón, A. (2018). *Servicio geológico colombiano. BANCO DE INFORMACIÓN PETROLERA.* http://srvags.sgc.gov.co

Waage, M., Serov, P., Andreassen, K., Waghorn, K. A., & Bünz, S. (2020). Geological controls of giant crater development on the Arctic seafloor. *Scientific Reports*, *10*(1), 8450. https://doi.org/10.1038/s41598-020-65018-9

Zhong, S., Zhang, J., Luo, J., Yuan, Y., & Su, P. (2021). Geological Characteristics of Mud Volcanoes and Diapirs in the Northern Continental Margin of the South China Sea: Implications for the Mechanisms Controlling the Genesis of Fluid Leakage Structures. *Geofluids*, *2021*. https://doi.org/10.1155/2021/5519264

Discussion

Towards a Seamless Coastal Framework

The research presented in this thesis was conceived to overcome the long-standing disciplinary and methodological divide between terrestrial and marine studies in coastal systems. The coastal zone has often been conceptualized as two separate subaerial and submerged realms, leading to incomplete reconstructions of geomorphological and environmental processes (Masselink et al., 2014; Armynot du Châtelet et al., 2016). This research attempts to demonstrate how cross-boundary approaches can generate a more coherent and process-based understanding of coastal and marine landscapes. The three projects that form the core of this thesis each address a distinct yet complementary dimension of this integration framework: conceptual, technical, and quantitative. Together, they demonstrate that merging land- and sea-based datasets not only enriches scientific interpretation but also strengthens applied outcomes, from geohazard mitigation to conservation and spatial planning (Barnard & Hoover, 2010; Prampolini et al., 2020).

The CresciBluReef project highlights the importance of conceptual integration: terrestrial geomorphological reasoning and stratigraphic interpretation can be successfully applied to marine settings, revealing new insights into the late quaternary evolution of coastal regions together with marine habitat extext and distribution. By combining high-resolution bathymetry and ROV video ground-truthing, this study reconstructed the morphology and distribution of coralligenous reefs off southeastern Sicily (Varzi et al., 2023). The correlation between biogenic structures, submerged terraces, and regional uplift rates provided a refined model for the tectonic and sea-level evolution of the investigate area (Varzi et al., 2025). These results demonstrate that the integration of geomorphic and biogenic archives can be used to quantify long-term environmental change and crustal dynamics, offering valuable proxies for assessing natural geohazards in active margins.

The BridgET project embodies technical integration through the development of reproducible workflows for producing seamless, high-resolution DEMs across the land–sea interface (Varzi et al., submitted). By combining UAV-based photogrammetry and LiDAR

together with MBES data, the Lachea islet and Cyclops Rocks case study created a continuous topo-bathymetric high-resolution surface spanning terrestrial and submarine domains, preserving positional accuracy through quasi-simultaneous temporal acquisition and enabling cross-domain geomorphometric and habitat-scale analyses. This integration follows a broader and recent international shift toward "seamless elevation products" designed to overcome the nearshore "white ribbon" gap, i.e., the systematic discontinuity between terrestrial topography and shallow-water bathymetry (Mason et al., 2006; Leon et al., 2013, 2014; Carvalho et al., 2017) that affects many coastal datasets. One of the key technological advances that has enabled the progressive mitigation of this limitation is the application of SfM photogrammetry, particularly from UAV platforms. Westoby et al. (2012) frame SfM photogrammetry as a low-cost, high-resolution 3D reconstruction approach whose accuracy hinges on survey design and ground control, providing the methodological basis for UAV photogrammetric blocks that can be rigorously tied to external reference frames. Building on this framework, Fonstad et al. (2013) demonstrate, through direct comparisons with GPS and airborne LiDAR data, that UAV-derived SfM topographic products can achieve accuracies broadly comparable to LiDAR in complex geomorphic environments (with acknowledged limitations in vegetated areas), supporting their role as an effective "onshore" component within integrated elevation models. Extending these approaches to the coastal transition zone, Leon et al. (2013) explicitly address the white ribbon problem by fusing multiple remote sensing-derived elevation sources into a seamless DEM for a reef-island system, emphasizing how multi-sensor integration and spatially explicit error handling are essential to ensure continuity and interpretability across domains. Along the same international trajectory, more recent coastal mapping frameworks increasingly combine surface and topographic sensors (UAV photogrammetry and LiDAR) with acoustic bathymetric data (MBES), often through multi-platform UAV-USV configurations, to ensure consistent referencing, assess accuracy and validate data integration, and to support joint analyses of coastal processes and hazards (Lewicka et al., 2022, Spetch 2024; Lopex et al., 2025; Tassetti et al., 2025, Casella et al.,

2025; Tang et al., 2025). Beyond its technical innovation, which is perfectly in line with recent advances, the BridgET project places strong methodological emphasis on the temporal simultaneity of terrestrial and marine data acquisition, a crucial aspect in the context of coastal regions, characterized by rapid and highly dynamic coastal processes. By acquiring UAV, LiDAR, and MBES data within the same temporal window, the project minimizes misalignment effects caused by short-term geomorphological changes, or coastal instability, thereby enhancing the internal coherence and reliability of the resulting topo-bathymetric DEM. This strategy represents a significant advancement over sequential acquisition approaches and strengthens the suitability of the dataset for process-based analyses and hazard assessment in dynamic coastal environments. In addition, BridgET demonstrated the societal relevance of such datasets: integrated DEMs are not only essential inputs for modelling floods, coastal erosion, and slope instability, but also powerful tools for education and communication (Carvalho et al., 2017; Barnard et al., 2019). Through immersive VR environments, the project translated complex geospatial data into interactive experiences that allow students and stakeholders to explore geohazards and their mitigation strategies (Barnard et al., 2019). This approach exemplifies how data integration and digital visualization can contribute simultaneously to research, teaching, and public engagement.

Finally, the Methane Seep Hunting project demonstrates the importance of quantitative analyses by combining satellite, morphological, and geophysical datasets to characterize active seepage systems in the Colombian Caribbean. The identification of seep-related features, including pockmarks and mud diapirs, revealed how subsurface fluid migration interacts with structural geology to produce potential geohazard-prone morphologies, which may be associated with gas emissions into the water column and potentially the atmosphere. This multi-method analysis provided a cost-effective and scalable workflow for seep detection and characterization. From a broader perspective, the project also underscores the significance of cross-disciplinary data integration for understanding coupled geological and ecological processes, such as fluid flow, benthic

community response, and methane emission under changing climatic conditions (Steneck & Pauly, 2019; Cooley et al., 2022).

Across these case studies, this research demonstrates that terrestrial–marine integration is not merely a technical exercise but a conceptual shift toward a systemic understanding of coastal systems. By merging data of different origin, scale, and nature, ranging from aerial imagery to bathymetric soundings and subsurface profiles, it becomes possible to describe the coastal zone as a continuum governed by interconnected processes (Inman & Brush, 1973; Cowell & Thom, 1994;). This framework supports the reconstruction of environmental evolution through time, the quantification of geohazard susceptibility, and the development of predictive models under climate and anthropogenic pressures (Prampolini et al., 2021; Cooley et al., 2022).

Implications for Coastal Geohazard Management and Environmental Change

The capacity to integrate terrestrial and marine data fundamentally improves the way we identify, model, and manage coastal and marine geohazards. Natural hazards such as coastal erosion, flooding, landslides, and submarine slope failures are rarely confined to a single domain; rather, they propagate across the land–sea boundary, requiring a continuous spatial representation for accurate risk assessment (Leon et al., 2014; Barnard et al., 2019). Seamless elevation datasets and integrated geospatial analyses, developed and tested in this thesis, directly address this requirement.

From a geomorphological perspective, the CresciBluReef results demonstrate that submerged terraces and reef systems act as long-term recorders of crustal movements, relative sea-level changes, and environmental stability (Rovere et al., 2016; Varzi et al., 2024). Quantifying their elevation, morphology, and internal structure enables reconstruction of uplift histories and paleo sea-level positions, which are critical for assessing regional tectonic hazards. In regions such as southeastern Sicily, characterized by active faulting and historical seismicity, these data provide valuable constraints for seismic hazard models and coastal vulnerability analyses (Varzi et al., 2024). The recognition that coralligenous bioconstructions preferentially develop on uplifted and morphologically stable substrates suggests that their presence can serve as an indicator of reduced sedimentation and tectonic quiescence, thereby linking geological processes with ecological stability.

At shorter time scales, spatially integrated datasets improve the predictive capacity of hazard models. The seamless DEMs generated through the BridgET workflows provide realistic coastal surfaces that can be directly incorporated into other types of analyses, such as hydrodynamic simulations of storm surge, wave run-up, and coastal flooding (Barnard & Hoover, 2010; Leon et al., 2014). Traditional models based on coarse or discontinuous topography often underestimate nearshore energy dissipation or misrepresent inundation

extents. In contrast, high-resolution integrated DEMs accurately capture critical morphological features such as cliffs, intertidal flats, and submerged reefs, which strongly influence wave propagation and coastal resilience (Masselink et al., 2014; Spadaro et al., 2025). This capability is essential for developing evidence-based adaptation strategies in the face of accelerating sea-level rise and extreme weather events (Cooley et al., 2022). Furthermore, integrated approaches enhance multi-hazard assessments by coupling morphometric analyses with ecological and anthropogenic information. In areas where human activities overlap with natural processes, such as ports, tourist developments, or coastal infrastructure, integrated geospatial models can identify zones of compounded risk (Rodríguez et al., 2009; Newton et al., 2020). By quantifying relationships between geomorphology, land use, and exposure, these models contribute to more robust coastal management and spatial planning frameworks. In this context, the BridgET project demonstrates how immersive VR environments can support not only academic training but also participatory decision-making, allowing non-specialists to visualize hazard scenarios and mitigation options (Tribbia & Moser, 2008; Barnard et al., 2019).

The Methane Seep Hunting project extends the implications of integration to submarine geohazards and climate-related processes. Methane seepage and pockmark formation are expressions of fluid migration that can destabilize slopes and trigger mass wasting events (Hovland et al., 2002; Judd and Hovland, 2007; Palomino et al., 2016: Micallef et al., 2019). Fine-scale geomorphological mapping, combined with the analysis of structural controls, is crucial for advancing the understanding of submarine landslide susceptibility and related geohazards (Prampolini et al., 2021). Moreover, it provides a robust baseline for monitoring temporal and spatial changes, enabling a deeper insight into the relationship between fluid seepage dynamics and their resulting geomorphological expression on the seabed. Moreover, seeps represent a key interface between geosphere and biosphere, linking geohazards with environmental change. In fact, seabed methane emissions may contribute to greenhouse gas fluxes, releasing large amounts of methane into the water column and possibly into the atmosphere, especially if present at shelfal depths

(Milkov et al., 2003; Etiope & Milkov, 2004; Etiope, 2005; Napoli et al., 2025; Joung et al., 2025). Other than this, seep-associated communities respond sensitively to variations in fluid flow and sedimentation (Suchley & Alvarez-Filip, 2018; Cooley et al., 2022). The integrative workflow developed in this project thus provides both a methodological template for geohazard detection and a foundation for evaluating the environmental implications of subsurface processes.

Collectively, the findings from these three projects underline the strategic value of integrated datasets for coastal and marine management. They enable the production of standardized, interoperable geospatial products that can be incorporated into CSDIs, supporting decision-making processes in ICZM and MSP (Kelly & Tuxen, 2003; Oliveira et al., 2014). By aligning scientific data with management needs, such infrastructures can facilitate early warning systems, monitor the effectiveness of nature-based solutions, and support sustainable development policies (Simmons, 2018; Schwartz-Belkin & Portman, 2023). The reproducibility and scalability of the workflows proposed in this thesis ensure that they can be adapted to different geographic and socio-economic contexts, from the Mediterranean to tropical or subpolar regions (Prampolini et al., 2020; Mazor et al., 2023).

Challenges and Future Perspectives

The methodological and conceptual advances developed in this thesis open several directions for future research and innovation. The next frontier lies in the convergence between integrated geospatial data, immersive visualization, and real-time digital modelling, fields increasingly represented by VR, AI, DT technologies (Chen et al., 2023; Yao et al., 2023).

The experience gained through the BridgET project demonstrated the potential of VR to transform static datasets into interactive analytical tools. Beyond its educational applications, VR offers a new mode of scientific inquiry, enabling users to explore complex three-dimensional geomorphological relationships at multiple scales. When combined with temporal datasets, such environments become virtual laboratories where processes such as erosion, sediment transport, and sea-level rise can be visualized and measured dynamically (Barnard et al., 2019). Future work should expand these applications toward collaborative VR platforms, allowing scientists and managers to jointly interpret data, simulate hazard scenarios, and test management strategies in real time.

The concept of the DTO and CDTs, virtual and continuously updated replicas of marine systems, represents a natural evolution of the integration framework established in this research (Jiang et al., 2021; Yao et al., 2023). By assimilating multi-sensor data streams (from satellites, drones, and in situ sensors) into dynamic models, digital twins enable real-time monitoring, prediction, and scenario testing. The seamless DEMs, data fusion workflows, and uncertainty quantification methods developed here form essential building blocks for such systems (Leon et al., 2014; Carvalho et al., 2017). Extending these frameworks to include biogeochemical, hydrodynamic, and socio-economic layers will enable comprehensive simulations of coastal evolution under changing climate and human pressures (Cooley et al., 2022).

According to literature, developing effective coastal digital twins will require addressing several challenges:

1. Establishing interoperable data standards and metadata protocols to ensure consistent integration of heterogeneous datasets (Simmons, 2018; Conti et al., 2018);

2. Advancing machine learning algorithms capable of automating feature detection and change analysis across temporal sequences (Ma et al., 2017; Hossain & Chen, 2019); and

3. Deploying open-access, cloud-based infrastructures that allow continuous data assimilation and stakeholder interaction (Conti et al., 2018; Chen et al., 2023). These efforts must also consider ethical and legal aspects of data sharing, ensuring transparency and equity in the use of digital environmental resources (Tribbia & Moser, 2008).

While the case studies presented in this thesis focused on regional-scale applications, the proposed methodologies are inherently scalable and adaptable to different spatial and temporal contexts. Extending these frameworks to broader spatial domains will support comparative analyses of tectonic, climatic, and anthropogenic controls on coastal evolution (Rovere et al., 2016). At the same time, a critical step forward lies in the coordinated and, where possible, simultaneous acquisition of terrestrial and marine datasets. Such integrated approaches are essential to capture the continuity of processes across the land-sea interface and to overcome the traditional fragmentation between terrestrial and submarine observations, which remain one of the major limitations. Equally important is the implementation of repeated surveys and long-term monitoring strategies. Time-series mapping, multi-temporal remote sensing, and sensor networks provide the only means to detect subtle geomorphological and ecological changes occurring at fine temporal scales, which still represent a significant knowledge gap in submarine and coastal environments. However, the realization of such monitoring frameworks is constrained by substantial

logistical, technological, and economic challenges, including the high costs of data acquisition, the need for multidisciplinary expertise, and the complexity of integrating heterogeneous technologies and datasets. These limitations currently restrict the widespread application of fully integrated monitoring systems, yet they also define a key frontier for future research and innovation.

In this perspective, the integration of simultaneous and repeated data acquisition strategies represents not only a methodological challenge but also a strategic opportunity for improving hazard assessment, environmental management, and decision-making processes. By enabling continuous observation of morphological, ecological, and socio-economic dynamics, such approaches would significantly enhance the predictive capabilities of CDTs and immersive modelling environments. Ultimately, advancing from episodic mapping toward systematic, multi-scale, and multi-temporal monitoring is crucial for identifying early warning signals of hazardous conditions and for evaluating the effectiveness of mitigation and adaptation measures (Leon et al., 2013; Prampolini et al., 2021). The future of integrated coastal and marine research therefore lies in the transition from mapping to modelling, from representation to simulation, and from disciplinary observation to systemic understanding. The technological, conceptual, and analytical foundations established in this thesis provide a pathway toward that transformation.

Conclusion

This thesis has demonstrated that integrating terrestrial and marine datasets represents both a methodological innovation and a conceptual change in thinking in coastal and marine geosciences. Through three complementary projects, it has shown that:

- Land-based geomorphological reasoning enhances the interpretation of submerged landscapes and biogenic structures;
- Multi-sensor workflows enable the creation of seamless and accurate digital representations of the land-sea continuum; and
- Quantitative analyses across these datasets reveal the spatial signatures of anthropogenic impacts and geohazard processes.

By addressing the *white ribbon gap* and developing reproducible integration workflows, this research contributes to the advancement of coastal geomorphology, hazard assessment, and environmental management. The methodologies proposed here support the generation of standardized datasets that can feed into CSDIs and emerging DT frameworks. As well, they promote a more inclusive and interactive approach to geoscientific communication using immersive technologies such as VR.

The findings confirm that the boundary between land and sea is not a limit but a continuum of processes and interactions. Understanding and managing this environment is crucial for addressing the challenges of a changing planet, where rising seas, shifting tectonics, and human pressures converge. The integrated approach developed in this thesis offers a foundation for future research and policy aimed at safeguarding coastal and marine environments through knowledge, innovation, and collaboration.

References

Armynot du Châtelet, E., Bout-Roumazeilles, V., Coccioni, R., Frontalini, F., Francescangeli, F., Margaritelli, G., Rettori, R., Spagnoli, F., Semprucci, F., Trentesaux, A., & Tribovillard, N. (2016). Environmental control on a land–sea transitional setting: integrated sedimentological, geochemical and faunal approaches. Environmental Earth Sciences, 75(2), 1–18. https://doi.org/10.1007/s12665-015-4957-7

Baatz, M. and Schape, A. (2000) Multiresolution Segmentation: An Optimization Approach for High Quality Multi-Scale Image Segmentation. In: Strobl, J., Blaschke, T. and Griesbner, G., Eds., Angewandte Geographische Informations-Verarbeitung, XII, Wichmann Verlag, Karlsruhe, Germany, 12-23.

Barnard, P.L., and Hoover, D., 2010, A seamless, high-resolution coastal digital elevation model (DEM) for southern California. U.S. Geological Survey Data Series 487, 8 p.
https://pubs.usgs.gov/ds/487/ds487_text.pdf

Barnard, P. L., Erikson, L. H., Foxgrover, A. C., Hart, J. A. F., Limber, P., O'Neill, A. C., van Ormondt, M., Vitousek, S., Wood, N., Hayden, M. K., & Jones, J. M. (2019). Dynamic flood modeling essential to assess the coastal impacts of climate change. Scientific Reports 2019 9:1, 9(1), 1–13. https://doi.org/10.1038/s41598-019-40742-z

Bialik, O. M., Varzi, A. G., Durán, R., le Bas, T., Gauci, A., Savini, A., & Micallef, A. (2022). Mesophotic Depth Biogenic Accumulations ("Biogenic Mounds") Offshore the Maltese Islands, Central Mediterranean Sea. Frontiers in Marine Science, 9. https://doi.org/10.3389/fmars.2022.803687

Blaschke, T. (2010). Object based image analysis for remote sensing. ISPRS Journal of Photogrammetry and Remote Sensing, 65(1), 2–16. https://doi.org/10.1016/J.ISPRSJPRS.2009.06.004

Bracchi, V. A., Marino, L., Voulaz, V., Savini, A., Fallati, L., Varzi, A. G., Bazzicalupo, P., & Basso, D. (2025). Mesophotic banks of Dendrophyllia ramea offshore Marzamemi (Sicily, Ionian Sea): a habitat classification model. Continental Shelf Research, 291, 105489. https://doi.org/10.1016/J.CSR.2025.105489

Carvalho, R. C., Hamylton, S., & Woodroffe, C. D. (2017). Filling the "white ribbon" in temperate Australia: A multi-approach method to map the terrestrial-marine interface. 2017 IEEE/OES Acoustics in Underwater Geosciences Symposium, RIO Acoustics 2017, 2018-January, 1–5.
https://doi.org/10.1109/RIOACOUSTICS.2017.8349743

Casella, E., Collin, A., Harris, D., Ferse, S., Bejarano, S., Parravicini, V., Hench, J. L., & Rovere, A. (2016). Mapping coral reefs using consumer-grade drones and structure from motion photogrammetry techniques. Coral Reefs 2016 36:1, 36(1), 269–275. https://doi.org/10.1007/S00338-016-1522-0

Casella, E., Scicchitano, G., & Rovere, A. (2024). Accuracy and Precision of Shallow-Water Photogrammetry from the Sea Surface. *Remote Sensing*, *16*(22), 4321. https://doi.org/10.3390/rs16224321

Chen, G., Yang, J., Huang, B., Ma, C., Tian, F., Ge, L., Xia, L., & Li, J. (2023). Toward digital twin of the ocean: from digitalization to cloning. Intelligent Marine Technology and Systems 2023 1:1, 1(1), 1–12. https://doi.org/10.1007/S44295-023-00003-2

Clapuyt, F., Vanacker, V., & van Oost, K. (2016). Reproducibility of UAV-based earth topography reconstructions based on Structure-from-Motion algorithms. Geomorphology, 260, 4–15. https://doi.org/10.1016/J.GEOMORPH.2015.05.011

Conti, L. A., Fonseca Filho, H., Turra, A., & Amaral, A. C. Z. (2018). Building a local spatial data infrastructure (SDI) to collect, manage and deliver coastal information. Ocean and Coastal Management, 164, 136–146. https://doi.org/10.1016/j.ocecoaman.2018.01.034

Cooley, S., D. Schoeman, L. Bopp, P. Boyd, S. Donner, D.Y. Ghebrehiwet, S.-I. Ito, W. Kiessling, P. Martinetto, E. Ojea, M.-F. Racault, B. Rost, and M. Skern-Mauritzen, 2022: Ocean and Coastal Ecosystems and their Services. In: Climate Change 2022: Impacts, Adaptation, and Vulnerability. Contribution of Working Group II to the Sixth Assessment Report of the Intergovernmental Panel on Climate Change [H.-O. Pörtner, D.C. Roberts, M. Tignor, E.S. Poloczanska, K. Mintenbeck, A. Alegría, M. Craig, S. Langsdorf, S. Löschke, V. Möller, A. Okem, B. Rama (eds.)]. Cambridge University Press, Cambridge, UK and New York, NY, USA, pp. 379-550. https://doi.org/10.1017/9781009325844.005

Cowell, P. J., & Thom, B. G. (1994). Morphodynamics of coastal evolution. Coastal evolution: Late Quaternary shoreline morphodynamics, 33-86.

EMODnet. (2023, August 31). Marine habitat mapping of the Croatian part of the Adriatic Sea [Use case]. European Marine Observation and Data Network. https://emodnet.ec.europa.eu/en/use-case/marine-habitat-mapping-croatian-part-adriatic-sea

Etiope, G., & Milkov, A. v. (2004). A new estimate of global methane flux from onshore and shallow submarine mud volcanoes to the atmosphere. *Environmental Geology*, *46*(8), 997–1002. https://doi.org/10.1007/s00254-004-1085-1

Etiope, G. (2005). Mud Volcanoes and Microseepage: The Forgotten Geophysical Components of Atmospheric Methane Budget. *Annals of Geophysics*, *48*(1). https://repository.geologyscience.ru/handle/123456789/42341

FAO, 2020b: The State of World Fisheries and Aquaculture 2020. Sustainability in Action. FAO, Rome, Italy. 244 pp.

Fonstad, M. A., Dietrich, J. T., Courville, B. C., Jensen, J. L., & Carbonneau, P. E. (2013). Topographic structure from motion: A new development in photogrammetric measurement. Earth Surface Processes and Landforms, 38(4), 421–430. https://doi.org/10.1002/ESP.3366;REQUESTEDJOURNAL:JOURNAL:10969837;WGROUP:STRING:PUBLICATION

Hossain, M. D., & Chen, D. (2019). Segmentation for Object-Based Image Analysis (OBIA): A review of algorithms and challenges from remote sensing perspective. ISPRS Journal of Photogrammetry and Remote Sensing, 150, 115–134. https://doi.org/10.1016/J.ISPRSJPRS.2019.02.009

Hovland, M., Gardner, J. v., & Judd, A. G. (2002). The significance of pockmarks to understanding fluid flow processes and geohazards. *Geofluids*, *2*(2), 127–136. https://doi.org/10.1046/j.1468-8123.2002.00028.x

Ierodiaconou, D., Schimel, A. C. G., Kennedy, D., Monk, J., Gaylard, G., Young, M., Diesing, M., Rattray, A., Ierodiaconou, D., Schimel, A. C. G., Kennedy, D., Monk, J., Gaylard, G., Young, M., Diesing, M., & Rattray, A. (2018). Combining pixel and object based image analysis of ultra-high resolution multibeam bathymetry and backscatter for habitat mapping in shallow marine waters. MarGR, 39(1–2), 271–288. https://doi.org/10.1007/S11001-017-9338-Z

Inman, D. L., & Brush, B. M. (1973). The coastal challenge. Science, 181(4094), 20–32. https://doi.org/10.1126/SCIENCE.181.4094.20

James, M. R., & Robson, S. (2012). Straightforward reconstruction of 3D surfaces and topography with a camera: Accuracy and geoscience application. Journal of Geophysical Research: Earth Surface, 117(3), 3017. https://doi.org/10.1029/2011JF002289;REQUESTEDJOURNAL:JOURNAL:21562202F;PAGEGROUP:STRING:PUBLICATION

Jiang, P., Meinert, N., Jordão, H., Weisser, C., Holgate, S., Lavin, A., Lütjens, B., Newman, D., Wainwright, H., Walker, C., & Barnard, P. (2021). Digital Twin Earth -- Coasts: Developing a fast and physics-informed surrogate model for coastal floods via neural operators. https://arxiv.org/pdf/2110.07100

Joung, D. J., Weber, T., Gregory, K., Dugan, J., & Kessler, J. (2025). Deep Gulf of Mexico seeps are not a significant source of methane to the atmosphere. *Communications Earth & Environment 2025 6:1*, *6*(1), 999-. https://doi.org/10.1038/s43247-025-03027-0

Judd, A., & Hovland, M. (2007). Seabed fluid flow: The impact on geology, biology, and the marine environment. In *Seabed Fluid Flow: The Impact on Geology, Biology, and the Marine Environment*. https://doi.org/10.1017/CBO9780511535918

Kelly, N. M., & Tuxen, K. (2003). WebGIS for Monitoring "Sudden Oak Death" in coastal California. Computers, Environment and Urban Systems, 27(5), 527–547. https://doi.org/10.1016/S0198-9715(02)00065-0

Kieu, H. T., & Law, A. W. K. (2021). Remote sensing of coastal hydro-environment with portable unmanned aerial vehicles (pUAVs) a state-of-the-art review. Journal of Hydro-Environment Research, 37, 32–45. https://doi.org/10.1016/J.JHER.2021.04.003

Leon, J. X., Heuvelink, G. B. M., & Phinn, S. R. (2014). Incorporating DEM Uncertainty in Coastal Inundation Mapping. PLOS ONE, 9(9), e108727. https://doi.org/10.1371/JOURNAL.PONE.0108727

Leon, J. X., Phinn, S. R., Hamylton, S., & Saunders, M. I. (2013). Filling the "white ribbon" - a multisource seamless digital elevation model for Lizard Island, northern Great Barrier Reef. International Journal of Remote Sensing, 34(18), 6337–6354. https://doi.org/10.1080/01431161.2013.800659

Lewicka, O., Specht, M., Stateczny, A., Specht, C., Dardanelli, G., Brčić, D., Szostak, B., Halicki, A., Stateczny, M., & Widźgowski, S. (2022). Integration Data Model of the Bathymetric Monitoring System for Shallow Waterbodies Using UAV and USV Platforms †. In *Remote Sensing* (Vol. 14, Issue 16). MDPI. https://doi.org/10.3390/rs14164075

López, I., Bañón, L., & Pagán, J. I. (2025). Integrating UAV and USV for Elaboration of High-Resolution Coastal Elevation Models. *Journal of Marine Science and Engineering*, *13*(8). https://doi.org/10.3390/jmse13081464

Ma, L., Li, M., Ma, X., Cheng, L., Du, P., & Liu, Y. (2017). A review of supervised object-based land-cover image classification. ISPRS Journal of Photogrammetry and Remote Sensing, 130, 277–293. https://doi.org/10.1016/J.ISPRSJPRS.2017.06.001

Maruca, G., Cipriani, M., Dominici, R., Imbrogno, G., Vespasiano, G., Apollaro, C., Perri, F., Bruno, F., Lagudi, A., Severino, U., Bracchi, V. A., Basso, D., Cellini, E., Mauri, F., Rosso, A., Sanfilippo, R., & Guido, A. (2025). Mapping benthic marine habitats featuring coralligenous bioconstructions: a new approach to support geobiological research. Ocean Science, 21(5), 1967–1986. https://doi.org/10.5194/OS-21-1967-2025

Mason, T., Rainbow, B., & McVey, S. (2008). Colouring the 'White Ribbon': Strategic coastal monitoring in the south-east of England. Hydro International. https://www.hydro-international.com/content/article/colouring-the-white-ribbon

Masselink, G., Hughes, M., & Knight, J. (2014). Introduction to Coastal Processes and Geomorphology. Routledge. https://doi.org/10.4324/9780203785461

Mazor, T., Watermeyer, K., Hobley, T., Grinter, V., Holden, R., MacDonald, K., & Ferns, L. (2023). Statewide Marine Habitat Map 2023: Habitat Complex Modelling Method (CBiCS Level 3) [Dataset]. The State of Victoria, Department of Environment, Energy and Climate Action. https://researchdata.edu.au/statewide-marine-habitat-map-2023/2287767

Micallef, A., Camerlenghi, A., Georgiopoulou, A., Garcia-Castellanos, D., Gutscher, M. A., lo Iacono, C., Huvenne, V. A. I., Mountjoy, J. J., Paull, C. K., le Bas, T., Spatola, D., Facchin, L., & Accettella, D. (2019). Geomorphic evolution of the Malta Escarpment and implications for the Messinian evaporative drawdown in the eastern Mediterranean Sea. *Geomorphology*, *327*, 264–283. https://doi.org/10.1016/j.geomorph.2018.11.012

Milkov, A. v., Sassen, R., Apanasovich, T. v., & Dadashev, F. G. (2003). Global gas flux from mud volcanoes: A significant source of fossil methane in the atmosphere and the ocean. *Geophysical Research Letters*, *30*(2). https://doi.org/10.1029/2002GL016358

Mishra, D. R., & Gould, R. W. (2016). Preface: Remote sensing in coastal environments. In Remote Sensing (Vol. 8, Issue 8). MDPI AG. https://doi.org/10.3390/rs8080665

Najdawi, A. R., & Ghatasha, N. (2012). Using concept mapping tools to enhance collaborative problem solving and innovation in corporate e-Learning. 2012 International Conference on Interactive Mobile and Computer Aided Learning, IMCL 2012, 197–199.
https://doi.org/10.1109/IMCL.2012.6396474

Napoli, S., Spatola, D., Casalbore, D., Lombardo, L., Tanyas, H., & Chiocci, F. L. (2025). Comprehensive global inventory of submarine mud volcanoes. *Scientific Data*, *12*(1). https://doi.org/10.1038/s41597-025-04726-1

Newton, A., Icely, J., Cristina, S., Perillo, G. M. E., Turner, R. E., Ashan, D., Cragg, S., Luo, Y., Tu, C., Li, Y., Zhang, H., Ramesh, R., Forbes, D. L., Solidoro, C., Béjaoui, B., Gao, S., Pastres, R., Kelsey, H., Taillie, D., … Kuenzer, C. (2020). Anthropogenic, Direct Pressures on Coastal Wetlands. Frontiers in Ecology and Evolution, 8, 512636. https://doi.org/10.3389/FEVO.2020.00144/FULL

Oliveira, A., Jesus, G., Gomes, J. L., Rogeiro, J., Azevedo, A., Rodrigues, M., Fortunato, A. B., Dias, J. M., Tomas, L. M., Vaz, L., Oliveira, E. R., Alves, F. L., & den Boer, S. (2014). An interactive WebGIS observatory platform for enhanced support of integrated coastal management. Https://Doi.Org/10.2112/SI70-086.1, 70(sp1), 507–512. https://doi.org/10.2112/SI70-086.1

Palomino, D., López-González, N., Vázquez, J. T., Fernández-Salas, L. M., Rueda, J. L., Sánchez-Leal, R., & Díaz-del-Río, V. (2016). Multidisciplinary study of mud volcanoes and diapirs and their relationship to seepages and bottom currents in the Gulf of Cádiz continental slope (northeastern sector). *Marine Geology*, *378*, 196–212. https://doi.org/10.1016/J.MARGEO.2015.10.001

Phinn, S. R., Roelfsema, C. M., & Mumby, P. J. (2012). Multi-scale, object-based image analysis for mapping geomorphic and ecological zones on coral reefs. International Journal of Remote Sensing, 33(12), 3768–3797. https://doi.org/10.1080/01431161.2011.633122;SUBPAGE:STRING:FULL

Piazzolla, D., Bonamano, S., Penna, M., Resnati, A., Scanu, S., Madonia, N., Madonia, A., Fersini, G., Coppini, G., Marcelli, M., & Piermattei, V. (2025). Combining USV ROV and multimetric indices to assess benthic habitat quality in coastal areas. Scientific Reports 2025 15:1, 15(1), 1–10. https://doi.org/10.1038/s41598-025-09845-8

Prampolini, M., Angeletti, L., Castellan, G., Grande, V., le Bas, T., Taviani, M., & Foglini, F. (2021). Benthic habitat map of the southern adriatic sea (Mediterranean Sea) from object-based image analysis of multi-source acoustic backscatter data. Remote Sensing, 13(15), 2913.

https://doi.org/10.3390/RS13152913/S1

Prampolini, M., Savini, A., Foglini, F., & Soldati, M. (2020). Seven good reasons for integrating terrestrial and marine spatial datasets in changing environments. In Water (Switzerland) (Vol. 12, Issue 8). MDPI AG. https://doi.org/10.3390/w12082221

Pulido Mantas, T., Roveta, C., Calcinai, B., di Camillo, C. G., Gambardella, C., Gregorin, C., Coppari, M., Marrocco, T., Puce, S., Riccardi, A., & Cerrano, C. (2023). Photogrammetry, from the Land to the Sea and Beyond: A Unifying Approach to Study Terrestrial and Marine Environments. Journal of Marine Science and Engineering, 11(4), 759. https://doi.org/10.3390/JMSE11040759/S1

Rodríguez, I., Montoya, I., Sánchez, M. J., & Carreño, F. (2009). Geographic Information Systems applied to Integrated Coastal Zone Management. Geomorphology, 107(1–2), 100–105. https://doi.org/10.1016/J.GEOMORPH.2007.05.023

Rovere, A., Stocchi, P., & Vacchi, M. (2016). Eustatic and Relative Sea Level Changes. Current Climate Change Reports, 2(4), 221–231. https://doi.org/10.1007/S40641-016-0045-7/FIGURES/3

Seabed 2030. (2025, June 21). Seabed 2030 announces millions of square kilometers of new seafloor data on World Hydrography Day. Seabed 2030. https://seabed2030.org/2025/06/21/seabed-2030-announces-millions-of-square-kilometers-of-new-seafloor-data-on-world-hydrography-day/

Schwartz-Belkin, I., & Portman, M. E. (2023). A review of geospatial technologies for improving Marine Spatial Planning: Challenges and opportunities. Ocean & Coastal Management, 231, 106280. https://doi.org/10.1016/J.OCECOAMAN.2022.106280

Selig, E. R., Hole, D. G., Allison, E. H., Arkema, K. K., McKinnon, M. C., Chu, J., de Sherbinin, A., Fisher, B., Glew, L., Holland, M. B., Ingram, J. C., Rao, N. S., Russell, R. B., Srebotnjak, T., Teh, L. C. L., Troëng, S., Turner, W. R., & Zvoleff, A. (2019). Mapping global human dependence on marine ecosystems. Conservation Letters, 12(2), e12617.
https://doi.org/10.1111/CONL.12617;PAGE:STRING:ARTICLE/CHAPTER

Sevilla, N. P. M., Adeath, I. A., le Bail, M., & Ruiz, A. C. (2019). Coastal Development: Construction of a Public Policy for the Shores and Seas of Mexico. Coastal Management: Global Challenges and Innovations, 21–38. https://doi.org/10.1016/B978-0-12-810473-6.00003-0

Simmons, S. (2018). Metadata and Spatial Data Infrastructure. Comprehensive Geographic Information Systems, 3, 110–124. https://doi.org/10.1016/B978-0-12-409548-9.09611-1

Smith, M. W., Carrivick, J. L., & Quincey, D. J. (2016). Structure from motion photogrammetry in physical geography. Progress in Physical Geography, 40(2), 247–275.
https://doi.org/10.1177/0309133315615805;WEBSITE:WEBSITE:SAGE;WGROUP:STRING:PUBLICATION

Spadaro, A., Chiabrando, F., Lingua, A., & Maschio, P. (2025). Photogrammetry and Traditional Bathymetry for High-Resolution Underwater Mapping in Shallow Waters. The International Archives of the Photogrammetry, Remote Sensing and Spatial Information Sciences, XLVIII-2-W10-2025(2/W10-2025), 279–286. https://doi.org/10.5194/ISPRS-ARCHIVES-XLVIII-2-W10-2025-279-2025

Specht, O. (2023). Land and Seabed Surface Modelling in the Coastal Zone Using UAV/USV-Based Data Integration. Sensors, 23(19), 8020. https://doi.org/10.3390/s23198020

Specht, M. (2024). Methodology for Performing Bathymetric and Photogrammetric Measurements Using UAV and USV Vehicles in the Coastal Zone. In *Remote Sensing* (Vol. 16, Issue 17). Multidisciplinary Digital Publishing Institute (MDPI). https://doi.org/10.3390/rs16173328

Steneck, R. S., & Pauly, D. (2019). Fishing through the Anthropocene. Current Biology, 29(19), R987–R992. https://doi.org/10.1016/j.cub.2019.07.081

Suchley, A., & Alvarez-Filip, L. (2018). Local human activities limit marine protection efficacy on Caribbean coral reefs. Conservation Letters, 11(5), e12571. https://doi.org/10.1111/CONL.12571;JOURNAL;JOURNAL:1755263X;WGROUP:STRING:PUBLICATION

Sullivan, E., Papagiannopoulos, N., Clewley, D., Groom, S., Raitsos, D. E., & Hoteit, I. (2025). Mapping Coastal Marine Habitats Using UAV and Multispectral Satellite Imagery in the NEOM Region, Northern Red Sea. Remote Sensing, 17(3), 485. https://doi.org/10.3390/RS17030485/S1

Tang, K. K. W., Yatim, M. H. M., Darwin, N., Aris, W. A. W., Yen, S. C., & Fadil, N. M. (2025). Seamless Multisource Topo-Bathymetric Elevation Modelling for River Basins: A Review of UAV and USV Integration Techniques. *Revue Internationale de Géomatique*, *34*(1), 587–602. https://doi.org/10.32604/rig.2025.065583

Tassetti, A. N., Simone, G., Avanzato, G., Malinverni, E. S., Memmola, F., Brocchini, M., & Penna, P. (2025). Integrated geomatics for seamless coastal mapping: a vulnerable coastline in the central Adriatic Sea. *Geomatics, Natural Hazards and Risk*, *16*(1). https://doi.org/10.1080/19475705.2025.2584699

Tribbia, J., & Moser, S. C. (2008). More than information: what coastal managers need to plan for climate change. Environmental Science and Policy, 11(4), 315–328. https://doi.org/10.1016/j.envsci.2008.01.003

Varzi, A. G., Fallati, L., Savini, A., Bracchi, V. A., Bazzicalupo, P., Rosso, A., Sanfilippo, R., Bertolino, M., Muzzupappa, M., & Basso, D. (2023). Geomorphology of coralligenous reefs offshore southeastern Sicily (Ionian Sea). Journal of Maps. https://doi.org/10.1080/17445647.2022.2161963

Varzi, A. G., Meschis, M., Fallati, L., Scicchitano, G., de Santis, V., Scardino, G., Basso, D., Bracchi, V. A., & Savini, A. (2024). New chronology for submerged relict paleoshorelines and associated rates of

crustal vertical movements offshore the Marzamemi village, Sicily (Southern Italy). Marine Geology, 474. https://doi.org/10.1016/j.margeo.2024.107326

Westoby, M. J., Brasington, J., Glasser, N. F., Hambrey, M. J., & Reynolds, J. M. (2012). 'Structure-from-Motion' photogrammetry: A low-cost, effective tool for geoscience applications. Geomorphology, 179, 300–314. https://doi.org/10.1016/J.GEOMORPH.2012.08.021

Yao, J. F., Yang, Y., Wang, X. C., & Zhang, X. P. (2023). Systematic review of digital twin technology and applications. Visual Computing for Industry, Biomedicine, and Art 2023 6:1, 6(1), 1–20. https://doi.org/10.1186/S42492-023-00137-4